To the Graduate Council:

I am submitting herewith a dissertation written by Russell Owen Colson entitled "Temperature and Compositional Dependence of Trace Element Partitioning in Silicate Systems." I have examined the final copy of this dissertation for form and content and recommend that it be accepted in partial fulfillment of the requirements for the degree of Doctor of Philosophy, with a major in Geology.

Lawrence A. Taylor

Lawrence A. Taylor, Major Professor

We have read this dissertation
and recommend its acceptance:

Accepted for the Council:

Vice Provost
and Dean of The Graduate School

TEMPERATURE AND COMPOSITIONAL DEPENDENCE OF TRACE ELEMENT PARTITIONING IN SILICATE SYSTEMS

A Dissertation

Presented for the

Doctor of Philosophy

Degree

The University of Tennessee, Knoxville

Russell Owen Colson

March 1986

ACKNOWLEDGEMENTS

To Dr. Lawrence Taylor, my advisor and committe chairman, and Dr. Gordon McKay, who had oversight of my research in Houston, I express my sincere gratitude for teaching me not only the facts of sicence but the philosophy as well. Without their instruction this dissertation would not have been possible. From each member of my dissertation committee I have received nothing but enthusiastic help and suggestions. My thanks goes to these also: Dr. Hap McSween, Dr. Ted Labotka, and Dr. Ben Oliver. A special note of thanks for outstanding instruction in the principles of thermodynamics goes to Dr. Dick Williams of the Johnson Space Center, Houston, and Dr. C. R. Brooks of the University of Tennessee Metallurgy department.

Many discussions with other University of Tennessee faculty and students, covering a wide range of subjects, have been an integral part of my study at the University of Tennessee. This dissertation has benefited from this intellectual stimulation, and I thank both faculty and students for their thoughts. Though the following list is in no way a complete listing of those whose discussions and interest have stimulated my own thoughts and interest in this and related projects, I would like to mention and thank the following people: Eyerett Rutherford, Steve Absher, Mary Lynn Dobson, Craig Clement, Jonathan Shireman, Christine Bowers, Dr. Nick Woodward, Dr. Kula Misra, Dr. Otto Kopp, and my wife, Mary Cudzil.

Thanks also goes to my parents, who first taught me a curiosity and wonder at the universe around me and gave me the strength and will to seek to understand it.

Funding and facilities for this study were provided in large part by a grant from the National Aeronautics and Space Administration. In this regard special recognition is made of the scientists and technicians of the solar system exploration division at the Johnson Space Center where the experimental work was completed. I am especially indebted to Dr. David Gust and Oscar Mullins for enlightening discussions and instruction of a greenhorn experimentalist.

ABSTRACT

Trace element partitioning between olivine and melt, and between orthopyroxene and melt, have been determined by microprobe analysis of synthetic olivine, orthopyroxene, and quenched basaltic glass equilibrated in latm gas mixing furnaces. Experiments were conducted in several compositional systems at temperatures ranging from 1180°C to 1420°C. Partitioning values are determined for the elements Eu, Ca, Mn, Fe, Ni, Sm, Gd, Y, Yb, Sc, Al, Zr, and Ti.

Equations expressing the temperature and compositional dependence of trace element partitioning are derived based on an evaluation of the substitution reaction between crystal and melt and the lattice energies of the trace element components. The lattice energies are modeled assuming that the crystals are ionically bonded. The derived expressions permit the prediction of trace element partitioning for compositions and temperatures not directly measured. The relation of enthalpies and entropies of exchange to cation size permits prediction of the partitioning of elements not experimentally investigated.

Based on these trace element partition coefficients and known phase equilibria for major elements, continuous fractional crystallization is not completely successful in modeling selected basaltic suites. Though major elements are modeled by fractional crystallization, Ni is better modeled by assuming all Ni has reequilibrated to the conditions of the lower temperature members of the suite. This suggests an olivine accumulation or olivine re-mixing model may be a

more realistic portrayal of the genetic relations of the Hawaiian suites investigated.

TABLE OF CONTENTS

LIST OF TABLES

LIST OF FIGURES

FIGURE PAGE

FIGURE PAGE

CHAPTER 1

INTRODUCTION

This study is an investigation of the effects of variations in intensive parameters on crystal/melt partitioning in silicate systems. Its focus is on the temperature and compositional dependence of REE, Sc, Al, and Ca partitioning among olivine, orthopyroxene and basaltic melts. By means of carefully formulated models, the results are extended into regions of temperature, pressure, fO_2, and composition not directly investigated. By relating partitioning to fundamental properties of each cation and phase, the results are extrapolated to include other elements and phases.

The second chapter reports olivine/melt and orthopyroxene/melt partitioning values for several divalent, trivalent, and tetravalent elements. It discusses the effect of variations in intensive parameters on partitioning. It is also concerned with the enthalpies, entropies, and mechanisms of the trace element substitutions. An ionic model for trace element lattice energies is developed to predict the variations in these values. Substitution mechanisms are investigated and nonidealities arising from local cation interactions are determined. The synthesis is based on published data and experimental data derived in this study.

The third chapter applies partitioning relations determined in this study to basaltic suites from the Hawaiian Islands. Its goal is to illustrate the practicality of applying rigorous thermodynamic con-

straints to real magma evolution problems. This chapter tests how well selected fractionation models predict the observed chemical trends when major and trace element partitioning is constrained to obey known thermodynamic relations.

The general implications of the temperature and compositional dependence of trace element partitioning on magma evolution are discussed throughout this thesis and a specific application given in chapter 4. However, the main thrust of the study is toward an understanding of the trace element energetics for its own sake. This is investigated from two perspectives:

1. A thermodynamic evaluation of activities, enthalpies, and entropies involved in the exchange of a trace element between crystal and melt.
2. A discussion of the crystal-chemical rational for relative partitioning relations.

The energies of exchange determined in the first approach are modeled on the basis of equations expressing lattice energies of ionic solids already well established in solid state physics.

This approach gives fundamental insight into the nature of trace elements in crystals and melt. Because of its fundamental nature, the approach is readily applied to other compositions, temperatures, phases, and even processes (such as diffusion or intra-crystalline partitioning). Therefore, the results become a more powerful tool in applied geochemistry than if trace element partitioning had been related to temperature and composition by purely empirical equations.

CHAPTER 2

TEMPERATURE AND COMPOSITIONAL DEPENDENCIES OF TRACE ELEMENT PARTITIONING IN OLIVINE AND ORTHOPYROXENE

Introduction

Trace elements, the REE in particular, are a useful tool in geochemical modeling of magma evolution. However, knowledge of the distribution of these elements between crystals and melt, critical to such studies, remains incomplete. There is an abundance of distribution coefficient data available (see Irving, 1978 for review of silicate partitioning data). However, these D values are functions of pressure, temperature, and phase composition (e.g., Ford et al., 1983; Mysen et al., 1982; Harrison, 1981).

The large number of variables on which trace element partitioning depends and the difficulty in resolving the individual contributions of each variable have impeded the integration of the partitioning data. Also, the impossibility of changing only a single variable while holding others constant has made partitioning studies difficult (Hart and Davis, 1978).

This study investigates the dependence of olivine/melt and orthopyroxene/melt partitioning for the REE and other selected elements on temperature and phase composition. Based on experiments in simplified systems of basaltic composition and on data available in the literature, a predictive, semitheoretical relation among D, temperature, crystal composition, and melt composition is formulated. Compositional

dependence is determined by formulating equilibrium constants for appropriate exchange reactions. Free energies of exchange are related to the size and charge of the trace cations by a simple ionic model. This study unifies olivine/melt and orthopyroxene/melt partitioning for many elements in many compositional systems.

Experimental Procedures

Twelve 5-component (CaO, SiO_2, Al_2O_3, FeO, MgO) synthetic basalts were made from oxides and homogenized by repeated fusing and grinding. Procedures for making the synthetic compositions are discussed in Appendix A along with the report of bulk compositions for experimental samples of this study. For each composition, experimental charges of approximately 80mg were doped with 0.5% to 4% REE (Sm, Gd, or Yb), and/or <1% Sc, Ni, and Co. Experiments were conducted in 1-atmosphere gas ($CO-CO_2$; anhydrous) mixing furnaces (Williams and Mullins, 1981) on Fe-plated platinum loops (Donaldson et al, 1975). Procedures for Fe-plating loops are discussed in Appendix B. Fe-Pt loops were not annealed prior to addition of the synthetic "basalt" to the loop. However, charges were fused at 50°C above the liquidus for two hours before beginning the preprogrammed cooling history. This history consisted of an initial temperature drop to approximately 30°C below the liquidus for 15-45 minutes to initiate nucleation. This was followed by a rapid (3-7 minutes) temperature increase to 2-5°C below the liquidus and a controlled cooling at 1/3 to 1/2°C per hour to 10 to 15° below the liquidus. Experiments were held at this final temperature for 15 to 30

hours and then air quenched. Final temperatures ranged from 1180 to 1420°C. Oxygen fugacities, measured using a solid ceramic oxygen electrolyte cell (Sato, 1971), were regulated at 1/2 log unit above the iron-wustite buffer.

Compositions of coexisting phases were analyzed by electron microprobe. Trace element partitioning was determined using techniques outlined by McKay and Seymour (1982) and McKay (1986). Analytical techniques are discussed further in Appendix C. To avoid error in the analyses due to fluorescence of the surrounding glass (McKay, 1982), only grains meeting certain size criteria were analyzed for trace elements. Olivine grains greater than 75 micrometers across for Yb, Sc, and Ni and greater than 200 micrometers across for Gd, Ca, Al, and Sm were selected for analysis. Orthopyroxene grains greater than 50 micrometers across for Yb, Sc, and Ni and greater than 100 micrometers across for Gd, Ca, Al, and Sm were selected.

In most cases, crystals in the final quenched charge constituted between 10 and 15 modal percent, minimizing REE zoning due to the increase in REE concentration in the melt with degree of crystallization. With one exception (run #90), no inhomogeneities or zoning of REE in olivine outside the 95% confidence interval of the analyses were detected. Major elements in olivine were homogeneous within 3% relative. Major elements in orthopyroxene were homogeneous within 10% relative, consistent with the lower diffusion rate in orthopyroxene than olivine.

No reversal experiments were conducted to confirm that these partitioning values represent equilibrium conditions. However, experiment

duration times were equal to or slightly greater than the experiments of McKay (1986), and thermal histories are similar. In the experiments of McKay (1986), reversal experiments indicated that equilibrium was attained within 48 hours.

Results

Experimental run conditions and compositions of run products are given in table 1 (olivine) and table 2 (orthopyroxene). Standard deviations of multiple analyses were usually within expectations from counting statistics. Reported temperatures are believed to be accurate within ±3°C. Reported fO_2 values are believed to be accurate within ±0.07 ln-units, unless otherwise specified. Weight% partitioning values (D_w = weight% trace oxide in crystal/weight% trace oxide in glass) between olivine and melt (table 3) and orthopyroxene and melt (table 4) are reported.

The variance in the D_w values reported in tables 3 and 4 can be related to five parameters. These are:

1. olivine composition,
2. melt composition,
3. temperature,
4. ionic radius of the cation, and
5. charge of the cation.

Reported D_w values for elements vary by over 100% (tables 3 and 4). Most of this variation can be associated with variations in crystal composition (%Fo, %En) and temperature. Figure 1 illustrates the

Table 1. Experimental run conditions and compositions of run products for olivine experiments. Row labels indicate the number of the experiment and the temperature in Kelvins. The uncertainties (in parentheses) represent one sigma standard deviations as derived from counting statistics or from multiple analyses, whichever is larger. If no standard deviation is reported, the value was calculated from the partition coefficient and not directly analyzed.

Run #	T(K)	$\ln fO_2$		SiO_2		Al_2O_3		FeO		MgO		CaO		Yb_2O_3		Sc_2O_3	Gd_2O_3		Sm_2O_3		Other	Total
68Yb	1473	-25.99	glass	41.740	(110)	15.910	(70)	23.960	(140)	6.980	(40)	8.580	(5)	1.734	(60)							98.9%
			olivine	35.910	(100)	0.059		33.020	(190)	30.050	(90)	0.270		0.06078								99.4%
78Yb	1513	-25.24	glass	46.080	(120)	17.860	(70)	13.150	(90)	10.650	(40)	9.650	(5)	2.586	(70)							100.0%
			olivine	39.200	(110)	0.059	(66)	17.490	(110)	43.190	(110)	0.189		0.06884								100.2%
79Sm	1471	-26.31	glass	42.090	(120)	15.580	(70)	23.860	(140)	6.770	(40)	8.430	(5)						2.968	(80)		99.7%
			olivine	36.330	(100)	0.056		33.730	(190)	30.470	(90)	0.281							0.00582			100.9%
79aYb	1471	-26.31	glass	43.970	(120)	15.830	(60)	21.910	(130)	7.940	(40)	8.590	(5)	1.724	(60)							100.0%
			olivine	36.850	(100)	0.061		30.140	(170)	32.820	(90)	0.229		0.05765								100.2%
79bYb	1471	-24.17	glass	43.050	(120)	16.700	(70)	21.760	(130)	7.500	(40)	8.960	(5)	1.049	(50)							99.0%
			olivine	36.780	(100)	0.080		31.000	(180)	32.390	(90)	0.256		0.03908								100.5%
79Gd	1471	-26.31	glass	42.840	(120)	16.440	(70)	22.420	(140)	7.480	(40)	8.830	(5)				1.602					99.6%
			olivine	36.600	(100)	0.061		31.610	(180)	31.980	(90)	0.237	(10)				0.00444	(60)				100.5%
80Gd	1471	-26.28	glass	43.400	(120)	15.560	(70)	23.170	(140)	6.910	(40)	8.550	(5)				1.656					99.2%
			olivine	36.140	(100)	0.054		33.570	(190)	30.340	(90)	0.267	(10)				0.00440	(60)				100.4%
81Yb	1473	-26.34	glass	45.060	(120)	15.930	(70)	20.240	(130)	7.660	(40)	8.340	(5)	1.803	(60)							99.0%
			olivine	37.040	(100)	0.070	(10)	30.200	(170)	33.150	(90)	0.228	(10)	0.05699								100.7%
82Gd	1513	-25.06	glass	47.300	(120)	18.150	(70)	10.430	(80)	11.460	(40)	10.240	(60)				1.866					99.4%
			olivine	40.300	(110)	0.101		13.460	(90)	46.500	(110)	0.179	(10)				0.00442	(60)				100.5%
85Yb	1513	-24.94	glass	46.720	(120)	18.880	(70)	10.510	(80)	11.530	(40)	9.950	(50)	2.090	(60)							99.7%
			olivine	39.740	(110)	0.070		13.690	(90)	45.790	(110)	0.180		0.5474								99.5%
85Gd	1513	-24.94	glass	46.840	(120)	18.360	(70)	10.480	(80)	11.280	(40)	10.180	(60)				1.761					98.9%
			olivine	39.590	(110)	0.074		13.650	(90)	45.890	(110)	0.174					0.00348	(60)				99.4%
85Sm	1513	-24.94	glass	45.830	(120)	17.820	(70)	10.680	(80)	11.310	(50)	9.840	(50)						4.492	(110)		100.0%
			olivine	40.150	(110)	0.073		13.750	(90)	46.510	(110)	0.193							0.00508			100.7%
89Yb	1514	-25.32	glass	48.690	(130)	18.100	(70)	9.990	(80)	11.370	(40)	10.020	(50)	1.127	(50)							99.3%
			olivine	40.180	(110)	0.067		13.020	(100)	46.450	(110)	0.184		0.02634								99.9%
90Yb	1559	-24.23	glass	49.336	(211)	20.490	(89)	0.064	(11)	15.010	(66)	11.833	(52)	2.244	(88)							99.0%
			olivine	42.655	(182)	0.113		D_w=1.216	(5)	55.845	(238)	0.167		0.06754								98.8%
92Yb	1539	-24.40	glass	48.420	(130)	19.720	(70)	4.860	(50)	13.340	(50)	10.560	(60)	3.201	(80)							100.1%
			olivine	41.340	(110)	0.107		6.450	(60)	51.530	(120)	0.227		0.07295								99.7%
94Yb	1561	-24.17	glass	39.530	(110)	10.840	(50)	32.090	(180)	8.810	(40)	5.590	(40)	3.203	(80)							100.1%
			olivine	36.020	(100)	0.049		33.850	(190)	29.710	(90)	0.200	(10)	0.10435								99.9%
94Gd	1561	-24.17	glass	38.000	(110)	10.440	(50)	33.870	(190)	8.140	(40)	5.630	(40)				2.698					98.8%
			olivine	35.840	(100)	0.068		35.490	(200)	28.920	(80)	0.336					0.00900	(80)				100.7%
99Sm	1512	-25.02	glass	43.700	(120)	17.790	(70)	13.730	(100)	10.280	(40)	9.730	(50)						4.342	(110)		99.6%
		(100)	olivine	39.430	(110)	0.096		17.710	(110)	43.180	(110)	0.206							0.00656			100.6%
101aYb	1550	-24.13	glass	44.620	(120)	11.380	(50)	22.740	(140)	10.960	(40)	5.790	(40)	3.900	(90)							99.4%
			olivine	37.670	(110)	0.046		25.890	(150)	36.400	(100)	0.141		0.09707								100.2%
101bYb	1550	-24.13	glass	40.610	(110)	10.030	(50)	28.690	(170)	10.120	(40)	5.260	(40)	0.790	(50)						3.37	98.9%
			olivine	37.170	(100)	0.023		28.490	(170)	34.080	(90)	0.140		0.01730							Ti02	99.9%
103	1457	-27.23	glass	49.062	(210)	14.914	(66)	19.776	(132)	6.762	(31)	8.107	(38)	0.215	(66)		0.536	(51)	0.409	(70)		99.8%
			olivine	43.226	(185)	7.808	(35)	25.586	(162)	18.221	(80)	4.427	(26)	0.01204								99.3%
104	1532	-25.68	glass	51.500	(220)	16.434	(73)	9.247	(76)	11.596	(52)	8.847	(41)	0.642	(59)		0.909	(56)	0.465	(65)		99.7%
			olivine	40.063	(172)	0.0711	(6)	12.800	(94)	46.098	(197)	0.181	(7)	0.02269								99.2%
105	1581	-24.01	glass	52.657	(225)	7.865	(35)	22.443	(146)	11.670	(52)	3.959	(24)	0.922	(65)		0.796	(56)	0.674	(74)		101.0%
			olivine	38.094	(163)	0.020		27.951	(174)	35.181	(151)	0.086		0.01713			0.00158		0.00060			101.4%
106a	1560	-25.52	glass	51.550	(221)	12.066	(54)	16.395	(114)	11.895	(53)	6.528	(33)				0.647	(52)	0.980	(73)		100.1%
			olivine	39.075	(167)	0.107		21.806	(142)	39.710	(171)	0.129		0.00000			0.00249		0.00313			100.8%

Table 1. (continued)

Run #	T(K)	$\ln fO_2$		SiO_2		Al_2O_3		FeO		MgO		CaO		Yb_2O_3		Sc_2O_3		Gd_2O_3		Sm_2O_3		Other	Total
106b	1560	-25.52	glass	51.318	(220)	12.308	(55)	15.590	(110)	11.755	(52)	6.579	(33)	0.918	(63)			0.632	(51)	0.756	(77)		99.9%
			olivine	38.780	(166)	0.025	(5)	20.913	(137)	40.847	(175)	0.115	(6)	0.02077									100.7%
107b	1482	-26.65	glass	50.723	(217)	16.615	(73)	11.333	(87)	9.638	(43)	9.137	(42)	1.690	(80)			0.653	(52)	0.551	(72)		100.3%
			olivine	39.789	(170)	0.144	(6)	17.248	(118)	43.288	(185)	0.207	(7)	0.06454									100.7%
108a	1503	-26.27	glass	48.328	(207)	11.921	(53)	21.651	(141)	8.990	(41)	6.443	(33)					1.068	(82)	0.579	(107)		99.0%
			olivine	37.095	(159)	0.015	(5)	31.142	(191)	32.968	(141)	0.138	(6)					0.00384		0.00207			101.4%
108b	1503	-26.27	glass	48.535	(207)	11.877	(53)	21.903	(142)	8.821	(39)	6.391	(32)	0.890	(96)			0.890	(82)	0.393	(99)		99.7%
			olivine	37.359	(160)	0.069	(6)	32.303	(196)	31.873	(137)	0.136	(7)	0.02462				0.00289					101.8%
109	1442	-27.12	glass	48.184	(206)	14.885	(66)	18.961	(127)	6.773	(31)	8.086	(38)	0.502	(77)			1.148	(88)	0.863	(144)		99.4%
			olivine	37.474	(161)	0.054	(6)	30.538	(187)	33.358	(143)	0.178	(7)	0.01643				0.00518		0.00318			101.6%
110a	1538	-25.70	glass	52.759	(225)	16.742	(73)	6.254	(59)	12.532	(55)	9.050	(41)	0.456	(78)			0.247	(55)	0.520	(89)		98.6%
			olivine	41.170	(176)	0.040	(5)	8.172	(70)	49.991	(213)	0.116	(6)	0.00885				0.00102					99.5%
112a	1475	-26.47	glass	44.943	(135)	14.706	(68)	22.757	(114)	6.944	(42)	9.028	(54)			0.970	(18)						99.3%
			olivine	36.407	(109)	0.068		34.140	(171)	30.111	(151)	0.307	(10)			0.236							101.3%
112b	1475	-24.46	glass	44.462	(133)	16.070	(64)	21.911	(110)	7.629	(46)	8.808	(63)			0.859	(17)						99.7%
			olivine	36.384	(109)	0.067		32.009	(160)	31.770	(159)	0.234	(9)			0.209							100.7%
113a	1610	-24.60	glass	54.896	(234)	14.190	(63)	7.036	(63)	14.106	(62)	7.937	(38)	0.410	(78)					0.578	(100)		99.2%
			olivine	41.378	(177)	0.030	(5)	7.623	(67)	50.706	(216)	0.108	(6)	0.00799						0.00136			99.9%
113b	1610	-24.60	glass	54.745	(164)	13.612	(54)	7.968	(48)	15.346	(77)	7.193	(43)					0.395	(15)				99.3%
			olivine	40.312	(121)	0.040	(7)	8.521	(51)	49.984	(200)	0.100	(7)					0.00180					99.0%
114a	1520	-25.99	glass	48.090	(126)	18.190	(72)	9.495	(54)	11.305	(60)	0.179	(56)	0.828	(20)	1.161	(22)						100.1%
			olivine	39.805	(109)	0.065		12.802	(68)	47.202	(205)	0.176		0.01533		0.207							100.3%
114b	1520	-25.99	glass	49.395	(127)	18.247	(72)	8.853	(62)	11.214	(59)	0.312	(57)	0.781	(20)	1.134	(21)						99.9%
			olivine	39.869	(109)	0.066		12.065	(65)	47.626	(206)	0.176		0.01705		0.206							100.0%
115a	1637	-24.26	glass	52.053	(133)	7.653	(40)	17.940	(89)	17.005	(85)	3.937	(29)			0.269	(9)	0.250	(13)	1.067	(25)		100.2%
			olivine	39.631	(109)	0.018		16.722	(84)	44.672	(195)	0.077				0.035		0.00103		0.00281			101.2%
115b	1637	-24.26	glass	51.736	(132)	8.208	(41)	17.043	(85)	16.754	(84)	4.070	(30)			0.257	(9)	0.336	(13)	1.430	(28)		98.8%
			olivine	39.228	(108)	0.017		15.948	(81)	43.835	(192)	0.076				0.033		0.00066		0.00074			99.1%
117a	1554	-25.39	glass	49.744	(128)	13.034	(56)	16.342	(82)	12.058	(64)	6.553	(41)	0.414	(16)	1.183	(22)	0.264	(12)	0.541	(19)		100.1%
			olivine	38.646	(107)	0.033		17.928	(89)	41.129	(181)	0.128		0.00998		0.203		0.00100		0.00247			98.1%
117b	1554	-25.39	glass	50.075	(128)	11.978	(53)	16.175	(82)	12.087	(64)	6.579	(41)	0.437	(17)	1.236	(22)	0.281	(13)	0.632	(20)		99.5%
			olivine	39.134	(108)	0.046		19.365	(95)	42.769	(188)	0.139		0.00925		0.226		0.00139		0.00255			101.7%
118a	1687	-23.63	glass	54.563	(138)	7.230	(38)	9.470	(54)	21.337	(101)	3.679	(28)	0.345	(16)	0.562	(12)	0.354	(13)	1.182	(25)		98.7%
		(100)	olivine	40.238	(110)	0.015		8.375	(50)	50.210	(216)	0.062		0.00717		0.069		0.00125		0.00276			99.0%
118b	1687	-23.63	glass	54.235	(137)	7.131	(38)	11.331	(62)	19.595	(94)	4.470	(32)	0.308	(15)	0.565	(12)	0.341	(14)	1.110	(26)		99.1%
		(100)	olivine	40.614	(111)	0.016		8.981	(52)	50.092	(216)	0.074		0.00491		0.069		0.00068		0.00220			99.9%
119a	1529	-25.83	glass	60.375	(130)	16.113	(66)	9.144	(53)	11.710	(62)	8.736	(50)	0.535	(18)	0.899	(18)	0.768	(18)	1.241	(26)		99.5%
			olivine	39.996	(110)	0.041		12.063	(65)	47.574	(206)	0.166		0.01564		0.158							100.0%
119b	1529	-25.83	glass	52.691	(134)	16.899	(68)	6.481	(42)	11.041	(59)	8.916	(51)	0.592	(18)	0.926	(18)	0.811	(18)	1.295	(27)		99.7%
			olivine	40.238	(110)	0.069		9.880	(56)	48.906	(211)	0.166		0.01240		0.195							99.5%
120a	1475	-26.62	glass	49.617	(128)	16.351	(66)	13.874	(72)	8.611	(50)	8.795	(51)			1.485	(27)	1.316	(25)				100.0%
			olivine	39.281	(108)	0.563	(13)	20.972	(101)	38.247	(170)	0.274	(9)			0.449							99.8%

				SiO_2		Al_2O_3		FeO		MgO		CaO		Y_2O_3		EuO		CoO		NiO		ZrO_2	
111a	1516	-25.77	glass	48.290	(145)	17.837	(71)	10.669	(64)	10.778	(54)	10.395	(63)	0.768	(17)	0.615	(18)	0.268	(8)	0.111	(19)	Ag not	99.7%
			olivine	37.962	(114)	0.061	(8)	14.326	(71)	41.304	(165)	0.215	(8)	0.00557		0.002		0.98800	(68)	0.83100	(257)	analyzed	95.7%
111b	1516	-25.77	glass	48.903	(147)	16.941	(68)	9.504	(57)	9.504	(57)	10.540	(63)	Zn not analyzed								3.147	98.5%
			olivine	38.777	(116)	0.134	(9)	12.760	(64)	44.709	(179)	0.240										(88)	96.6%

Table 2. Experimental run conditions and compositions of run products for orthopyroxene experiments. Row labels indicate the number of the experiment and the temperature in Kelvins. The uncertainties (in parentheses) represent one sigma standard deviations as derived from counting statistics or from multiple analyses, whichever is larger. If no standard deviation is reported, the value was calculated from the partition coefficient and not directly analyzed.

Run #	T(K)	$\ln fO_2$		SiO_2		Al_2O_3		FeO		MgO		CaO		Yb_2O_3		Sc_2O_3		Gd_2O_3		Sm_2O_3		Total
103	1457	-27.23	glass	49.062	(185)	14.914	(66)	19.776	(132)	6.762	(31)	8.107	(38)	0.215	(51)			0.536	(51)	0.409	(70)	99.8%
			pyroxene	53.538	(229)	2.175	(15)	18.278	(124)	25.070	(108)	0.898	(12)	0.02748								100.0%
105	1581	-25.01	glass	49.748	(212)	7.265	(33)	24.752	(158)	11.432	(51)	3.780	(24)	0.877	(63)			0.854	(67)	0.655	(69)	99.4%
			pyroxene	54.717	(234)	0.344		17.445	(119)	26.609	(115)	0.334		0.04968								99.5%
106b	1560	-25.52	glass	51.318	(220)	12.308	(55)	15.590	(110)	11.755	(52)	6.579	(33)	0.918	(63)			0.632	(51)	0.756	(77)	99.9%
			pyroxene	55.297	(236)	1.009	(11)	12.645	(94)	29.958	(128)	0.521	(9)	0.07518								99.5%
107b	1482	-26.65	glass	51.198	(218)	16.699	(73)	10.298	(81)	9.495	(43)	9.195	(42)	1.559	(78)			0.631	(53)	0.570	(74)	99.6%
			pyroxene	55.294	(236)	3.589	(20)	9.762	(78)	30.519	(131)	0.966	(12)	0.33146								100.5%
108b	1503	-26.27	glass	48.421	(207)	11.910	(53)	22.010	(143)	8.808	(40)	6.347	(32)	0.845	(97)			0.815	(77)	0.567	(91)	99.7%
			pyroxene	53.223	(227)	1.042	(11)	19.474	(130)	25.003	(108)	0.702	(10)	0.06457								99.5%
109	1442	-27.12	glass	48.292	(207)	15.027	(66)	18.890	(127)	6.914	(31)	8.006	(38)	0.330	(54)			0.935	(58)	0.920	(84)	99.3%
			pyroxene	53.000	(227)	1.693	(13)	19.280	(129)	24.598	(106)	1.085	(13)	0.05092								99.7%
113a	1610	-24.60	glass	54.413	(232)	13.320	(59)	7.123	(64)	16.332	(71)	7.347	(36)	0.405	(76)					0.422	(91)	99.4%
			pyroxene	58.040	(248)	0.714	(9)	4.578	(49)	35.669	(152)	0.228	(7)	0.01514								99.2%
115a	1637	-24.26	glass	52.053	(133)	7.653	(40)	17.940	(89)	17.005	(85)	3.937	(29)			0.269	(9)	0.250	(13)	1.067	(25)	100.2%
			pyroxene	57.032	(143)	0.242		10.335	(58)	32.871	(147)	0.232				0.064						100.8%
115b	1637	-24.26	glass	51.736	(132)	8.208	(41)	17.043	(85)	16.752	(84)	4.070	(30)			0.257	(9)	0.336	(13)	1.430	(28)	99.8%
			pyroxene	56.661	(142)	0.371		10.125	(57)	32.492	(145)	0.256				0.095						100.0%
117a	1554	-25.39	glass	49.727	(128)	14.184	(60)	15.881	(81)	12.167	(65)	6.451	(40)	0.396		1.169	(22)	0.286	(12)	0.538	(19)	100.8%
			pyroxene	55.513	(140)	1.097		12.351	(66)	30.472	(138)	0.522		0.02933		0.765						100.7%
117b	1554	-25.39	glass	50.606	(130)	12.787	(55)	15.277	(78)	12.566	(66)	6.340	(40)	0.448	(17)	1.139	(22)	0.300	(13)	0.635	(20)	100.1%
			pyroxene	55.426	(139)	1.090		12.189	(65)	30.489	(138)	0.511		0.03247		0.741						100.5%
118a	1687	-23.63	glass	54.563	(138)	7.230	(38)	9.470	(54)	21.337	(101)	3.679	(28)	0.345	(16)	0.562	(12)	0.354	(13)	1.182	(25)	98.7%
		(100)	pyroxene	57.880	(144)	0.173		5.056	(36)	37.458	(164)	0.108		0.01041		0.120		0.00205		0.00531		100.8%
118b	1687	-23.63	glass	54.235	(137)	7.131	(38)	11.331	(62)	19.595	(94)	4.470	(32)	0.308	(15)	0.565	(12)	0.341	(14)	1.110	(26)	99.1%
		(100)	pyroxene	57.486	(144)	0.173		5.164	(36)	35.943	(158)	0.138		0.00621		0.122		0.00144		0.00257		99.1%
119a	1529	-25.83	glass	51.283	(131)	16.402	(66)	5.936	(40)	12.497	(65)	8.911	(51)	0.536	(18)	0.944	(18)	0.797	(18)	1.247	(27)	98.6%
			pyroxene	57.151	(143)	1.525	(17)	2.915	(26)	36.452	(160)	0.212		0.01411		0.725	(14)	0.00453		0.00479		99.0%
119b	1529	-25.83	glass	51.790	(132)	17.629	(70)	3.504	(29)	12.636	(65)	9.485	(53)	0.610	(18)	0.867	(17)	0.809	(18)	1.270	(27)	98.6%
			pyroxene	56.078	(141)	2.303	(20)	3.008	(26)	35.400	(156)	0.323		0.04002		0.905	(17)	0.00811		0.00771		98.1%
120a	1475	-26.62	glass	49.617	(128)	16.351	(66)	13.874	(72)	8.611	(50)	8.795	(51)			1.485	(27)	1.316	(25)			100.0%
			pyroxene	51.396	(132)	5.398	(32)	13.333	(70)	26.733	(123)	1.116				2.464	(41)	0.06278				100.5%

Table 3. Weight percent partitioning values (D_w) between olivine and coexisting melt. Experiment number and temperature in Kelvins are reported in the left column. Numbers in parentheses represent one sigma standard deviation.

Run #	T(K)	D_w(Yb)		D_w(Mn)		D_w(Sc)		D_w(Ca)		D_w(Gd)		D_w(Sm)		D_w(Al)		D_w(Ni)	D_w(Ti)	D_w(Fe)
68Yb	1473	0.03505	(40)	1.127	(54)			0.031470	(68)					0.003716	(27)			
78Yb	1513	0.02662	(20	1.044	(80)													
79Sm	1471			1.048	(54)			0.033290	(70)			0.00196	(9)	0.003616	(30)			
79aYb	1471	0.03344	(39)	1.142	(56)			0.026690	(62)					0.003872	(27)			
79bYb	1471	0.03725	(41)					0.028530	(63)					0.004778	(28)			
79Gd	1471			1.270	(66)					0.00277	(22)			0.003701	(30)			
80Gd	1471			1.024	(57)					0.00266	(20)			0.003452	(30)			
81Yb	1473	0.03161	(40)	1.083	(54)													
82Gd	1513			0.846	(24)					0.00237	(16)			0.005546	(44)			
85Yb	1513	0.02619	(19)					0.018080	(46)					0.003711	(21)			
85Gd	1513			0.990	(70)			0.017130	(45)	0.00198	(40)			0.004055	(22)			
85Sm	1513			0.789	(20)			0.019630	(35)			0.00113	(9)	0.004106	(24)			
89Yb	1514	0.02337	(31)	0.906	(59)			0.018410	(50)					0.003702	(122)			
90Yb	1559	0.03010	(300)					0.014120	(37)					0.005536	(83)			1.216
92Yb	1539	0.02279	(54)	0.774	(69)			0.021460	(42)					0.005423	(708)			
94Yb	1561	0.03258	(33)	0.942	(32)									0.004527	(36)			
94Gd	1561			1.005	(40)			0.059714	(127)	0.00334	(25)			0.006504	(71)			
99Sm	1512			1.054	(100)			0.021175	(56)			0.00151	(8)	0.005396	(35)			
101aYb	1550	0.02489	(45)	0.875	(24)			0.024282	(138)					0.004035	(37)			
101bYb	1550	0.02190	(59)	0.961	(62)			0.026590	(85)					0.002327	(60)		0.011	
103	1457			1.237	(5)													
104	1532	0.03534	(85)	0.794	(67)													
105	1581	0.01858	(237)	0.798	(31)			0.021774	(191)	0.00198	(41)	0.00089	(70)	0.002529	(61)			
106a	1560			0.894	(87)			0.019696	(63)	0.00385	(47)	0.00320	(35)	0.008843	(52)			
106b	1560	0.02263	(149)	0.889	(500)													
107a	1482			1.208	(12)													
107b	1482	0.03819	(90)	1.201	(11)													
108a	1503			1.052	(38)					0.00360	(39)	0.00357	(35)					
108b	1503	0.02766	(65)	1.057	(41)					0.00325	(33)							
109	1442	0.03273	(304)	1.125	(49)					0.00451	(41)	0.00368	(63)					
110a	1538	0.01940	(170)	0.705	(61)					0.00414	(80)							
110b	1538			0.992	(103)													
112a	1475			1.257	(53)	0.24318	(96)							0.004618	(33)			
112b	1475			1.099	(50)	0.24370	(157)							0.004167	(24)			
113a	1610	0.01949	(183)	0.786	(62)							0.00235	(49)					
113b	1610			0.756	(64)					0.00456	(212)							
114a	1520	0.01852	(71)	0.989	(70)	0.17800	(69)	0.017304	(86)					0.003565	(23)			
114b	1520	0.02183	(71)	0.928	(62)	0.18170	(69)	0.017037	(105)					0.003590	(23)			
115a	1637			0.749	(42)	0.13110	(166)	0.019680	(80)	0.00413	(40)	0.00264	(33)	0.002327	(52)			
115b	1637			0.700	(40)	0.12990	(171)	0.018580	(80)	0.00197	(34)	0.00052	(28)	0.002038	(49)			
117a	1554	0.02410	(129)	0.862	(61)	0.17172	(61)	0.019470	(65)	0.00375	(35)	0.00456	(64)	0.002566	(37)			
117b	1554	0.02116	(189)	0.986	(68)	0.18250	(62)	0.019700	(65)	0.00496	(35)	0.00404	(62)	0.003822	(41)			
118a	1687	0.02077	(169)	0.773	(45)	0.12280	(83)	0.016820	(71)	0.00355	(31)	0.00233	(31)	0.002099	(49)			
118b	1687	0.01595	(167)	0.786	(99)	0.12220	(84)	0.016540	(76)	0.00200	(31)	0.00199	(36)	0.002273	(55)			
119a	1529	0.02923	(94)	0.961	(104)	0.17540	(64)	0.019020	(42)					0.002559	(23)			
119b	1529	0.02094	(90)	1.073	(116)	0.21110	(70)	0.018620	(40)					0.004074	(24)			
120a	1475			1.274	(110)	0.30217	(87)									24		
		D_w(Y)		D_w(Mn)		D_w(Eu)		D_w(Ca)		D_w(Co)		D_w(Ni)		D_w(Al)		D_w(Zr)		
111a	1516	0.00725	(97)			0.00321	(990)					7.82						
111b	1516			0.9525	(726)			0.022780	(4)							0.001		

Table 4. Weight percent partitioning values (D_w) between orthopyroxene and coexisting melt. Experiment number and temperature in Kelvins are reported in the left column. Numbers in parentheses represent one sigma standard deviation.

Run #	T(K)	D_w(Yb)		D_w(Mn)		D_w(Sc)		D_w(Ca)		D_w(Gd)		D_w(Sm)		D_w(Al)		D_w(Ni)
103	1457	0.12780	(294)													
105	1581	0.05665	(175)					0.088318	(348)							
106b	1560	0.08190	(204)											0.047311	(98)	
107b	1482	0.21261	(244)													
108b	1503	0.07641	(78)													
109	1442	0.15430	(425)													
113a	1610	0.03729	(209)													
115a	1637					0.23950	(223)	0.058900	(125)					0.031580	(94)	
115b	1637					0.36940	(230)	0.062830	(125)					0.045180	(98)	
117a	1554	0.07407	(274)			0.65480	(160)	0.080880	(141)					0.077340	(119)	
117b	1554	0.07248	(259)			0.65070	(155)	0.080640	(150)					0.085250	(168)	
118a	1687	0.03016	(310)	0.4990	(495)	0.21330	(118)	0.029460	(99)	0.00581	(40)	0.00450	(37)	0.023980	(89)	
118b	1687	0.01016	(350)	0.4086	(455)	0.21530	(119)	0.030840	(109)	0.00421	(42)	0.00231	(38)	0.027130	(97)	
119a	1529	0.02632	(140)			0.42290	(230)	0.023740	(56)	0.00569	(21)	0.00384	(35)	0.026240	(49)	
119b	1529	0.06560	(136)			0.88740	(207)	0.034010	(60)	0.01002	(20)	0.00607	(35)	0.087860	(81)	
120a	1475			1.0836	(550)	1.50105	(199)	0.126839	(110)	0.04771	(26)			0.234300	(174)	7.355

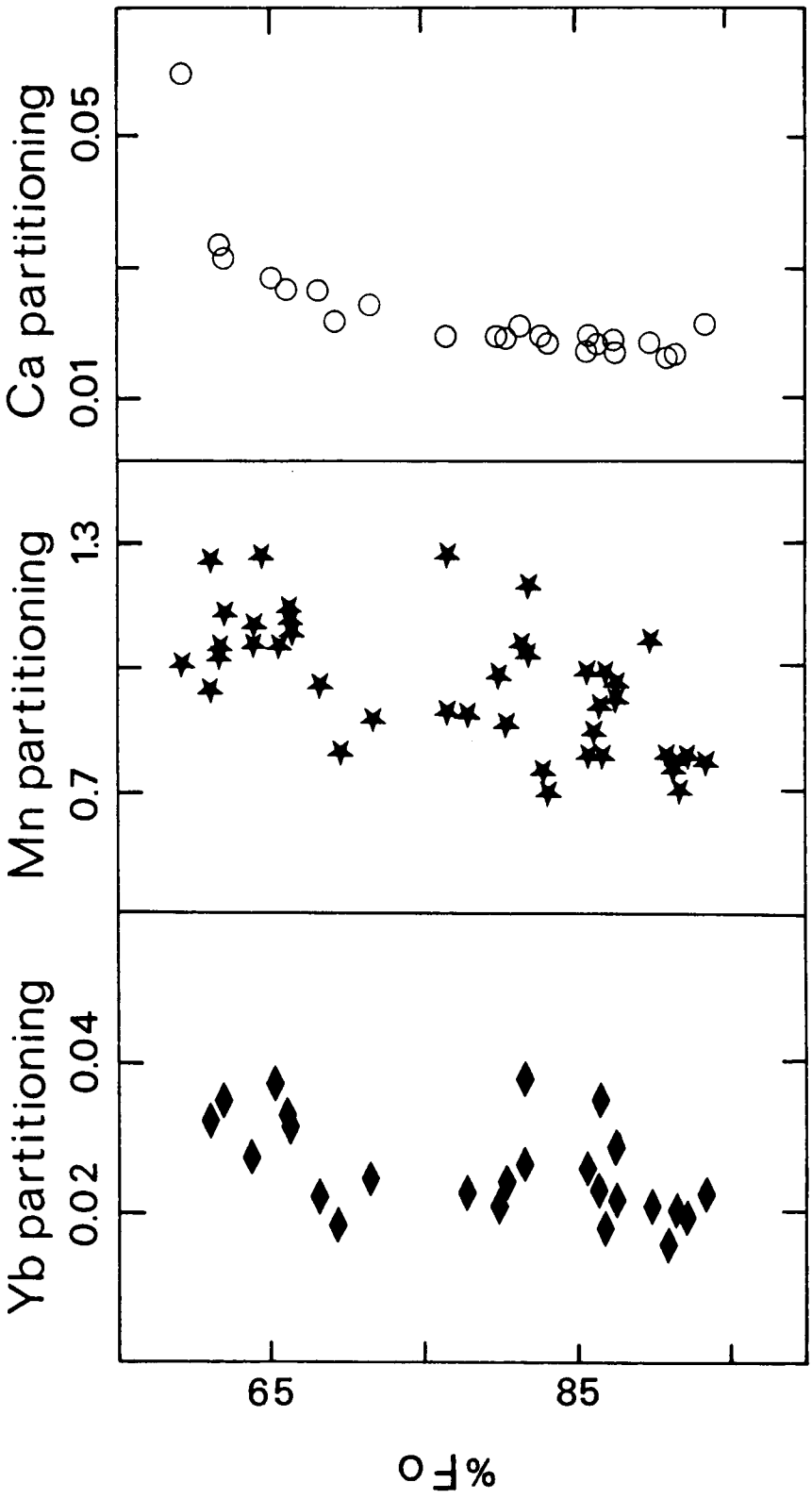

Figure 1. Dependence of weight-percent D values of Yb, Ca, and Mn on olivine composition without consideration of the effects of temperature or melt composition. Weak negative trends are seen.

dependence of Yb, Ca, and Mn partitioning between olivine and melt on olivine composition. It is clear that D_w values decrease with an increase in %Fo (or %En), as Harrison (1981) expected. With the exception of Ca, there is a large amount of scatter in these data. This is related to variations in temperature or melt composition.

Similar dependence on temperature could be shown. However, a large part of the temperature-dependent variation is a reflection of covariation of temperature with Fe content of the system.

D_w is strongly dependent on the size of the cation as expected by Nagasawa (1981) (figure 2). Based on Philpotts' (1978) discussion of "Onuma" diagrams, we expect to find some "optimum radius" where partitioning reaches a maximum. From figure 2 this optimum radius is constrained to lie between the radii of Sc and Al. Figure 2 also illustrates the offset introduced by a difference in the valence of the trace cations. Between divalent and trivalent cations, this difference is about 1 log unit.

Interpretation of Results

The goal of this study is to determine the dependence of partitioning on the five parameters listed above. This is best accomplished by constraining the data into the form of thermodynamic relations already established. This will give good insight into the energy states of trace elements in crystals and melt. More importantly, it will allow prediction of partitioning values for temperatures, compositions, and elements not included in this study.

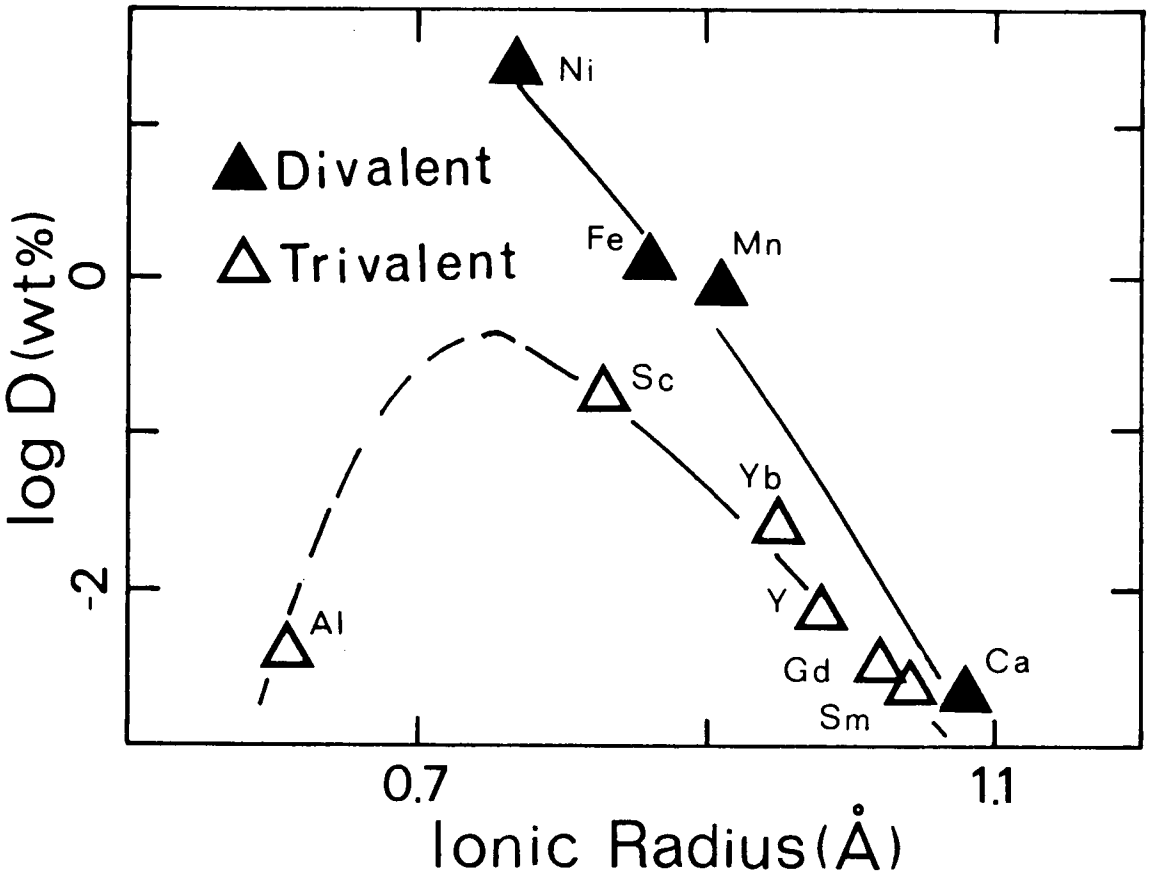

Figure 2. "Onuma" diagram for the divalent and trivalent olivine/melt partitioning data of this study (averages are plotted). The "optimum radii" is constrained to lie between the radii of Al and Sc. Ionic radii are from Whittaker and Muntus (1970). Error estimates are the size of the symbols of smaller. Values are averages of the data reported in Table 2.

The steps taken to achieve these results were:

1. A substitution equation was chosen to express the reaction:

Trace element in melt = Trace element in crystal.

This required a determination of any charge-balancing, coupled substitutions associated with the reaction. Once this reaction was determined, an equilibrium constant was derived to express the compositional dependence of partitioning.

2. The relation of activity to composition for components in the crystal and melt was modeled. A model for melt activities from Bottinga and Weill (1972) was assumed. A nonideal mixing of Mg and Fe around the trace cation in olivine and orthopyroxene was determined using a nonlinear regression of the data.

3. In addition to the energy arising from any coupled substitutions, enthalpies of exchange were related to the size and charge of the cations exchanging on octahedral sites (trace cation, Mg, and Fe). Standard equations for ionically bonded crystals were used to model the lattice energies. Standard state chemical potentials in the melt were modeled in the same manner.

4. The derived model was applied to the experimental data from this study, as well as to published data. Linear regression of the data to this model was used to determine: (a) unknown coefficients in the ionic model; (b) enthalpies associated with coupled substitutions; and (c) the dependence of the entropy of substitution on cation size.

Equilibrium Constants

The exchanges considered between olivine or orthopyroxene and melt are:

$$\text{trivalent trace cation} = Fe^{2+},$$
$$\text{trivalent trace cation} = Mg^{2+},$$
$$\text{divalent trace cation} = Fe^{2+}, \text{ and}$$
$$\text{divalent trace cation} = Mg^{2+}.$$

The notation and equations for the trace-Fe^{+2} exchange are exactly analogous to the trace-Mg^{+2} exchange. Also, with the exception that a different substitution mechanism is chosen, the orthopyroxene equations are analogous to the olivine exchange equations. Therefore, only the equations for the trace-Mg^{+2} exchange between olivine and melt will be derived here. The notation used in these derivations is:

G_i, H_i, S_i = Free energy, enthalpy, or entropy arising from the reaction expressed in Equation i.

XN = mole fraction component N,

M, M^{+2}, or M^{+3} = symbol for the trace cation.

X_{Mgol} = XMg/(XMg + XFe + X(trace element)) ≈ XMg/(XMg + XFe), where trace elements are in low concentration.

X_{MgM} = $XMgMSiO_4/(XMgMSiO_4 + XFeMSiO_4)$ if M is divalent, or

$XMg_{0.8}M_{0.8}\square_{0.4}SiO_4/(XMg_{0.8}M_{0.8}\square_{0.4}SiO_4 + XFe_{0.8}M_{0.8}\square_{0.4}SiO_4)$ if M is trivalent. In both cases, X_{MgM} = the atomic fraction Mg on those octahedral sites associated with the trace cation.

γ_{Mg} = the activity coefficient which arises when Mg and Fe in the olivine are assumed to mix randomly between the $MgMSiO_4$ and $FeMSiO_4$ components (or the $Mg_{0.8}M_{0.8}\square_{0.4}SiO_4$ and $Fe_{0.8}M_{0.8}\square_{0.4}SiO_4$ components for the case of a trivalent trace cation).

K_{Mg} and lnKMg = Equilibrium constant and natural log of the equilibrium constant for the exchange of a divalent or trivalent trace cation with Mg between olivine and melt.

X_{Mol} = X(cation M) in olivine/(XMg + XFe + XM)in olivine.

X_{Nmelt} = X(cation N) in melt/ΣX(cations in melt).

The equilibrium constants for the divalent cation substitutions are straightforward and derived from the exchange equations:

$$Fo + M^{+2} = MgM^{+2}SiO_4 + Mg \quad . \qquad (1)$$

However, for the trivalent cations which are replacing divalent Mg and Fe in the crystal lattice, there must be a charge-balancing substitution coupled to this reaction. Several substitutions are possible. Charge balance could be achieved by: (1) a coupled substitution of Na for Mg and Fe in the octahedral sites, (2) a coupled substitution of Al for Si in the tetrahedral site, (3) a vacancy substitution of [2 M^{+3} + vacancy] substituting for 3 (Mg^{+2} + Fe^{+2}).

In this study, the reactions are written assuming that each M^{+3} exists in olivine coupled with 1/2 vacancy, an assumption supported by analysis of the Sc-containing data of this study; there is insufficient Al in the olivines to accomplish the Sc charge balance. The following exchange reactions were chosen for the trivalent cations:

$$5/4(Fo) + M^{+3} = 5/4(Mg_{0.8}M^{+3}{}_{0.8}\square_{0.4}SiO_4) + 1.5Mg \quad . \qquad (2)$$

It is apparent that this exchange is a nonunique expression of the more general exchange in olivine: $2nM^{+3} + n\square = 3nM^{+2}$. This form of these exchange reactions was selected to minimize the presence of non-unity exponents in the equilibrium constant. The equilibrium constant for the reaction expressed in Equation (2) is:

$$K_{Mg} = (a(Mg_{0.8}M^{+3}{}_{0.8}\square_{0.4}SiO_4))^{5/4} \cdot (a(Mg_{melt}))^{1.5} \; / \; (a(Mg_{ol}))^{2.5} \cdot (a(M{+}3_{melt})) \quad . \qquad (3)$$

Selection of standard state components and formulations of composition-activity relations are necessary before this equation can be utilized. The model chosen for melt component activities was a simplified 2-lattice mixing model after Bottinga and Weill (1972). Activities were estimated assuming that all Si and Al act as network formers while all other elements act as network modifiers. Melt activities are defined as

$$a_{\text{network modifiers}} = X_{\text{modifiers}}/\Sigma\, X_{\text{modifiers}} \text{ and}$$
$$a_{\text{network formers}} = X_{\text{formers}}/\Sigma\, X_{\text{formers}}.$$

Activities in olivine and orthopyroxene were modeled based on the study of Kerrick and Darken (1975). They derived an ideal solution model for multi-site crystalline silicates based on statistical thermodynamic modeling. By their model, a component of the form $A_u^{\alpha}C_v^{\beta}Z_w$ in the solid solution $(A,B)_u^{\alpha}(C,D)_v^{\beta}Z_w$ has the activity:

$$a(A_uC_vZ_w) = (X_A^{\alpha})^u(X_C^{\beta})^v \quad ;$$

where X_A^{α} and X_C^{β} equal the molar concentration of A on site α and C on site β respectively. The activity of Mg_2SiO_4, which has two octahedral sites, is expressed as $(X_{Mgol})^2$.

By analogy, and considering charge-balance restrictions, the activity of the component $Mg_{0.8}M^{+3}{}_{0.8}\square_{0.4}SiO_4$ in the solution $(Mg,Fe)_{0.8}(M^{+3},Mg,Fe)_{0.8}(\square,Mg,Fe)_{0.4}SiO_4$ is:

$$a(Mg_{0.8}M^{+3}{}_{0.8}\ {}_{0.4}SiO_4) = (X_{MgM+3})^{0.8}(2 \cdot X_{M+3ol})^{0.8} \quad .$$

The factor of 2 in the X_{M+3ol} term assumes all M^{+3} is on one site (either M1 or M2) by analogy to ordering in the ferrifayalite structure (Zhizhong, 1980). The quantity X_{MgM+3} cannot be directly measured. The concentration measured by microprobe analysis is X_{Mgol}. Therefore, (X_{MgM+3}) is expressed as $(\gamma_{Mg}X_{Mgol})$.

The activity coefficient (γ_{Mg}) is a relation between the proportion of Mg on normal octahedral sites to the proportion of Mg on sites near a large trace cation. Therefore, this apparent nonideality can be interpreted to reflect an energetic preference for Fe or Mg on sites associated with the large trace cations. For divalent cations, this energetic preference is mathematically expressed by the exchange reaction:

$$1/2Fo + FeM^{+2}SiO_4 = 1/2Fa + MgM^{+2}SiO_4 \quad . \qquad (4)$$

The ΔG for this reaction expresses the difference in the exchange energy of Fe and Mg when the Fe and Mg are associated with the M^{+2} cation, as opposed to the Fe-Mg exchange between pure Fo and Fa.

The equilibrium constant can be expressed:

$$-\Delta G_4/RT = \ln[Fa^{1/2}\cdot(MgM^{+2}SiO_4)/(Fo^{1/2}\cdot(FeM^{+2}SiO_4))]$$
$$= \ln[(X_{Feol}\cdot X_{MgM+2})/(X_{Mgol}\cdot(1-X_{MgM+2}))] \quad (5)$$

where ΔG_4 = the free energy of exchange for the reaction in Equation (4). Substituting $X_{MgM+2} + X_{FeM+2} = 1$ and $\gamma_{Mg} X_{Mgol} = X_{MgM+2}$ yields:

$$\gamma_{Mg} = (Q/X_{Mgol})/(1+Q) \quad . \quad (6)$$

where

$$Q = X_{Mgol}/X_{Feol}\ EXP(-\Delta G_4/RT).$$

An analogous expression can be derived for the behavior of Fe and Mg around trivalent trace cations. This formulation presents an expression for the temperature and composition dependence of the activity coefficient. It also offers an interpretation of this nonideality.

From the discussions above, the equilibrium constants for the reactions expressed by Equations (1) and (2) are:

$$K_{Mg\text{-}trivalent} = (\gamma_{Mg})(X_{M+3ol})(a_{Mg})_{melt}^{1.5} \ /$$
$$(X_{Mgol})^{1.5}(a_{M+3})_{melt} \quad (7)$$

and

$$K_{Mg\text{-}divalent} = (\gamma_{Mg})(X_{M+2ol})(a_{Mg})_{melt} \ /$$
$$(X_{Mgol})(a_{M+2})_{melt} \quad . \quad (8)$$

Free Energy Terms

Mole percent partitioning values (D_m) are defined as $(X_{Mol})/(a_M)_{melt}$. Also, lnKMg = $-\Delta G_1/RT$, and $\Delta G_1 = \Delta H_1 - T\Delta S_1$, where ΔG, ΔH, and ΔS are free energy, enthalpy, and entropy. Equation (7) becomes:

$$\ln(D_m) = \Delta S_1/R - \Delta H_1/RT - \ln KMg + 1.5 \cdot \ln X_{Mgol} - 1.5 \cdot \ln(a_{Mg})_{melt} \quad , \tag{9}$$

where ΔS_1 and ΔH_1 are different for each trace element. The goal of this section is to relate ΔS_1 and ΔH_1 to simple, readily available properties of the trace cations.

A qualitative relationship of the free energy of the partitioning reaction with cationic size and charge is intrinsic in Goldschmidt's (1937) rules for substitution. The present study attempts to quantify this relationship and is based on the following reasoning. It is assumed that: (a) there exists a hypothetical "average" Madelung constant for each component in the melt and (b) the component internal energies for both melt and crystal can be approximated by an ionic model. The lattice energies for melt and crystal can be estimated from equations of the type:

$$U = N(\alpha Z^+ Z^-/d + \sigma y e^{-d/p}) \quad , \tag{10}$$

where

N = number of molecules,

α = Madelung constant, a value dependent on crystal structure only,

σ = number of nearest neighbors,

Z = charge,

y = constant,

d = nearest-neighbor internuclear distance, and

p = range of repulsion parameter.

The first term is the Madelung (or electrostatic) energy term; the second is an energy term arising from repulsive interactions (Kittel, 1976; O'Keefe, 1981; Tosi, 1964).

Internal energies can be formulated for both crystal and melt for each cation. The difference in the internal energies of the trace component between the melt and crystal can be expressed as:

$$U = k1_{crystal} \cdot Z^{+}/d - k1_{melt} \cdot Z^{+}/d - k2_{crystal} \cdot EXP((d2-d')/p) - k2_{melt} \cdot EXP((d2-d')/p) \quad , \tag{11}$$

where

k1 = $N\alpha Z^{-}$,

k2 = Nzy,

d' = d/0.707 (distance between surrounding oxygens), and

d2 and p are repulsion parameters from Miyamoto and Takeda (1983).

An analogous expression can be written for the internal energy of Mg leading to the expression for the internal energy of exchange:

$$\Delta U = (k1_{crystal} - k1_{melt})(Z^{+}_{M}/d_{M} - Z^{+}_{Mg}/d_{Mg}) - (k2_{crystal} - k2_{melt})(Z^{+}_{M} \cdot EXP((d2-d'_{M})/p) - Z^{+}_{Mg} \cdot EXP((d2-d'_{Mg})/p) \quad . \tag{12}$$

$dH = dU + d(PV)$. Calculations of pressure-volume work at 1 atm when volumes are linearly related to ionic size (Brown, 1970) indicate that $dPV << dU$. Therefore, Equation (12) is an expression for the enthalpy of the trace element-Mg exchange.

For the trivalent cations, an additional enthalpy term is associated with the charge balancing substitution. The enthalpy of this substitution is considered to be independent of the $M^{+3} - M^{+2}$ exchange.

No theoretical relation between cationic size and the entropy of exchange was derived. However, ΔS_1 was fit empirically to the difference in the inverses of cationic volume as:

$$\Delta S_1 = A(1/r^3 - 1/(0.83)^3) \quad ,$$

where r = cationic radius (0.83 = average radius of Mg and Fe in octahedral coordination). Justification for setting the intercept to zero comes from the reasoning that where Mg or Fe substitute for themselves, ΔS_1 should equal zero.

Regressions

Data for nine elements for olivine and four elements for orthopyroxene are empirically fitted to the equations:

$$\ln D_m = \Delta S_1/R - \Delta H_1/RT - \text{LnKMg} \qquad (13)$$

and

$$\ln D_m = \Delta S_1/R - \Delta H_2/RT - \text{LnKFe} \qquad (14)$$

where

$\ln D_m$ = the natural log of D_m,

T = temperature.

For olivine:

$LnKMg = \ln((a_{Mg})_{melt}) - \ln(X_{Mgol}) - \ln\gamma_{Mg}$ for divalent trace cations; and

$LnKFe = 1.5 \cdot \ln((a_{Fe})_{melt}) - 1.5 \cdot \ln(X_{Feol}) - \ln\gamma_{Fe}$ for trivalent cations.

$\gamma_{Mg} = (Q/X_{Mgol})/(1+Q)$

$\gamma_{Fe} = (1 - \gamma_{Mg}(X_{Mgol}))/(X_{Feol})$.

where

$Q = (X_{Mgol}/X_{Feol}) \cdot EXP(\Delta H_4/RT)$ and

ΔH_4 = enthalpy of the Mg-Fe exchange reaction of Equation (4).

The entropy of the exchange is assumed equal to 0 ($\Delta S_4 = 0$), analogous to a regular solution model.

For orthopyroxene, the terms are analogous except that for trivalent cations:

$$\ln KFe = \ln((a_{Fe})_{melt}) - \ln(X_{Feopx}) + \ln((a_{Si})_{melt}) - \ln((a_{Al})_{melt}) - \ln\gamma_{Fe} ,$$

reflecting a different substitutions mechanism as discussed later in this paper.

Results of linear regressions against these parameters are reported in tables 5 and 6. Included in these regressions were the olivine and orthopyroxene data of this study and the olivine data from McKay (1985),

Table 5. Results of regressions for the olivine data for nine elements to the equations:

$$\ln D_m = \Delta S_1/R - \Delta H_1/RT - \ln KMg \text{ and}$$
$$\ln D_m = \Delta S_1/R - \Delta H_2/RT - \ln KFe$$

The lnKMg and lnKFe coefficients are fixed at -1. "No." labels the number of data points used in the regression.

Element	No.	$\Delta S_1/R$	error	$(\Delta H_1/R)/10^4$	error	$(\Delta H_2/R)/10^4$	error	$\Delta H_4/10^4$	error	Rsqr
Yb	39	0.692	0.970	-0.858	0.150	-0.493	0.125	-0.116	0.044	0.15
Sc	17	-0.087	0.534	-0.394	0.080	-0.104	0.080	-0.035	0.064	0.90
Al	31	-5.980	1.380	0.008	0.210	0.148	0.210	0.112	0.090	0.25
Gd	25	3.350	2.140	-1.640	0.330	-1.230	0.330	-0.156	0.158	0
Sm	24	4.730	3.000	-1.970	0.460	-1.530	0.460	-0.184	0.220	0
Ni	39	-2.650	0.380	0.541	0.060	0.816	0.060	-0.077	0.037	0.85
Co	48	-0.196	0.187	-0.023	0.029	0.203	0.029	-0.030	0.014	0.86
Mn	113	0.445	0.130	-0.305	0.020	.000	0.020	-0.124	0.016	0.60
Ca	27	0.272	0.687	-0.945	0.106	-0.487	0.106	-0.289	0.034	0.71

Table 6. Results of regressions for the orthopyroxene data for nine elements to the equations:

$$\ln D_m = \Delta S_1/R - \Delta H_1/RT - \ln KMg \text{ and}$$
$$\ln D_m = \Delta S_1/R - \Delta H_2/RT - \ln KFe$$

The lnKMg and lnKFe coefficients are fixed at -1. "No." labels the number of data points used in the regression.

Element	No.	$\Delta S_1/R$	error	$(\Delta H_1/R)/10^4$	error	$(\Delta H_2/R)/10^4$	error	$\Delta H_4/10^4$	error	Rsqr
Yb	13	-9.32	2.10	1.040	0.33	1.310	0.33	-0.357	0.20	0.75
Sc	9	-5.24	1.30	0.911	0.21	0.828	0.21	-0.050	0.06	0.95
Al	16	-9.32	2.00	1.170	0.31	1.140	0.31	0.222	0.40	0.85
Ca	16	-0.46	0.71	-0.613	0.11	-0.209	0.11	-0.482	0.24	0.94

Takahashi (1978), and Lindstrom (1976). Estimates of parameter significance and correlation coefficients (R^2) for each regression are reported. Regressions and parameter estimates were performed using the SAS statistical package.

For olivine, consistent variations of ΔH_1, ΔH_2, and ΔS_1 with trace element size occur. The meaning of the variations of ΔH_1 and ΔH_2 was discussed above. The variation of ΔS_1 with size (figure 3) illustrates that the entropy of exchange becomes systematically greater as the size of the substituting trace cation increases. This may reflect a disordering in the olivine crystal resulting from distortion caused by the insertion of larger trace cations. ΔH_4 also varies systematically with cationic size (figure 4). The interpretation of this is as follows: Fe tends to congregate around large cations like Ca ($X_{Mgol} > X_{MgM}$), Mg tends to congregate around small cations like Al ($X_{Mgol} < X_{MgM}$), and there is no congregation around middle-sized cations like Co. Consistent variations in the orthopyroxene data are less significant. This probably reflects the smaller data set.

Values of ΔS_1, ΔH_1, ΔH_2, and ΔH_4 for the various trace cations are related to ionic size by the following equations:

$$\Delta S_1/R = A\cdot(1/r^3 - 1.749) \quad , \tag{15}$$

$$\Delta H_1/R = B\cdot(Z_M^+/d - .9434) + C\cdot(Z_M^+\cdot EXP((3.585 - (d/.707)/.208) - 32.42) + D+Z_M^+ \quad , \tag{16}$$

$$\Delta H_2/R = B\cdot(Z_M^+/d - .9174) + C*(Z_M^+\cdot EXP((3.585 - (d/.707)/.208) - 21.56) + D+Z_M^+ \quad , \tag{17}$$

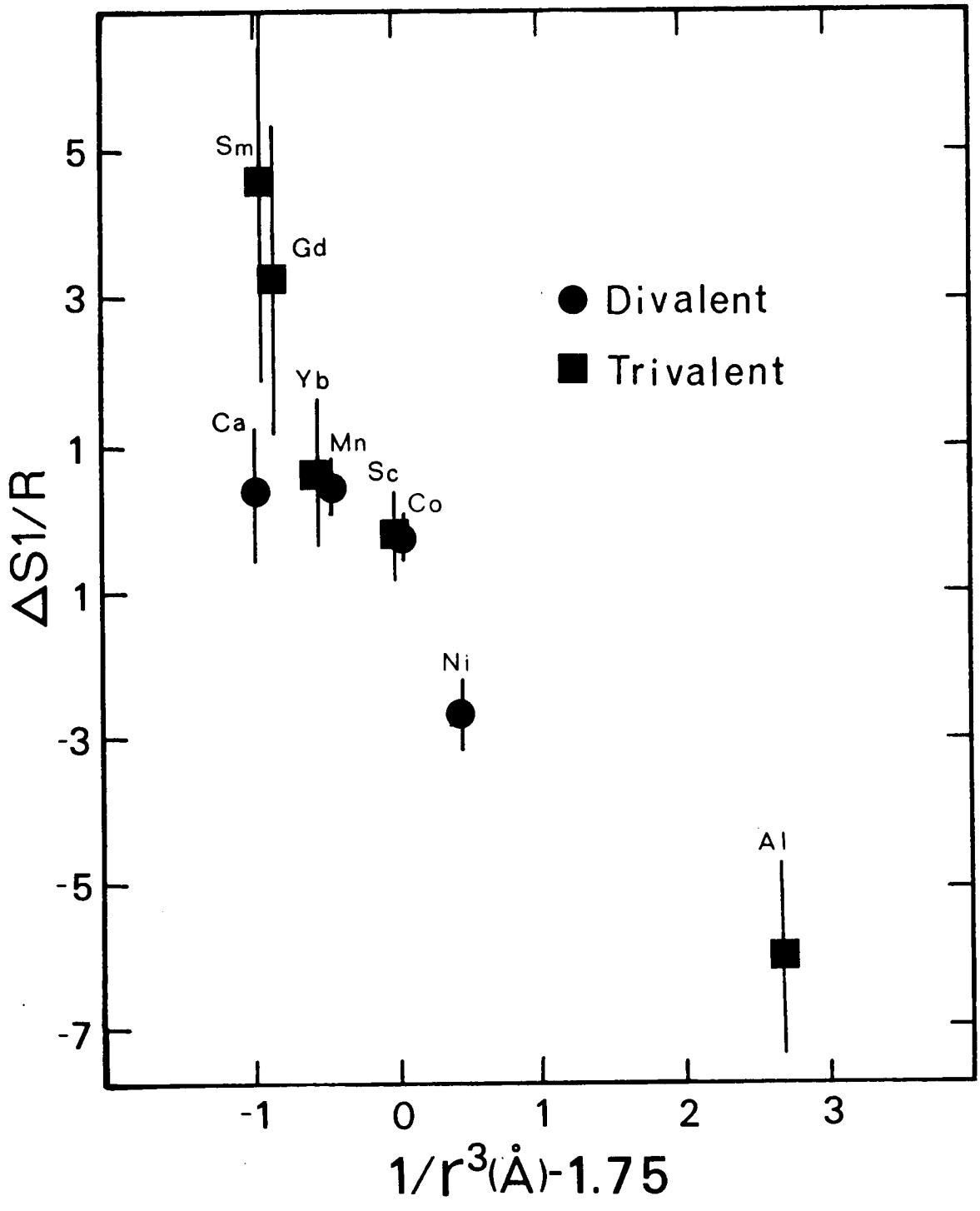

Figure 3. Dependence of entropy of exchange on ionic size, where $\Delta S_1/R$ is the entropy of the exchange expressed in either equation 1 (for divalent cations) or equation 3 (for trivalent cations) divided by the gas constant. The coordinate axis plots the change in $1/r^3$ between the trace cation and the average of Mg and Fe. Bars = 1 σ error estimate.

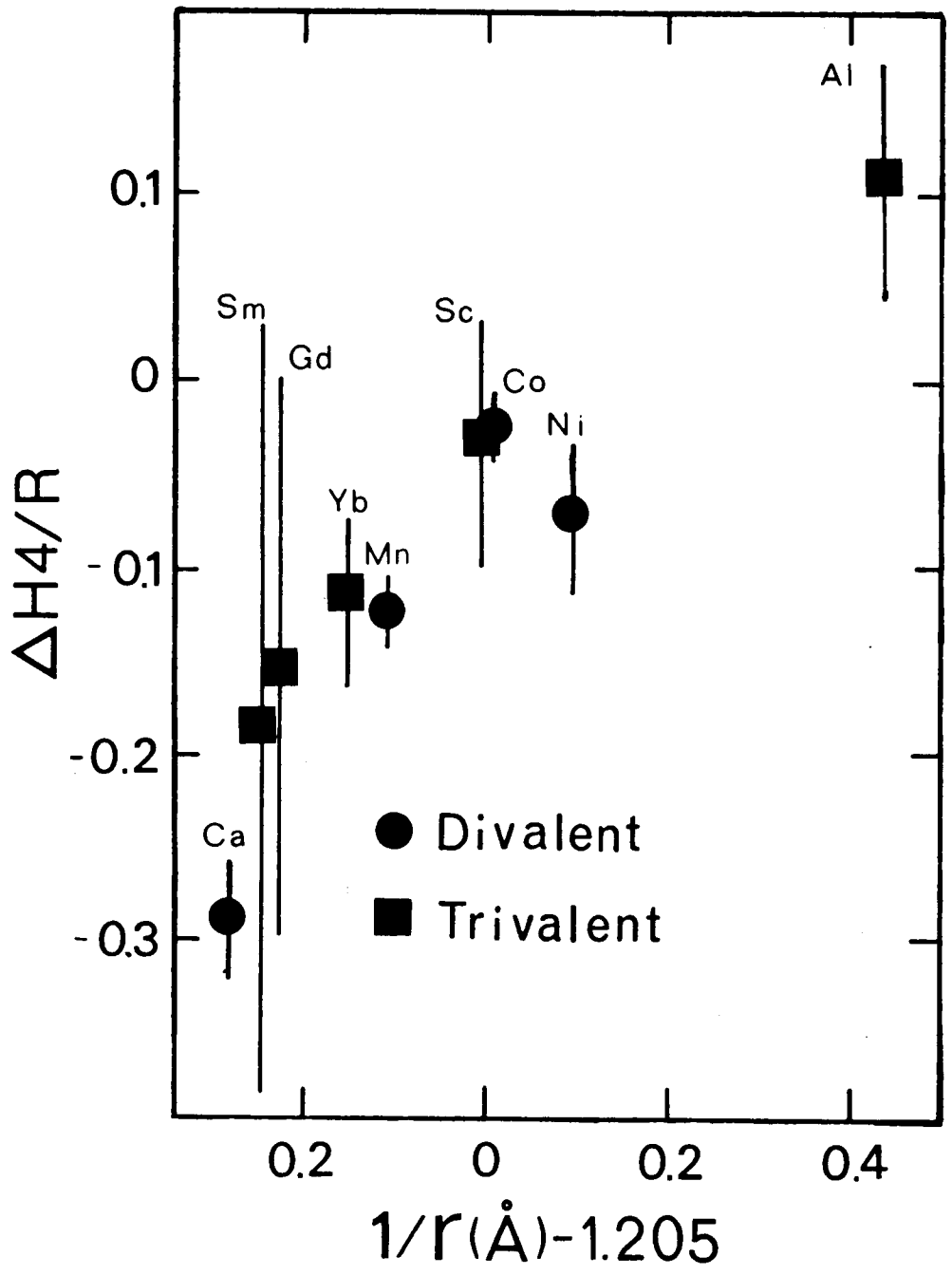

Figure 4. Dependence of the nonideality term $\Delta H_4/R$ on ionic size, where $\Delta H_4/R$ is the enthalpy of the exchange expressed in equation 4 divided by the gas constant. The coordinate axis plots the change in 1/r between the trace element and the average of Mg and Fe. The consistency of the variation of $\Delta H_4/R$ with size supports the belief that this nonideality is real. Bars = 1 σ error estimate.

and

$$\Delta H_4/R = E + F\cdot(1/r - 1.205) \quad , \tag{18}$$

where

r = cationic radius from Whittaker and Muntus (1970),

R = gas constant,

d = internuclear distance (trace-oxygen),

Z_M^+ = cationic charge,

B = $(k1_{crystal} - k1_{melt})$,

C = $(k2_{crystal} - k2_{melt})$, and

$D+Z_M^+$ = the enthalpy associated with the charge balancing coupled substitution.

A and B are constant, but C and D are functions of the charge of the substituting cation. Results are reported in tables 7 and 8 of regression to these equations for all the trivalent and divalent data of this study and the studies listed above.

Available data are currently insufficient for a rigorous analysis of the substitution of tetravalent cations in olivine. Using values for A, B, and C derived from all the data (table 7), the ΔG of the charge-balancing coupled substitution associated with the tetravalent cations is estimated at 12590 (or D+4 = -12590). As expected, this coupled substitution is more restricting than the trivalent coupling (enthalpy of exchange is approximately twice as high).

Test of Model

In order to evaluate the model presented above, two different aspects were considered: (1) a discussion of how well the data is

Table 7. Coefficients to the equations given in the text (equations 13-18). Coefficients are determination is by linear regression. Note that values for all the data are closely modeled by values determined from single elements.

Data			A	error	$B/10^4$	error	$C+3/10^4$	error	$C+2/10^4$	error	$D+3/10^4$	error	$D+2/10^4$	error	Rsqr	$E/10^4$	$F/10^4$
Divalent	227 pts.	LnKMg	-1.64	0.37	13.90	0.46	--	--	-0.0052	0.0011	--	--	0.114	0.02	0.98	-0.084	0.635
		LnKFe	-1.90	0.87	9.92	0.70	--	--	-0.0003	0.0017	--	--	0.123	0.02	0.96		
Trivalent	138 pts.	LnKMg	-2.73	1.00	12.14	0.56	-0.0099	0.0024	--	--	-5.78	0.26	--	--	0.89	-0.059	0.415
		LnKFe	-2.62	0.94	11.41	0.55	-0.0110	0.0023	--	--	-5.31	0.29	--	--	0.89		
All data	365 pts.	LnKMg	-1.58	0.55	12.15	0.35	-0.0136	0.0013	-0.0052	0.0024	-5.73	0.16	0.110	0.02	0.99	-0.075	0.465
		LnKFe	-2.77	0.59	11.20	0.38	-0.0099	0.0014	-0.0003	0.0026	-5.49	0.19	-0.08	0.02	0.99		
Yb calculated			-1.19		14.04		--		--		-6.17		0.000		--	0	0.748
Mn calculated			-1.05		11.73		--		--		--		0.240		--	0	1.17

Table 8. Coefficients to the orthopyroxene partitioning equations are estimated by regressions for selected data sets. These equations are given in the text (equations 13-18).

Data			A	error	$B/10^4$	error	$C+3/10^4$	error	$C+2/10^4$	error	$D+3/10^4$	error	$D+2/10^4$	error	Rsqr
Yb-Sc-Al	39 pts.	lnKMg	-2.64	0.92	11.72	0.6	-0.00080	0.0026	--	--	-5.17	0.27	--	--	0.96
		lnKFe	-2.53	0.74	7.80	0.5	-0.00600	0.0018	--	--	-3.27	0.24	--	--	0.97
All data	67 pts.	lnKMg	-3.22	0.61	12.05	0.5	-0.00680	0.0015	0.0033	0.0033	-5.33	0.20	0.150	0.04	0.99
		lnKFe	03.10	0.62	8.35	0.5	-0.00510	0.0016	0.0011	0.0033	-3.75	0.23	-0.045	0.03	0.97

modeled, and (2) a discussion of how well the results fit with what is theoretically expected. Because most of the theory was built into the model before it was applied, much of the following discussion falls into the first category.

Figures 5 (olivine) and 6 (orthopyroxene) plot the measured $\ln D_m$ versus that predicted by the Equations (13)-(18) whose coefficients are given in tables 3 and 4, pp. 10 and 11. Each is a graphical test of the goodness of fit of the linear regressions. For clarity, only a fraction of the 408 data points from these studies are plotted. The Mn data of Watson (1977) and data for the elements Nd, Y, Eu^{+2}, Zn, and Fe were not included in the regression and illustrate the models predictive capability. It is noted that as the measured $\ln D_m$ becomes low, the scatter about the line becomes large. This is especially noticeable for Nd, Sm, Gd, and Eu^{+2} for which analytical difficulties have been reported previously (McKay, 1982).

Further support is given the model by the observation that most of the information in the regression can be found in the data of a single element. Table 7 lists the parameter coefficients calculated from the regression of only Yb and Mn data. Two unknowns (B and D+2 or D+3) are calculated from two equations of exchange (trace-Mg and trace-Fe). These values are close to the values of the coefficients of regression for all the data. Figure 7 is analogous to figure 5, plotting model vs measured lnD. The model $\ln D_m$ values of figure 7 are based only on the regression of the Yb data. Only those elements from this study whose ionic radius is within ±0.12 Å that of Yb are plotted. Estimations of

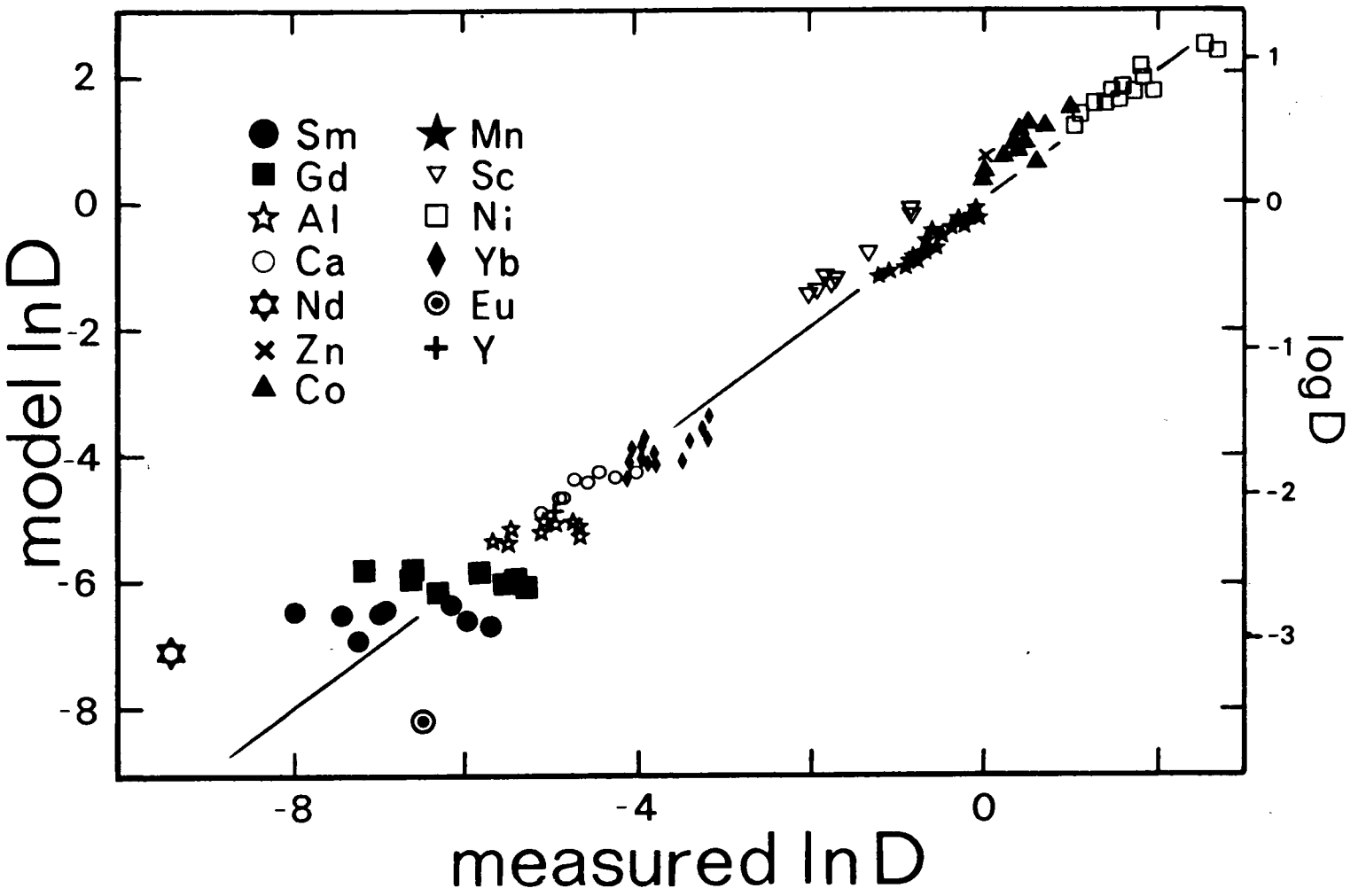

Figure 5. Measured versus modeled olivine $\ln D_m$ for 365 data points and 13 trivalent and divalent elements based on a regression for all the data. Plot represents a test of the goodness of fit of the model. Data are from this study, McKay (1986), Takahashi (1978), Lindstrom (1976), and Watson (1977). $R^2 = 0.99$ (from table 7).

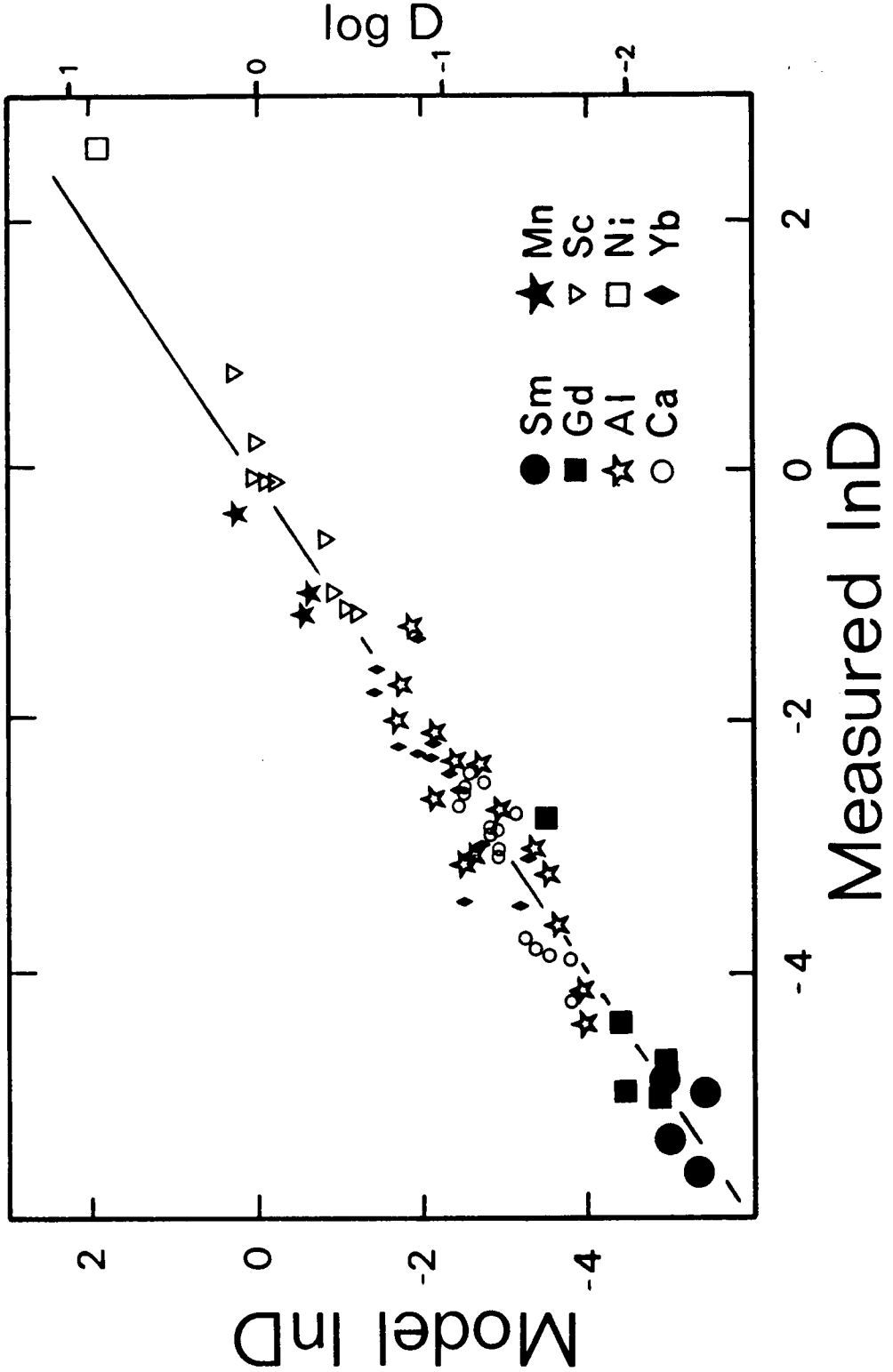

Figure 6. Measured versus model orthopyroxene lnD_m values for 67 data points and 8 elements. Plot represents a test of the "goodness of fit" of the model. $R^2 = 0.99$ (from table 8).

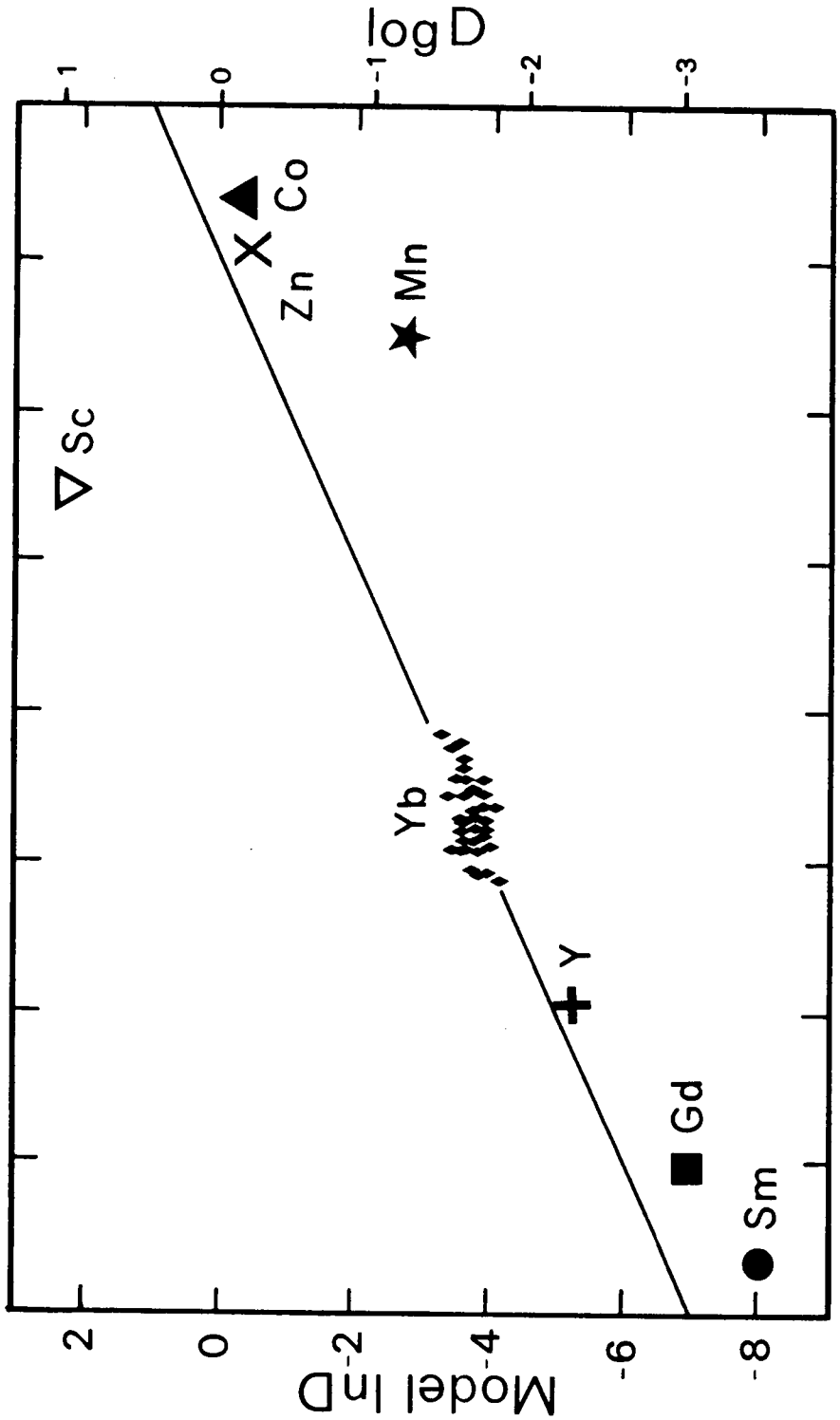

Figure 7. Measured versus modeled $\ln D_m$ based on regressions only for the Yb data. Averages are plotted for all elements except Yb. Plot represents the capability of predicting partitioning of one element based upon knowledge of how partitioning of another element changes with temperature.

partitioning based on a single element fail where the repulsion term (C+2,C+3) becomes significantly different from that of the element from which the estimates are made. The systematically low predictions for the large cations (e.g., Sm, Gd) and the high predictions for Sc reflect the absence of the repulsion term. The prediction of the divalent cations appears poor since the measured values for Mn (which has an ionic radius near that of Yb) are considerably higher than modeled. However, this error could result from only a 6% error in the estimation of the D+3 term. In reality, the prediction is within the error expected from the scatter of the Yb data. The closeness of these predictions based on the data of a single element suggests the model has wide application in predicting partitioning behavior in compositional systems and for elements for which experimental data are not available.

Model versus measured $\ln D_m$ values for three tetravalent cations are illustrated in figure 8. The data are from this study and Lindstrom (1976). Because there are three elements defining the D+4 term, two degrees of freedom remain. The assumption appears good that, for this limited data set, the B and C terms have the same value as those derived for the divalent data, and the D+4 term is constant.

If all is well with this model, B and C are expected to remain constant for all cations regardless of charge. D+2 is expected to be zero, since there is no charge-balancing substitution coupled to the exchange of divalent for divalent cations. C+2 and C+3 are expected to have negative values. B, C, and D+Z should be the same for both trace-Mg and trace-Fe exchanges. If we assume that the charge-balancing

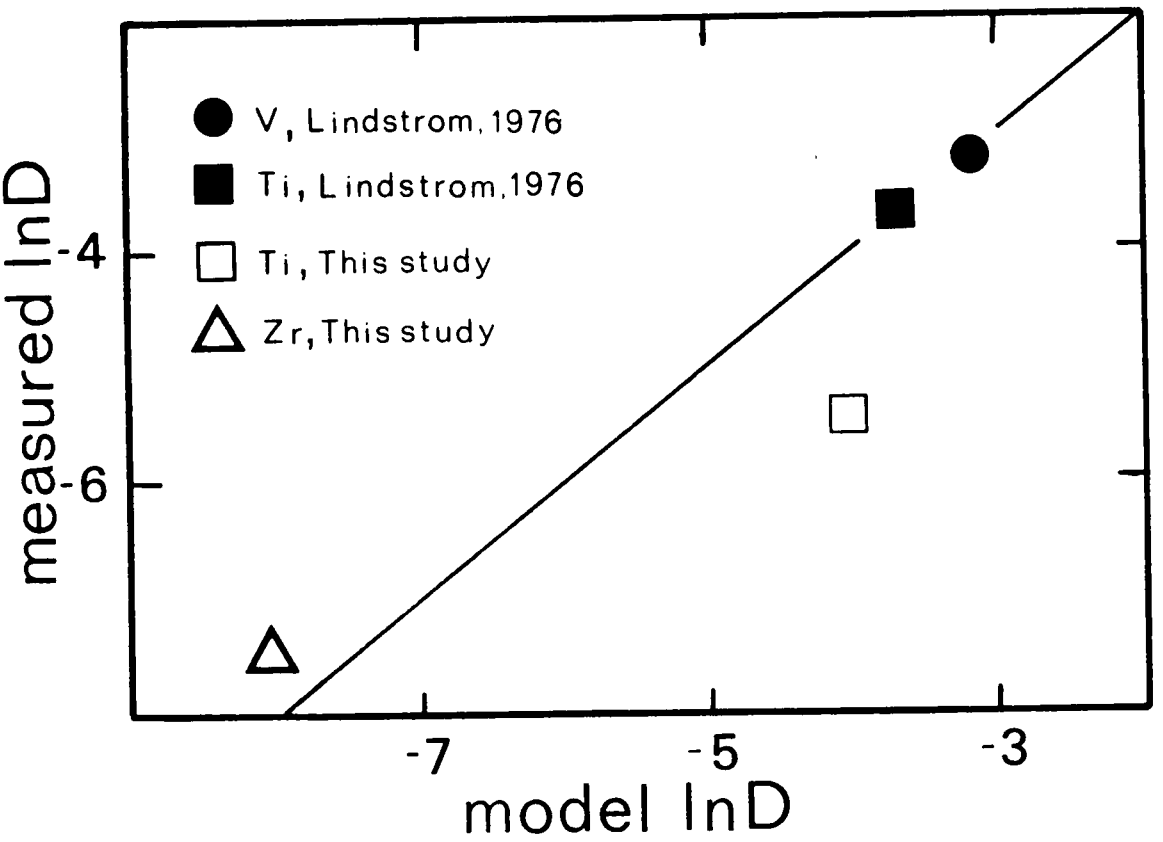

Figure 8. Model $\ln D_m$ versus measured $\ln D_m$ for tetravalent cations in olivine. The data of Lindstrom (1976) are averages of multiple analyses; the data of this study are single analyses. Data is modeled based on the regression for the divalent data reported in Table 7.

substitution associated with tetravalent cations is simply two of whatever charge balances trivalent cations, then we expect D+4 to be approximately twice D+3.

Most of the results fit these theoretical expectations. Inspection of tables 7 and 8 reveals that, for both olivine and orthopyroxene partitioning, B is nearly the same for divalent and trivalent cations. The B values determined from the olivine data are nearly equal for both Fe-trace and Mg-trace exchanges. C coefficients are all negative, except for the C+2 value derived for orthopyroxenes which is near zero. As expected, D+2 is nearly 0 for both olivine and orthopyroxene and D+4 is approximately twice D+3.

In orthopyroxene, the value derived for B by regression to the trace-Fe exchange is different from the value when the trace-Mg exchange is considered. Also, C+2 and C+3 are not the same in either olivine or orthopyroxene. This is a minor defect of the model.

The repulsion term (the exponential portion of Equation (10)) is interpreted to reflect the increasing interference of oxygens surrounding the cation as the cation becomes small. Consistent with this interpretation, oxygen-oxygen internuclear distances are used in the repulsion term (d') along with oxygen-oxygen repulsion parameters (d2,p) taken from Miyamoto and Takeda (1983). For oxygens surrounding a cation in octahedral coordination, internuclear distances are computed as a function of cation size as (d' = d/.707). This interpretation of the repulsion term is supported by the observation that the "optimum radius" of Philpotts (1978) typically corresponds approximately to the minimum

cation radius where oxygens "just touch" in a site of given coordination number (figure 9). Phases with uncertain or variable coordination or asymmetric sites (e.g. amphibole, K-spar) deviate from this relation.

In summary, the proposed model takes into account energies in the melt which are likely to be important; it explains the parabolic nature of trace element partitioning (Philpotts, 1978)(the exponential repulsion term); it predicts the value of the trivalent-divalent offset mentioned by Philpotts (1978) (D+2=0, D+3 calculated from Yb data only); it predicts the optimum radius of partitioning (figure 9); and it accurately models the systematic variation in H_1, H_2, and S_1 based only on readily available ionic radii.

Discussion

Partitioning Dependence on T and X

Figures 10, 11, and 12 illustrate the effects of temperature and composition on $\ln D_m$. Figures 10 and 11 plot lnD against the remainder of the equilibrium constant when the ordinate axis is normalized to temperature by the $\Delta G_1/RT$ term. Figure 10 plots divalent data and figure 11 plots trivalent data. Figure 12 plots the entire equilibrium constant against 10^4/temperature, illustrating the relation $\ln K = -\Delta G/RT$. It also illustrates the dependence of $\ln D_m$ on temperature when the rest of the equilibrium constant does not vary. The tightness of the fit of the data, which come from McKay (1986), Takahashi (1978), Watson (1977), Lindstrom (1976), as well as this study, illustrates the model's versatility in the interpretation of data derived in a wide

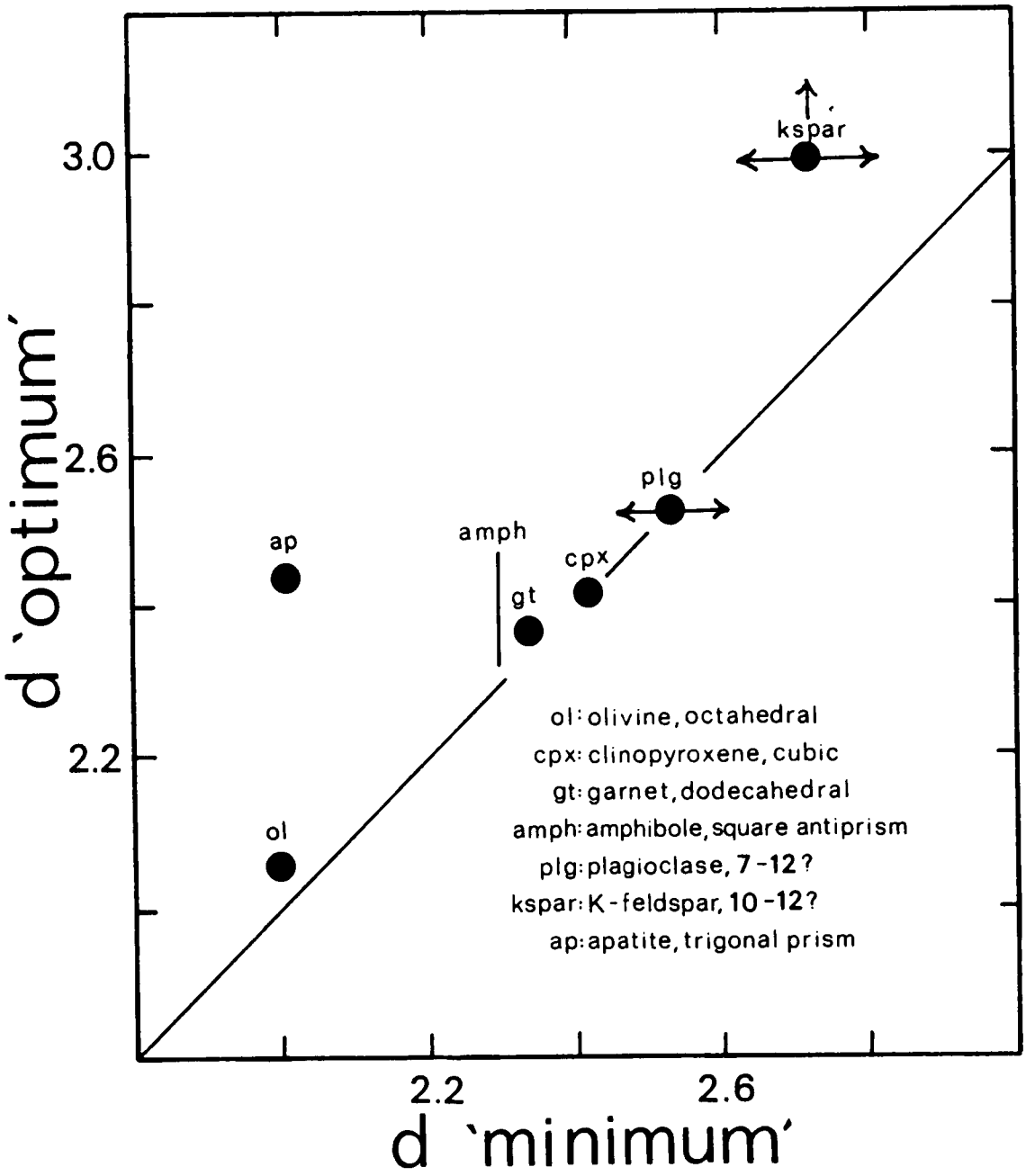

Figure 9. Plot of the radius of maximum partitioning coefficient versus radius at which oxygen ions "just touch." Plot "predicts" the optimum radii at which partitioning reaches a maximum. Data are from Reviews in Mineralogy, Volumes 2, 5, 7, 9a, Philpotts (1978), Irving (1978), Long (1978), Leeman (1975), Hurlbut and Klein (1977), Watson and Green (1981), and this study.

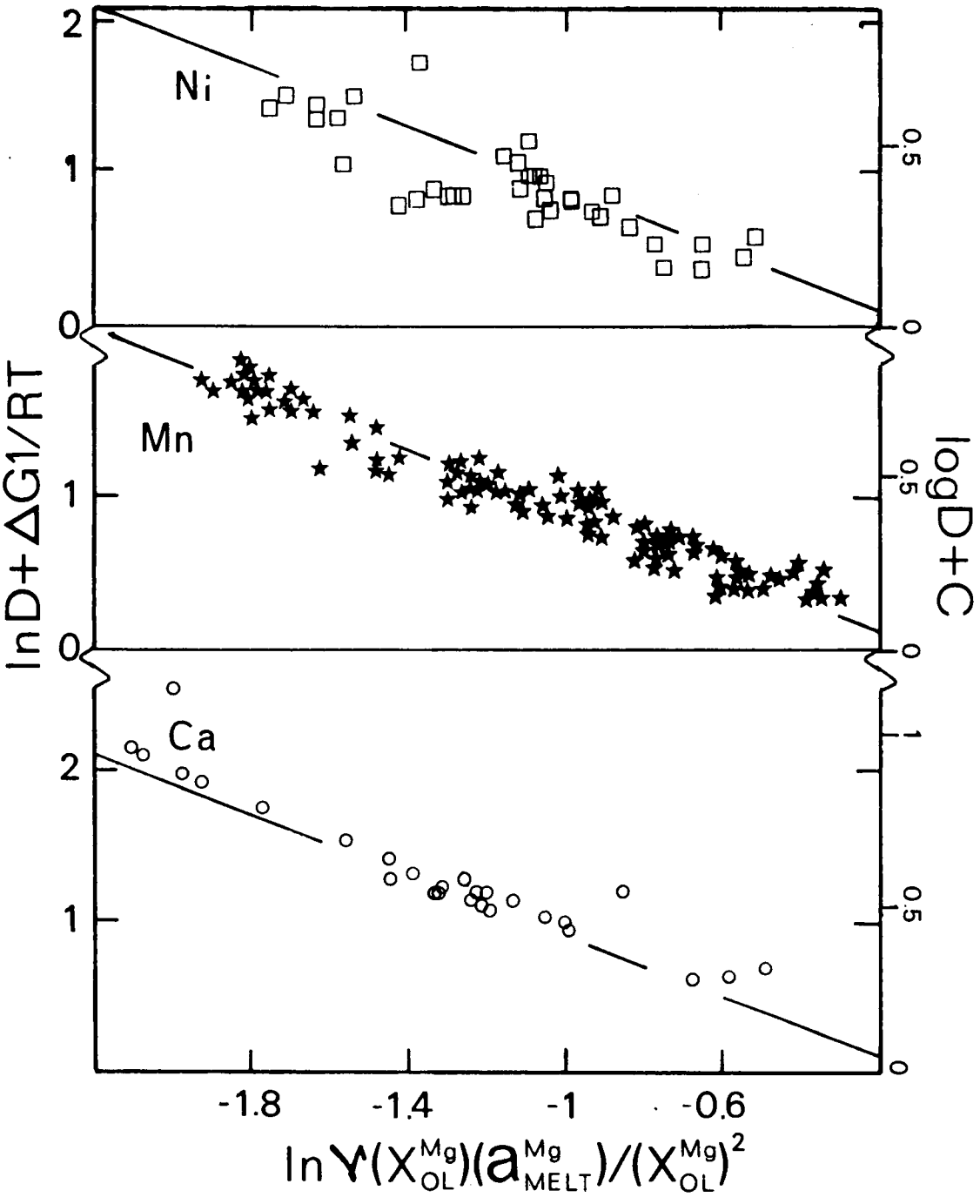

Figure 10. Compositional dependence of divalent partitioning between olivine and melt. $\Delta G_1/R$ is the free energy change in the reaction expressed in equation 1 divided by the gas constant. Coordinate axis plots the remainder of the equilibrium constant after the partition coefficient is removed. Regression coefficients are reported in Table 5.

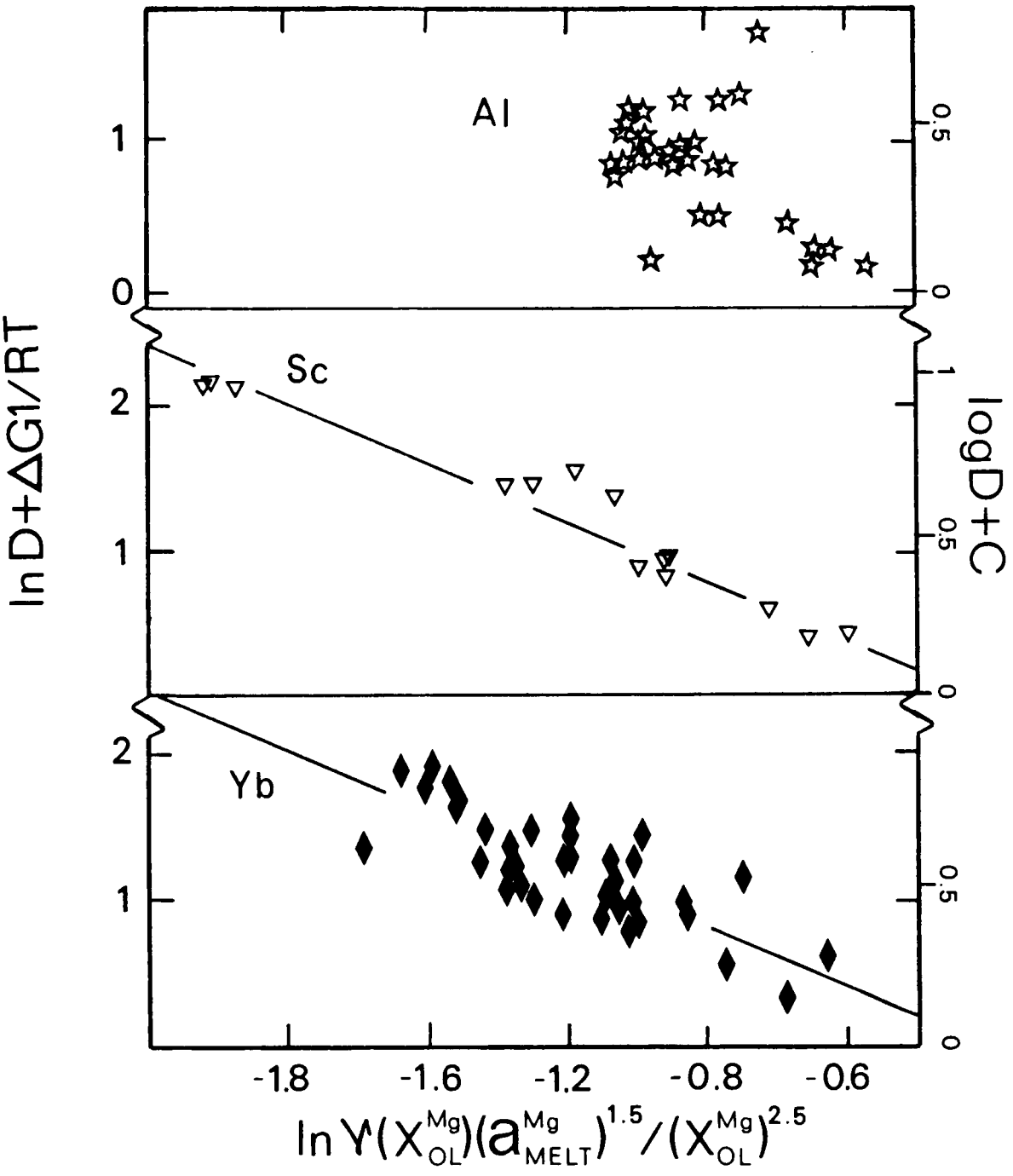

Figure 11. Compositional dependence of trivalent partitioning between olivine and melt. $\Delta G_1/R$ is the free energy change in the exchange expressed by equation 2 divided by the gas constant. Coordinate axis plots the remainder of the equilibrium constant after the partition coefficient is removed.

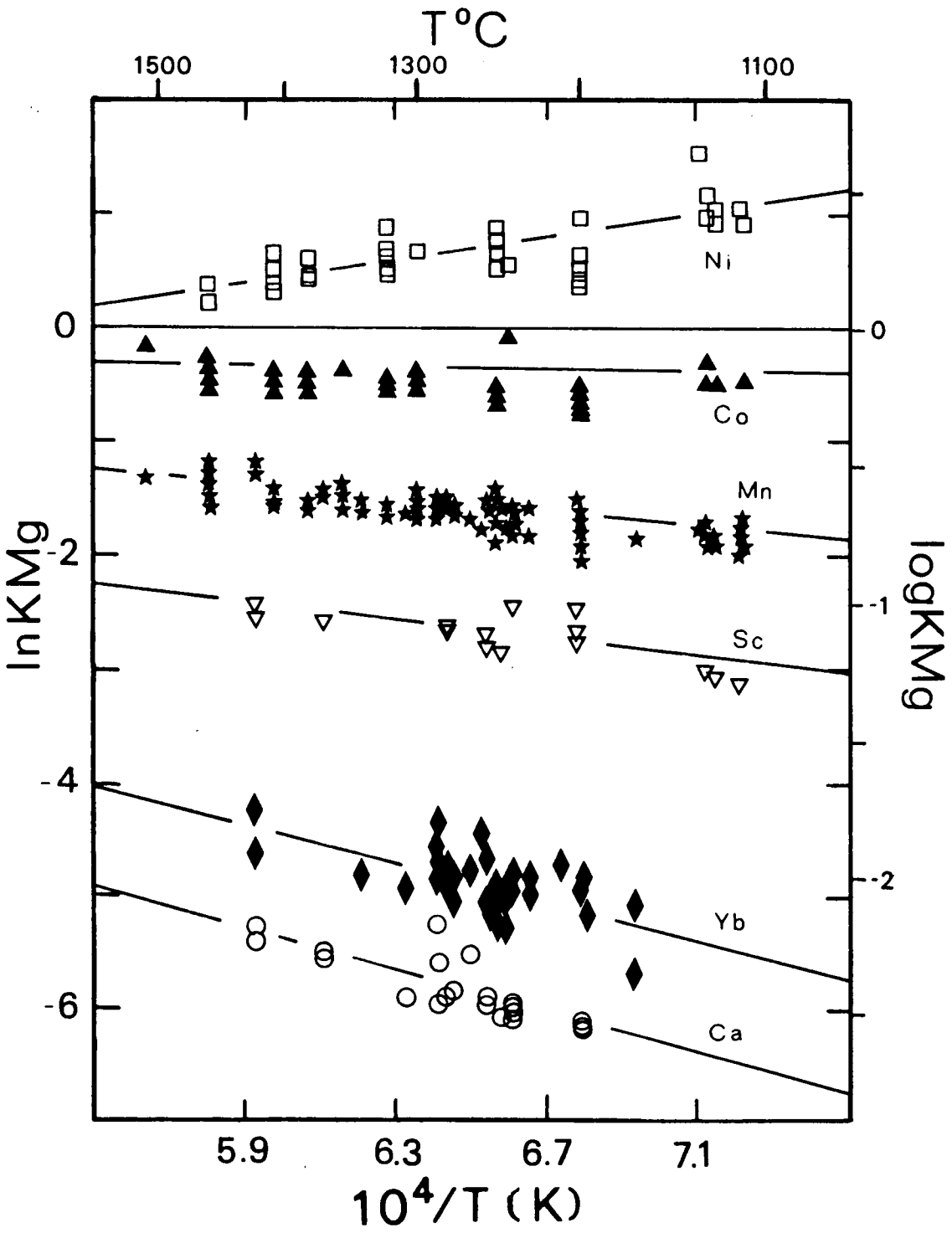

Figure 12. Plot of the equilibrium constant versus 10000/temperature. Where all the compositions involved in the equilibrium constant remain constant except those of the trace element, this represents the temperature dependence of partitioning between olivine and melt.

variety of experimental systems and by different investigators. It is seen that both temperature and composition affect $\ln D_m$ significantly, and variations of an order of magnitude in $\ln D_m$ are expected over typical basaltic compositions and temperatures.

fO_2 Effects

Oxygen fugacity is expected to have two major effects on partitioning. The first effect is due to the changing valence state of Fe. As Fe changes valence state the activities of the Fe^{+2} in olivine and melt change, thereby altering the value of the lnKMg and LnKFe parameters. The second effect is the alteration of the valence state of the trace cation. With the exception of Eu, V, and Ti, the cations of this study are generally found in only a single valence state in basaltic systems. Therefore, for these elements, the main effect of fO_2 is expected to be due to changing valence of Fe. If the relative proportions of Fe^{+3} and Fe^{+2} in the phases are known (Sack et al., 1980), this fO_2 effect is accounted for by the equilibrium constant already formulated.

The fO_2 dependence of $\ln D_m$ arising from multiple valences of the trace cation can be modeled by determining a partitioning value for each of the valence states in which the cation exists. The total partitioning value for the element can be expressed as $\Sigma X_i D_i$, where D_i is the partition value of the cation with charge i, and X_i is the fraction which valence i constitutes of the total amount of the cation. An illustration of this relation is given in figure 13 using the Cr data of Schreiber and Haskin (1976). Model $\ln D_m$ values are computed from the regression coefficients for all the data given in table 7, p. 31. The

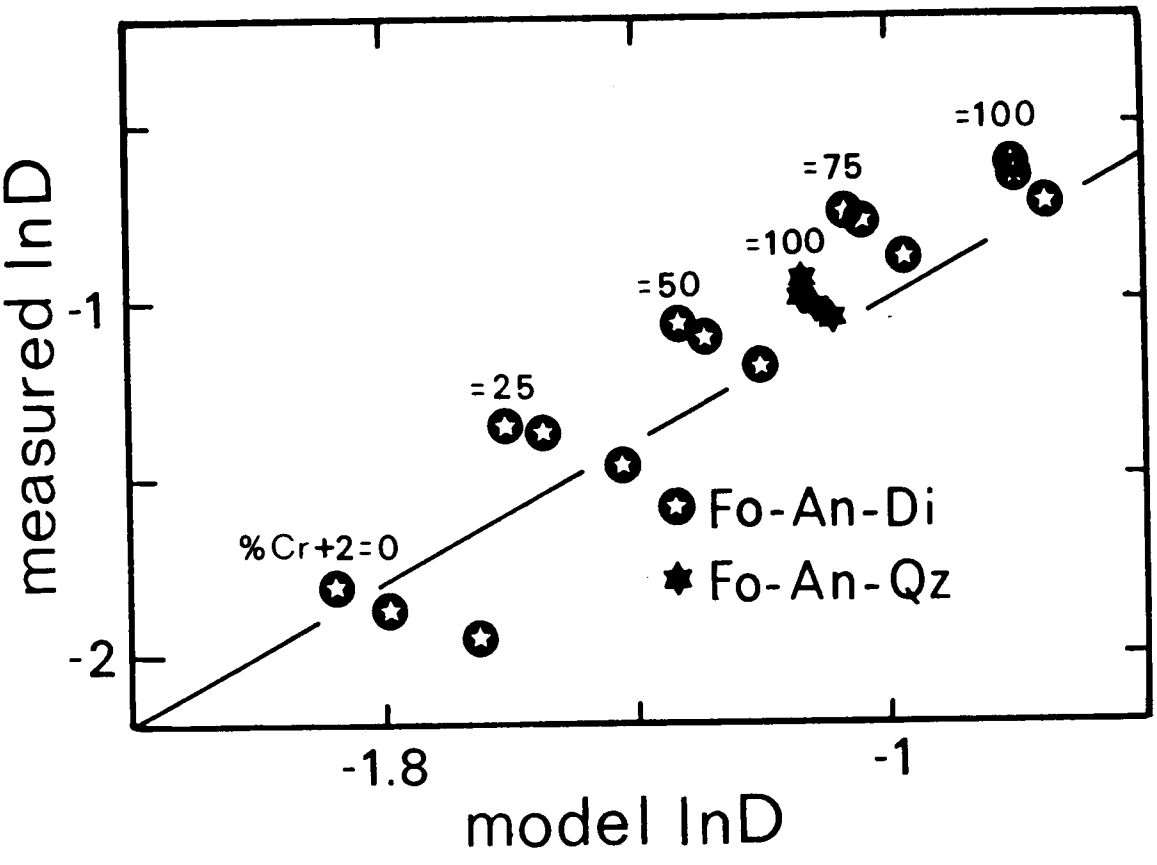

Figure 13. Dependence of Cr partitioning on valence state in low-Al systems. Data is modeled based on the regressions for the divalent and trivalent data to the equations given in the text. These regression coefficients are reported in Table 7. Data are from Schreiber and Haskin (1976).

dependence of partitioning on valence is accurately predicted for the FAD (Fo-An-Di) system of Schreiber and Haskin (1976).

Substitution Mechanism

Three substitution mechanisms for incorporating trivalent cations into olivine were considered. These involved couplings with (1) vacancies in octahedral sites, (2) Al in the tetrahedral site, and (3) Na in an octahedral site.

In orthopyroxene, only one substitution coupled to the M^{+3}-M^{+2} exchange was found to be dominant. This is the Al-Si substitution on tetrahedral sites. This conclusion was based on the systematic variation of tetrahedral Si with trivalent cations, illustrated in figure 14. The slope of the best fit line through the data of this graph is -0.5, consistent with this interpretation of coupled substitution.

Based on reasoning already stated, the mechanism believed to dominate in olivine is a vacancy substitution. If this is the true mechanism of substitution, the coefficients for the lnK terms are expected to be -1. Actual coefficient values determined by linear regression are reported in table 9 (coefficient Y). These values are near -1. It is believed that deviation from -1 results from uncertainty in formulation of component activities in the melt.

Supporting evidence for the vacancy substitution is found in previous studies. Morlotti and Orttonello, (1984) reported evidence for a vacancy-structure $Sm_4(SiO_4)_3$ component in olivine. This component was inferred by analogy to the vacancy structure of ferrifayalite (Zhizhong, 1980).

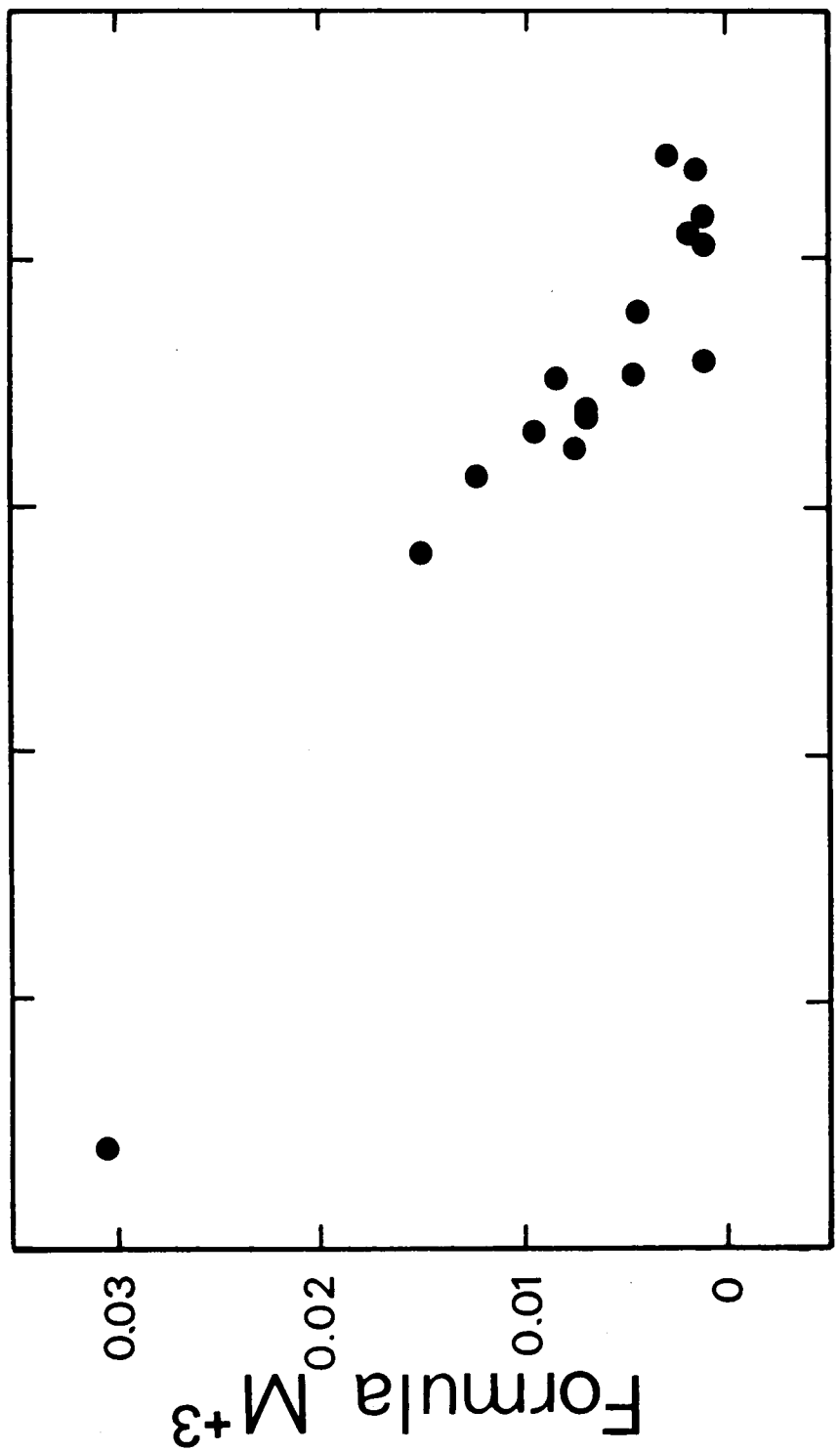

Figure 14. Correlation of tetrahedral Si to trivalent cation concentrations in orthopyroxene. This supports the interpretation that trivalent cations in octahedral sites in orthopyroxene are charge balanced by the coupled substitution of Al for Si.

Table 9. Results of regressions for the olivine data for seven elements to the equation: $\ln D_m = \Delta S_1/R - \Delta H_1/R - Y(\ln KMg)$. The closeness of the "Y" parameter to -1 tests the validity of restricting the lnKMg and lnKFe coefficients to -1. For each element the regression is performed with and without the inclusion of the ΔH_4 nonideality term. "No." labels the number of data points used in the regression.

Element	No.	$\Delta S_1/R$	error	$(\Delta H_1/R)/10^4$	error	Y	error	Rsqr
Yb	40	-3.420	1.900	-0.268	0.325	-0.762	0.320	0.18
Yb(H_4)	39	-2.780	1.530	-0.382	0.260	-0.722	0.190	0.31
Sc	17	-4.090	1.500	0.182	0.260	-0.602	0.190	0.90
Sc(H_4)	17	-3.790	1.500	0.129	0.260	-0.627	0.180	0.90
Al	32	-12.960	2.600	1.020	0.460	0.175	0.460	0.29
Al(H_4)	31	-12.220	2.600	0.880	0.550	0.025	0.690	0.29
Ni	39	-2.370	0.940	0.490	0.180	-1.020	0.260	0.89
Ni(H_4)	39	-3.050	0.600	0.630	0.110	-0.830	0.150	0.91
Co	48	-1.620	0.600	0.240	0.160	-0.530	0.160	0.84
Co(H_4)	48	-1.610	0.340	0.243	0.060	-0.610	0.090	0.90
Mn	152	0.236	0.260	-0.260	0.050	-1.090	0.060	0.90
Mn(H_4)	113	0.310	0.330	-0.280	0.060	-0.980	0.060	0.86
Ca	27	7.490		-2.250	0.280	-4.200	0.400	0.81
Ca(H_4)	27	0.870		-1.060	0.170	-1.100	0.100	0.82

Although the model derived in this study only considers the vacancy component, other components may be important in olivine for some of the trivalent cations. The relative significance of each component may vary with composition and temperature. Also, the substitution mechanism may be related to the size of the substituting cation. In fact, as seen in figure 11, p. 43, the variation in the partitioning values for Al in olivine is not explained by assuming a vacancy-coupled substitution. Variation in Al partitioning is better explained by assuming that charge balance is accomplished by Al substituting for Si in the tetrahedral site. This is seen in table 10 where the equilibrium constant coefficients are near -1 only for the Al-Si substitution. This suggests the possibility that the Al-Si substitution may be important in charge balancing smaller cations.

A test of this might be partitioning of Cr^{+3}. It was seen in figure 13 that Cr^{+3} partitioning is accurately modeled by assuming vacancy substitution. However, the FAD system of Schreiber and Haskin (1976) has little Al. Their Fo-An-SiO_2 (FAS) system has more Al. Cr^{+3} partitioning in the FAS system deviates sharply from the value predicted and is not plotted in figure 13. This leads to the most obvious possibility that the $MgCrAlO_4$ component in olivine is significant at higher melt Al concentrations.

Na was not included in the experiments of this study, and the contribution of the $NaM^{+3}SiO_4$ component to the trivalent cation partition coefficient was not investigated. However, an estimation of the relative effect of this component can be made by computing an energy for the Mg-Na exchange from the regression results of table 7, p. 31. This

Table 10. Regression of the olivine data for Al partitioning to the equations:

$$\ln D_m = \Delta S_1/R - \Delta H_1/RT - Y(\ln KMg) \text{ and}$$
$$\ln D_m = \Delta S_1/R - \Delta H_2/RT - Y(\ln KFe),$$

where lnKMg and lnKFe are formulated differently for each of two possible substitution mechanisms. This tests how well each substitution mechanism models the composition dependence of the olivine/melt Al partitioning data of this study. $\Delta S_1/R$, $\Delta H_1/R$, and $\Delta H_2/R$ are not reported.

Substitution		Coeff.	Conf. Lev.	Rsqr
Al-Si	LnKMg	-0.60	0.93	0.37
	LnKFe	-1.36	0.99	0.50
Vacancy	LnKMg	0.18	0.30	0.29
	LnKFe	-0.16	0.26	0.29

energy can be compared to the vacancy substitution energy (D+3). The $\Delta G/R$ estimated for the Mg-Na exchange is 63700-T·(1.58); compared to $\Delta G/R$ = 57300 for the vacancy coupled substitution. At a temperature typical of this study (1524K), the concentration of the $lnNaM^{+3}$ component is predicted to be 1 to 1.5 log-units below the vacancy substitution component. Considering also the typically low concentration of Na in basalt, this substitution mechanism is not expected to be significant for trivalent substitution. It is noted that this analysis considers the Na^{+} and M^{+3} substitutions independently and ignores any enthalpies arising from their interaction. A stabilizing enthalpy is expected between the large trivalent cations and Na by analogy to the "ΔH_4" interaction of Fe with the larger cations.

Magma Modeling

Trace element D values for olivine/melt and orthopyroxene/melt vary by an order of magnitude or more with temperature and composition. However, the effect on concentrations of large cations in the melt during fractional crystallization is small due to low D values. However, the temperature and composition dependence derived here for the large cations may be significant for partial melting models in which the degree of partial melting is low.

The dependence of the compatible elements (e.g., Ni) on temperature and composition is likely to be significant in fractionation models. Figure 15 illustrates the projected Ni line of descent for a Hawaiian basalt, assuming fractional crystallization of olivine. In one case partitioning is allowed to vary with temperature and composition, in the

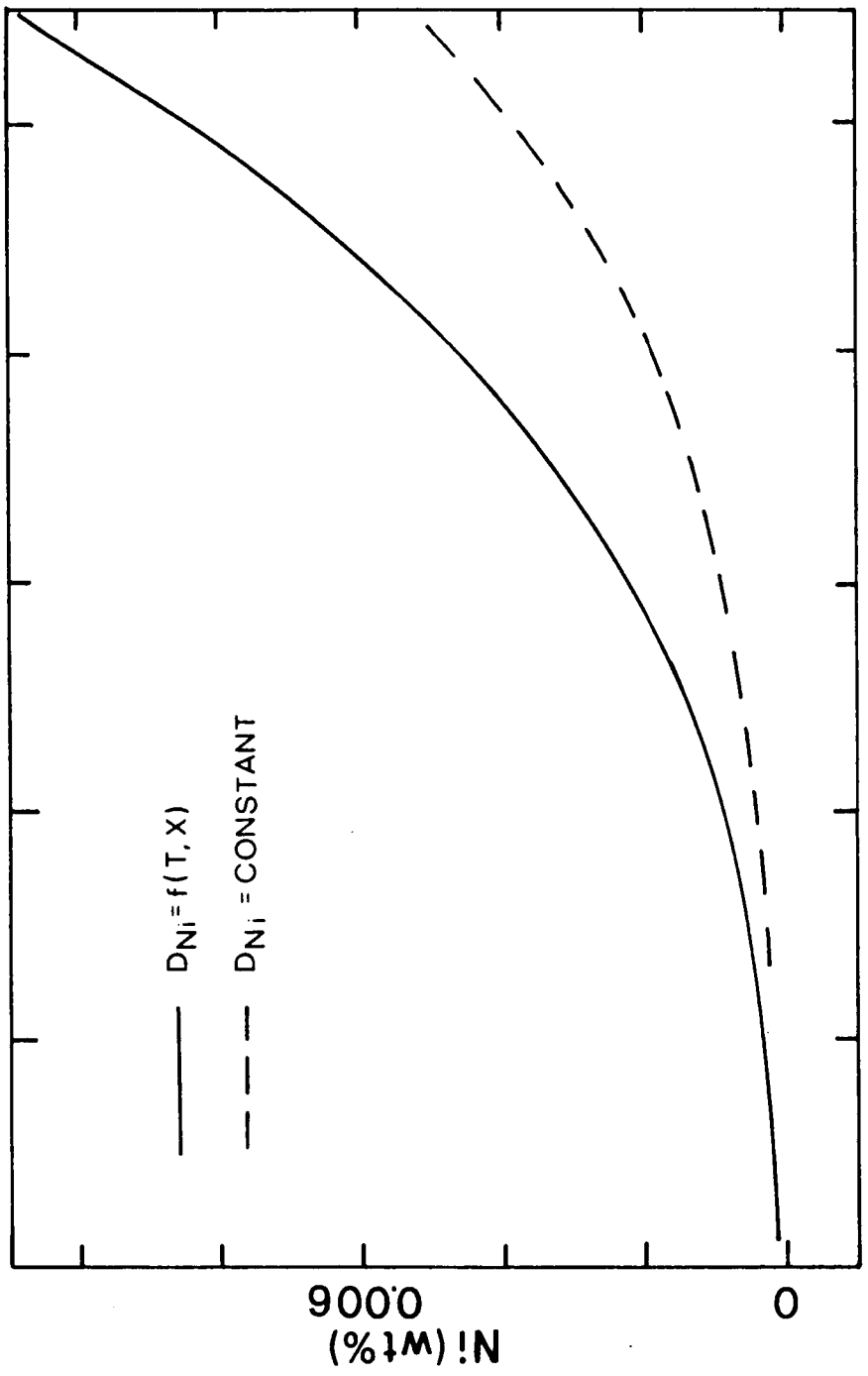

Figure 15. Comparison of projected basaltic "line of descent" (assuming crystal fractionation) for the two cases: Ni D varies with temperature and composition; Ni D is held constant at a value typical of basalts.

other case it is not. The difference in the two trends is nearly 100% after 25% fractional crystallization. The difference will be even larger for greater degrees of fractionation. This difference will be significant in most magma evolution studies.

Enthalpies of exchange differ between elements. Therefore, the temperature dependencies of different elements are not the same. Consequently, the degree of fractionation between elements will change with temperature. This can be seen by investigating changes in the fractionation "slopes" between elements which have similar chemical properties, such as the REE.

Figure 16 plots log D_m (olivine) for four selected REE. The curves were calculated from the model given in this paper. The temperatures are typical of olivine-liquid assemblages. The lower two temperatures represent a range of basalt compositions at one atmosphere pressure. The higher temperature is typical of peridotitic compositions and/or higher pressures. The trend seen with increasing temperature is an increase in partitioning (D_m) values and a decrease in the steepness of the slope. Though the steepness of the slope increases as temperature decreases, the change with temperature is not great.

Comparisons of Olivine and Orthopyroxene

Over the range of typical basaltic compositions and temperatures in which orthopyroxene is as table liquidus phase, D values for trivalent cations (e.g., Sc) between orthopyroxene and melt vary by nearly an order of magnitude. As Colson et al. (1985) pointed out, this is a considerably greater variation than exhibited by olivine over the same

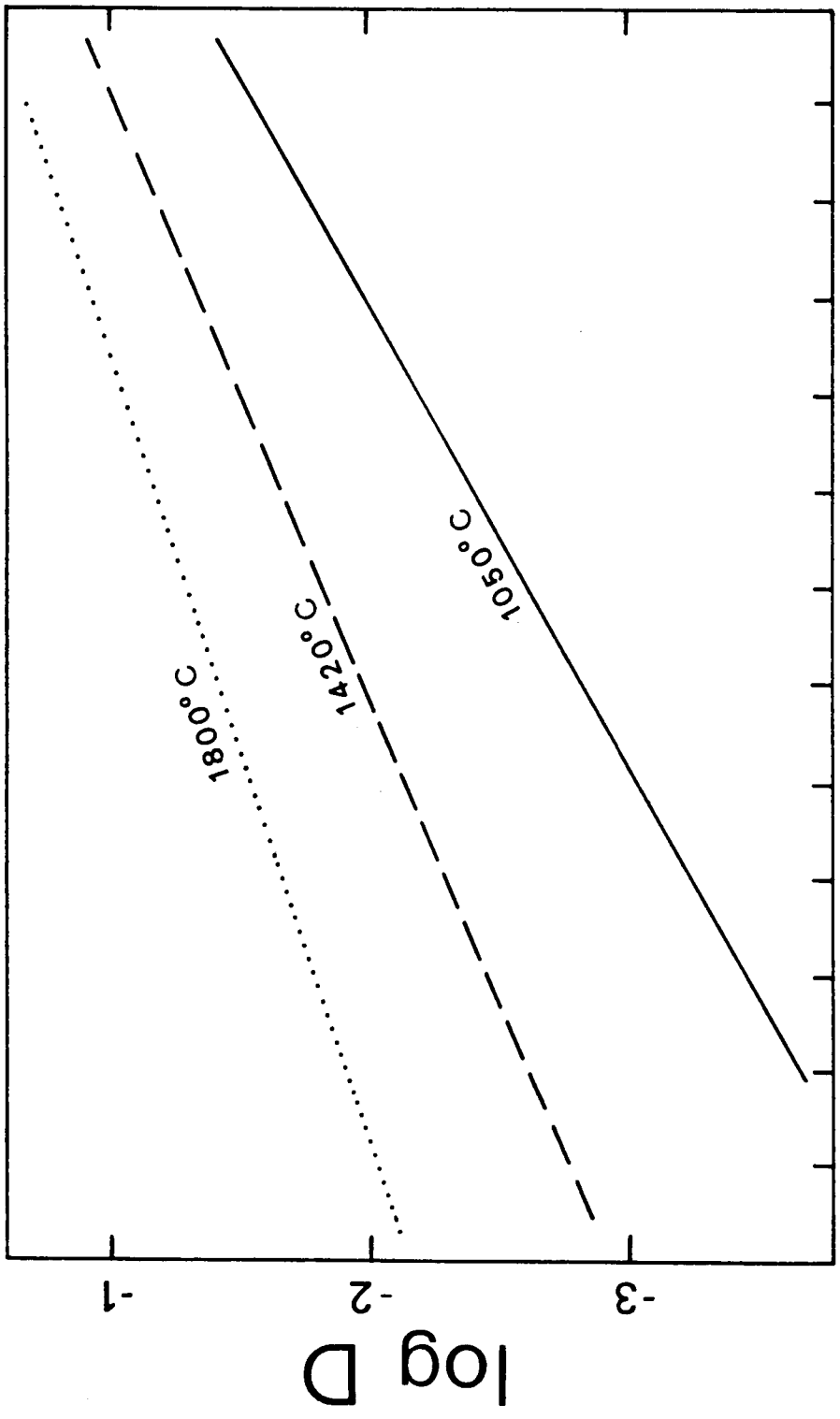

Figure 16. Temperature dependence of the REE pattern slope for olivine/melt partitioning. These slopes are not measured but rather calculated from the equations and data discussed in the text. The slope becomes steeper at lower temperatures. This indicates that olivine will fractionate between REE to a greater degree at low temperature.

T-X range. Colson et al. (1985) noted that the difference in temperature-composition sensitivity does not arise from differences in energies of exchange in the octahedral sites. It probably arises from differences in the type and energy of the coupled substitution. This is confirmed here by the closeness of the B values between olivine and orthopyroxene.

Values for all the regression parameters are nearly the same for olivine and orthopyroxene (tables 7 and 8, pp. 31 and 32). This was expected from the similarities in site coordination. In orthopyroxenes, the ΔH_4 parameter is more sensitive to trace ion size than it is in olivine as illustrated in figure 17. The ΔS_1 term is also more sensitive to cation size (A = -1.58 for olivine, -3.22 for orthopyroxene).

In the preceding sections, many of the energy relations are interpreted on the basis of free energies of reactions and electrostatic potentials. These can also be interpreted on the basis of the edge-sharing nature of adjacent polyhedra. Edge-sharing relations for olivine and orthopyroxene are listed in table 11 (Prewitt, 1980 and Ribbe, 1982). These edge-sharing properties place constraints on the size of polyhedra relative to adjacent polyhedra. For example, consider placing a large trace cation in an octahedral site sharing edges with considerably smaller octahedra. To accommodate the change, the bond angle between small and large octahedra must be distorted into configurations which are less energetically favorable. This offers a conceptual explanation for the tendency of the crystal to reject the larger cations. This also offers an explanation of the ΔH_4 term:

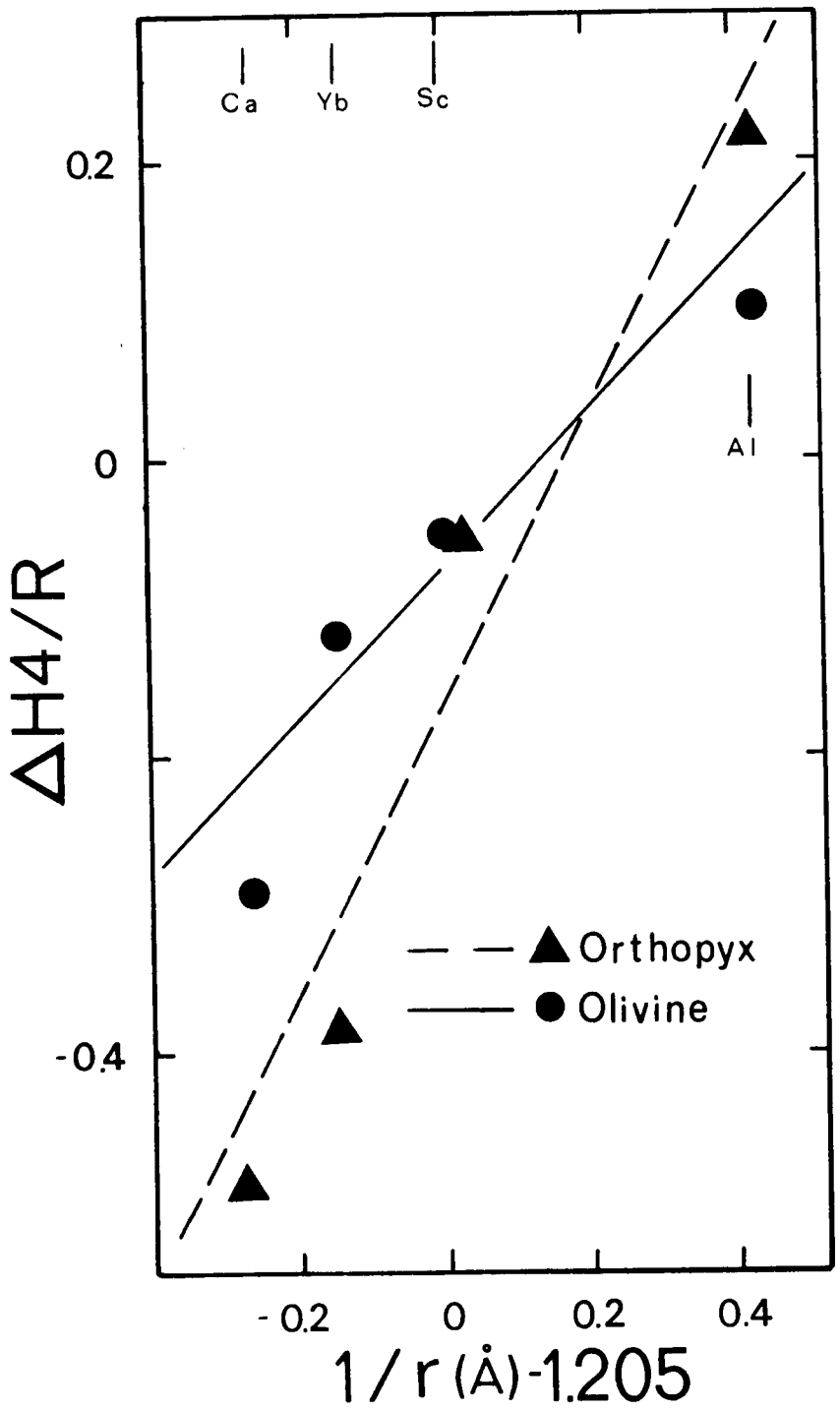

Figure 17. Comparison of the dependence on cation size of the trace element nonideality in olivine to that in orthopyroxene. The dependence of $\Delta H_4/R$ on cation size is much steeper in the orthopyroxene. The coordinate axis plots the change in 1/r between the trace element and the average of Mg and Fe. $\Delta H_4/R$ is the enthalpy change for the reaction expressed in equation 4 divided by the gas constant.

Table 11. Polyhedral edge sharing relationships in orthopyroxene and olivine. Data are from Prewitt (1980) and Ribbe (1982).

Phase	Lattice Site	Number of Shared Edges
Ol:	M1:	2 with M1, 2 with M2, 2 with T
	M2:	2 with M1, 1 with T
	T:	2 with M1, 1 with M2
Opx:	M1:	2 with M1, 3 with M2
	M2:	3 with M1, 1 with TA
	TA:	1 with M2
	TB:	

because of similarities in size, there will be less distortion caused by a shared edge between a large cation and Fe^{+2} than between a large cation and the smaller Mg. In addition, the greater dependence on cation size of orthopyroxene ΔH_4 than olivine ΔH_4 can be explained by the observation that the M2 site in olivine shares two edges with adjacent M1 whereas the M2 site in orthopyroxene shares three edges with adjacent M1.

Al is found to enter the TB site in orthopyroxene. This is interpreted as due to the larger size of the TB site and the absence of shared edges with M2 (Prewitt, 1980; Papike and Ross, 1970). Based on this interpretive premise, we would expect tetrahedral Al to be less energetically favorable in olivine which shares three edges with octahedra, than in orthopyroxene which shares no edges. This offers an explanation for the apparent dominance of the Al-coupled substitution in orthopyroxene, whereas other substitutions appear important in olivine. Using more complex reasoning, an increasing importance of Al coupling in olivine with decreasing cation size can be rationalized. The network of edge sharing around the tetrahedral site in olivine is such that if the size of one of the octahedra is decreased (the trace cation), the effect is to squeeze one of the shared tetrahedral edges. However, the edges shared with the two adjacent octahedra are also squeezed, having the effect of expanding the two edges these octahedra share with the tetrahedron. The overall effect of one squeeze and two expansions is to decrease the energy necessary to put the larger Al in the tetrahedral site. This makes the Al substitution more energetically favorable for the smaller trace cations.

Conclusions

1. Enthalpies of exchange for a large number of elements can be predicted on the basis of a simple ionic model. Much of the information needed by the model can be derived from partitioning data of a single element. This points out the potential of extrapolating from such data to elements and systems not yet investigated.

2. Trivalent cations in olivine are not always charge-balanced by Al on the tetrahedral site. A vacancy substitution is assumed. Al coupling may be more important for smaller trivalent trace cations. In orthopyroxenes, trivalent cations are charge balanced by the coupled substitution of Al for Si in tetrahedral sites.

3. A "ΔH_4" term is derived and interpreted to reflect a local ordering effect in olivine in which the larger trace cations have a tendency to be surrounded by octahedra filled by Fe rather than Mg.

4. Effects of variable redox state (+2 to +3) for trace cations can be modeled by a linear combination of predicted divalent and trivalent partition coefficients.

CHAPTER 3

TRACE ELEMENT REEQUILIBRATION DURING CRYSTAL FRACTIONATION

The igneous petrologist is concerned with formulating a sequence of events which links the chemical trends in a suite of rocks with inferred mechanisms of magma evolution. Many models which have traditionally been invoked to explain chemical trends, such as fractional crystallization, are essentially equilibrium models. Therefore, constraining these models to known phase equilibria allows nonequilibrium effects to be more completely evaluated. This study investigates how well an olivine fractionation model, when constrained by thermodynamic relations, explains trends seen in basaltic suites in which olivine is the major liquidus phase. Two suites of Hawaiian basalts (Rhodes, 1983; Gunn, 1971), a suite of Tertiary basalts from N. E. Greenland (Upton et al., 1984), and Apollo 12 basalts (Compston et al. 1971) are considered. Fractional crystallization models are only partially successful. It is suggested that olivine typically has reequilibrated or partially reequilibrated with the basaltic melt and that "fractionation" trends often represent mechanical olivine mixing or accumulation.

Liquidus temperatures and compositions of the evolving magma are modeled using a computer routine (reported in Appendix D). Major element partitioning (MgO, FeO, SiO_2) between olivine and melt is modeled on the basis of the study of Nielsen and Dungan (1983). Trace element partitioning is modeled on the basis of the present study which is presented in the preceding chapter of this thesis. Activities in the

melt are estimated using a two-lattice mixing model (Bottinga and Weill, 1972). Fe^{+3}/Fe^{+2} ratios are modeled after Sack et al. (1980) assuming the melt is approximately buffered at QFM. A liquidus temperature is calculated for the basalts by computing the highest temperature at which the melt is in equilibrium with olivine. This temperature is calculated from the data of Nielsen and Dungan (1983). Given a fractionation model, both amount and composition of olivine relating a suite of rocks are fixed by thermodynamic relations. Fractional crystallization, batch crystallization, and equilibrium crystallization with mechanical remixing of olivine are modeled. In addition,the computer routine permits selected elements in the olivine to reequilibrate with the melt while others do not.

The liquidus temperature of the basalt is equal to the system temperature at the time the basalt melt was separated from the evolving magma. Therefore, this temperature is linked to the degree of fractionation. Consequently the calculated temperature is a useful coordinate against which to plot chemical variations in the suite of rocks. This has the advantage that the coordinate system does not need to change if different magma evolution models are chosen.

Systematic variations in major elements in the Hawaiian suites are modeled well by assuming a crystal fractionation model (see figures 18-19). This is not surprising considering that Gunn (1971) and Rhodes (1983) interpret these suites to reflect olivine fractionation only. However, this computer modeling imposes the additional constraints that composition and amount of olivine crystallized are known functions of

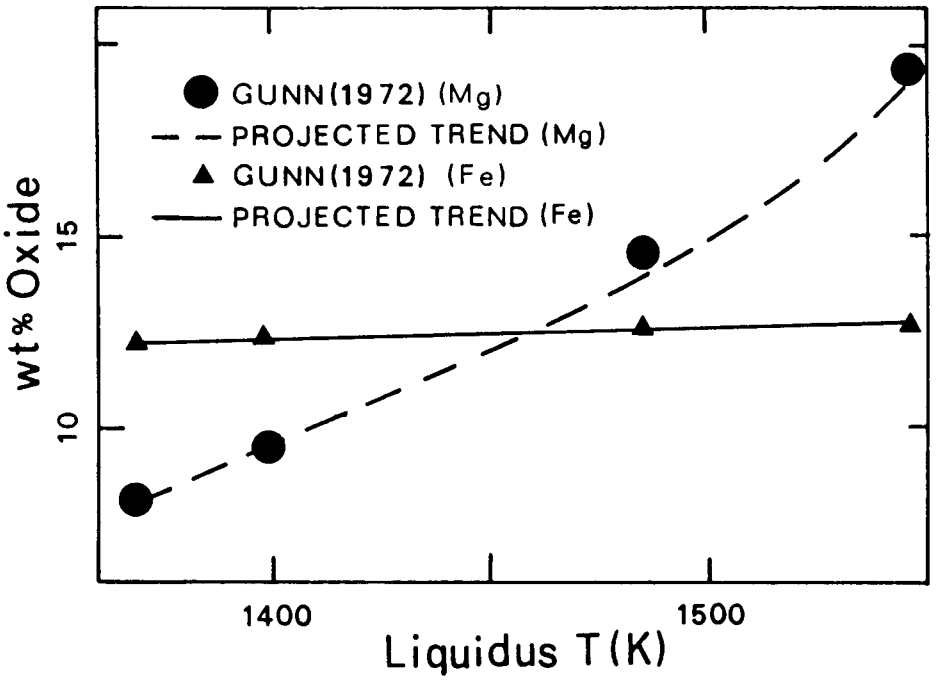

Figure 18. Projected Mg and Fe descent versus observed chemistries of the basaltic suites reported in Gunn (1972).

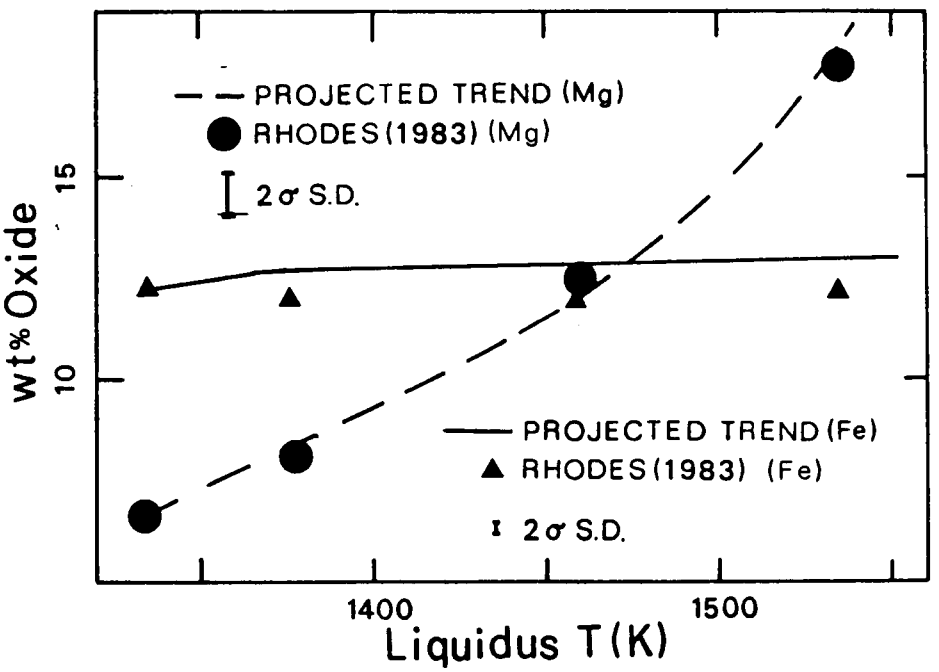

Figure 19. Projected Mg and Fe descent versus observed chemistries of the basaltic suites reported in Rhodes (1983).

temperature. This means that neither olivine composition nor the amount of olivine removed is allowed to vary to achieve a "fit" to the data.

With the exception of Ni, trace elements are also modeled well (see figures 20-23). The variation in Ni concentration cannot be modeled by assuming continuous crystal fractionation. However, the trends can be modeled if Ni is assumed to reequilibrate to the temperature and melt-composition conditions of the lowest temperature basalt in the suite. This is illustrated in figures 24 and 25.

This is similar to the conclusions of Hart and Davis (1978), whose trends in basaltic suites were modeled by olivine accumulation. They observed that Ni-Mg trends in basaltic suites tended to be linear, whereas the trends are expected to be curved based on known thermodynamic relations. They interpreted this to indicate that the suites are not related by continuous fractionation. Instead they are related by the accumulation of olivine of constant composition, in which components have equilibrated to intermediate temperature-composition conditions.

Walker et al. (1976) also inferred olivine accumulation in relating compositions of Apollo 12 basalts reported by Compston et al. (1971). In this study, trends in the Apollo 12 basalts are consistent with fractional crystallization of major elements, but Ni is modeled best by assuming it has reequilibrated (figures 26 and 27).

The possibility that all elements may reequilibrate was considered. However, major elements cannot be modeled by assuming this (figures 28 and 29). It is puzzling why Ni should reequilibrate while Mg and Fe, which have higher diffusion coefficients, do not. This can be explained

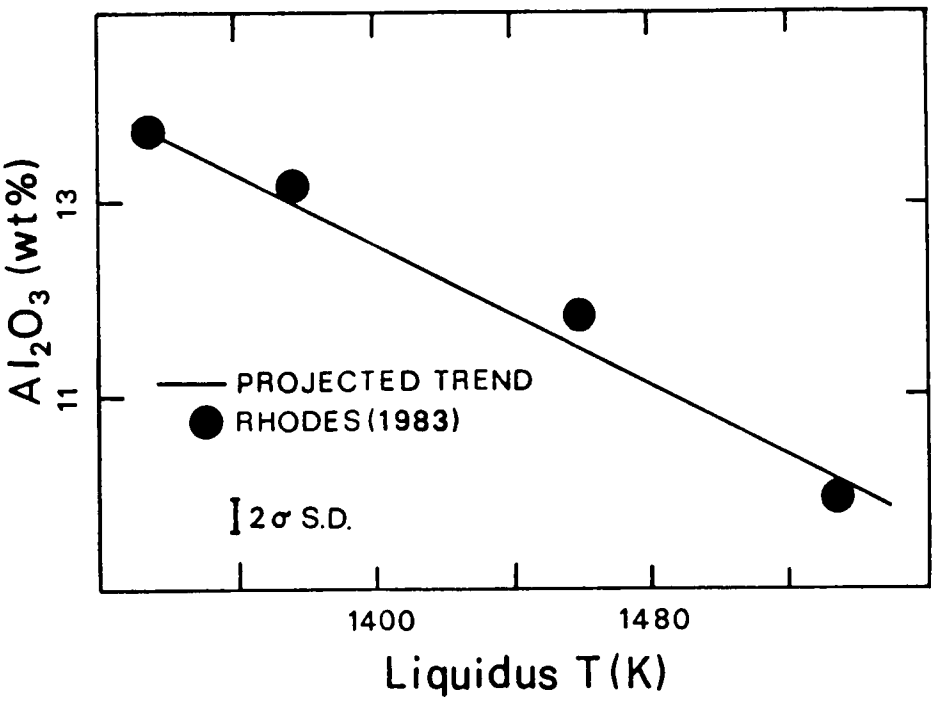

Figure 20. Projected Al descent versus observed chemistries of the basaltic suites reported in Rhodes (1983).

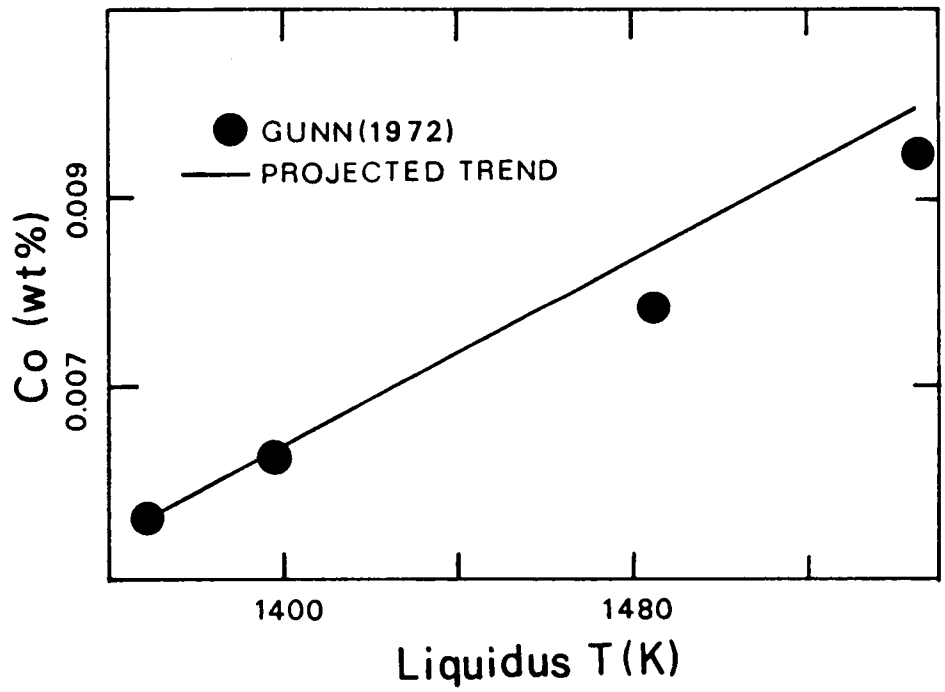

Figure 21. Projected Co descent versus observed chemistries of the basaltic suites reported in Gunn (1972).

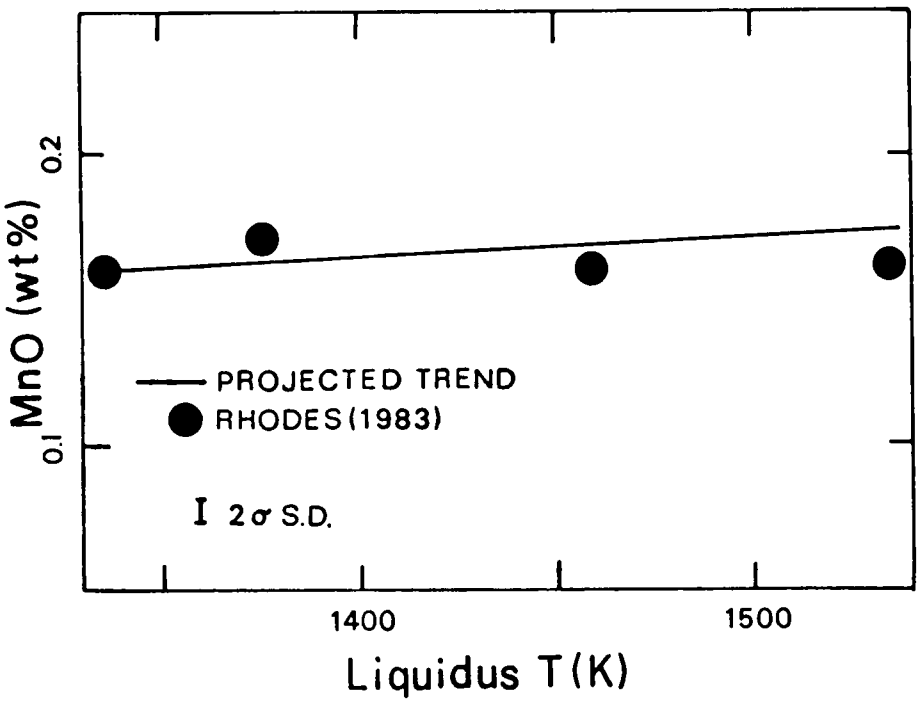

Figure 22. Projected Mn descent versus observed chemistries of the basaltic suites reported in Rhodes (1983).

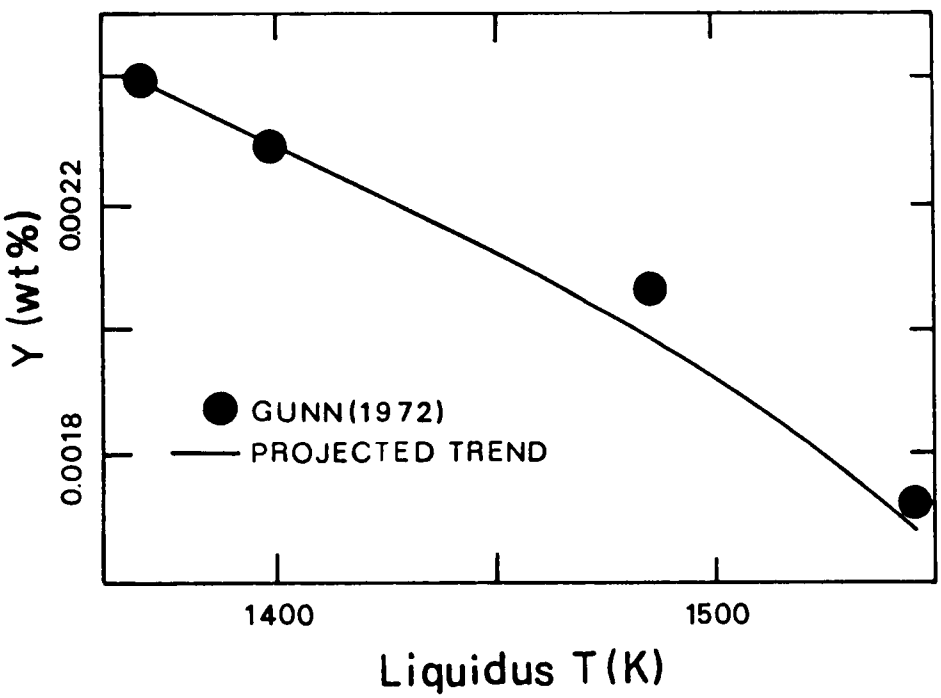

Figure 23. Projected Y descent versus observed chemistries of the basaltic suites reported in Gunn (1972).

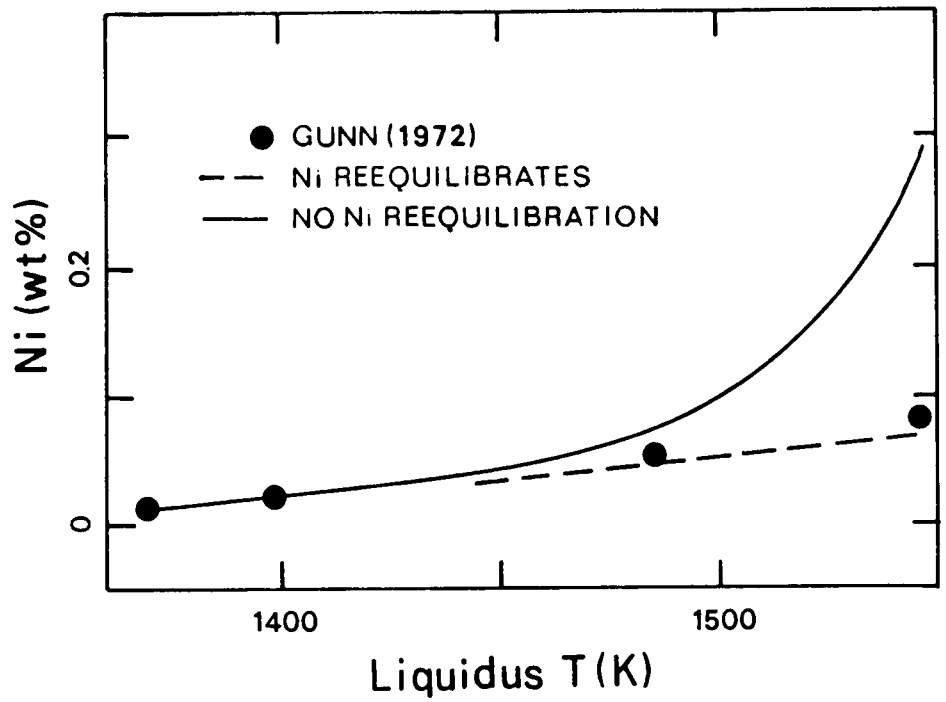

Figure 24. Comparison of Ni descent line assuming Ni is fractionally crystallized to that assuming Ni reequilibrates to the conditions of the lowest temperature basalt of the suite (data from Gunn, 1972).

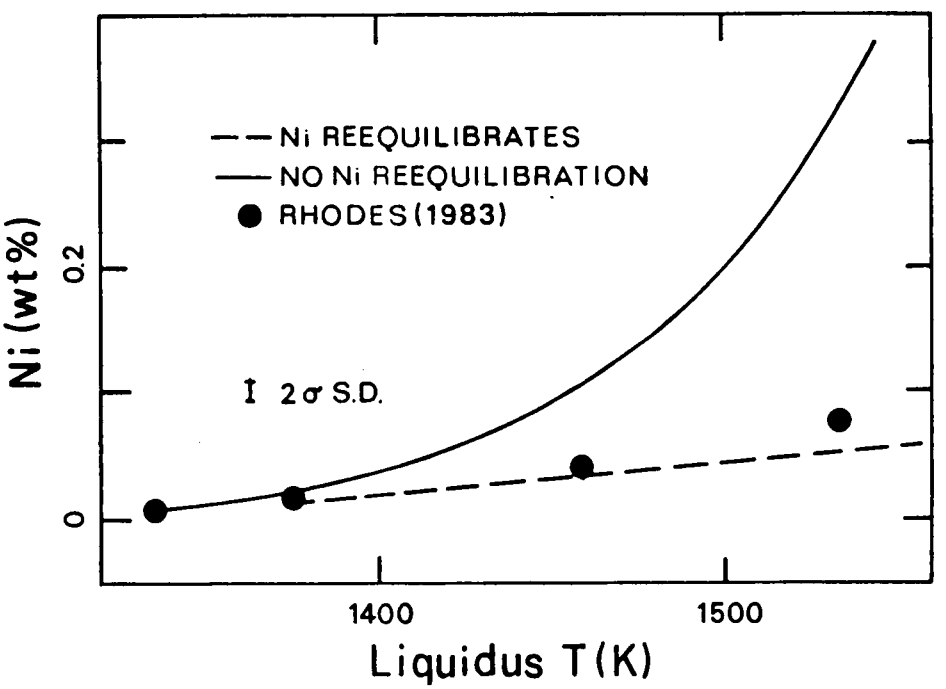

Figure 25. Comparison of Ni descent line assuming Ni is fractionally crystallized to that assuming Ni reequilibrates to the conditions of the lowest temperature basalt of the suite (data from Rhodes, 1983).

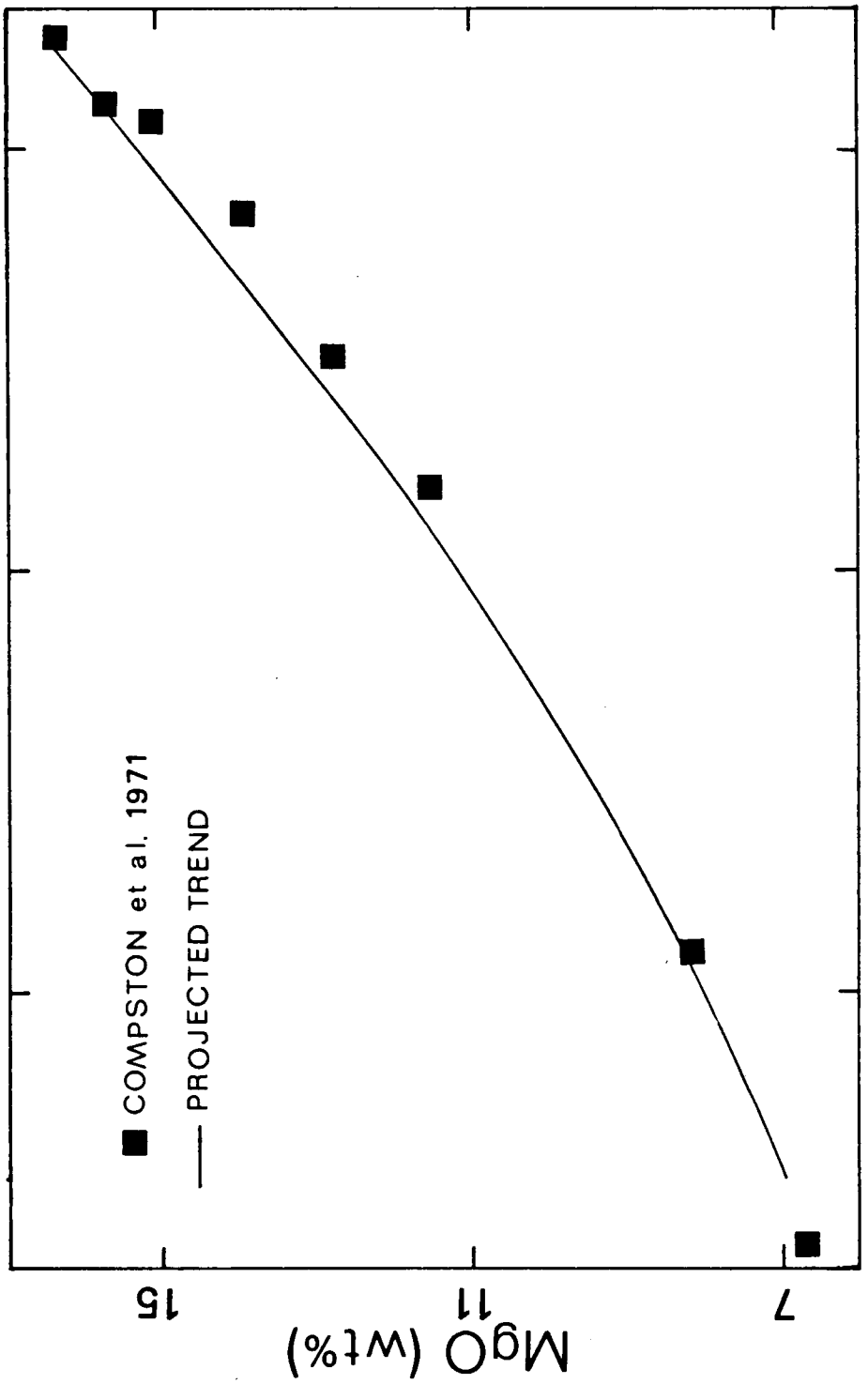

Figure 26. Projected MgO descent versus observed chemistries of the basaltic suites reported in Compston et al. (1971).

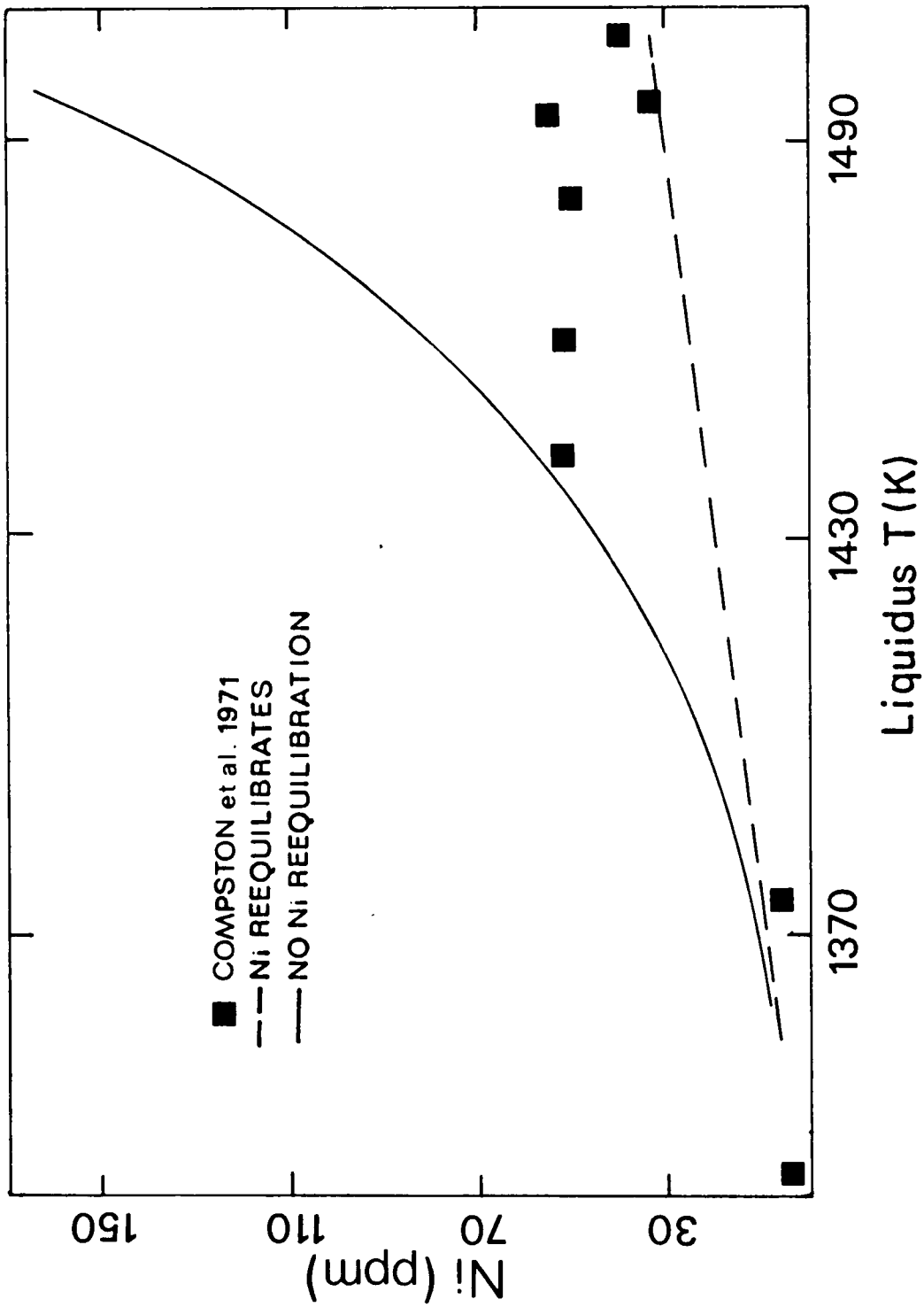

Figure 27. Comparison of Ni descent line assuming Ni is fractionally crystallized to that assuming Ni reequilibrates to the conditions of the lowest temperature basalt of the suite (data from Compston et al., 1971).

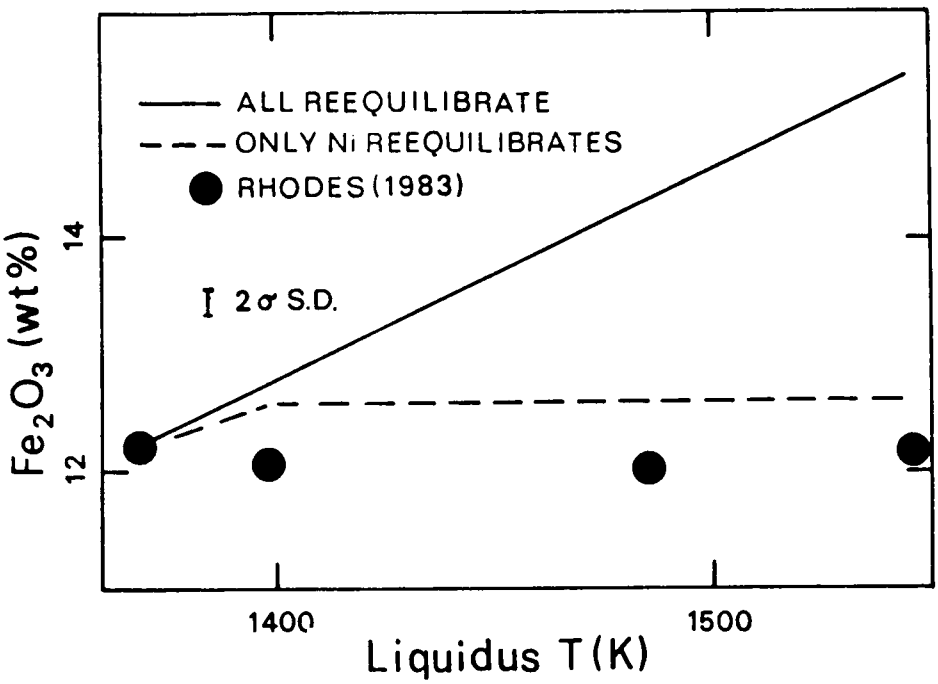

Figure 28. Comparison of projected Mg and Fe lines of descent when all elements reequilibrate to final conditions to the case when all elements continuously fractionally crystallize (data from Rhodes, 1983).

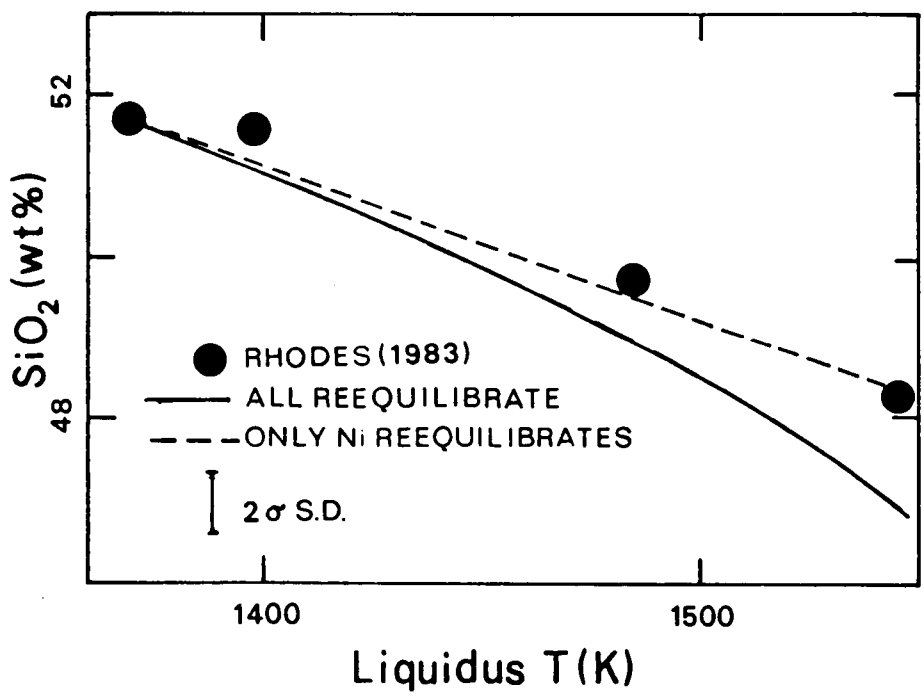

Figure 29. Comparison of projected Si line of descent when all elements reequilibrate to final conditions to the case when all elements continuously fractionally crystallize (data from Rhodes, 1983).

by observing from the equations in the preceding chapter that Ni chemical potential in the olivine relative to the melt is expected to change more with temperature than the chemical potentials of Mg and Fe. This makes the effective concentration gradient of Ni larger and therefore the diffusion rate higher. Trace element trends other than Ni are not sensitive to temperature and composition and so cannot be tested for reequilibration. However, in other basaltic suites, partial equilibration of Ni or complete reequilibration of all elements are possibilities implied by the reequilibration of Ni.

In fact, the chemical variations in the suite of basalts analyzed by (Upton et al., 1984) can only be explained by reequilibration of all the elements. When both major and trace elements are assumed to reequilibrate to conditions of the lowest temperature basalt in the suite, concentrations of all elements are predicted within 5% of the total variation (e.g., figure 30).

The possibility that other phases were present and effected the Ni trends was considered. The two phases most likely to have been in equilibrium with the melt are chromite and an immiscible melt. The amount of chromite removed from the melt can be estimated from the Cr trends in the basaltic suites. This amount is too small to explain the Ni trends. The Ni trends observed in these basaltic suites indicate that Ni was removed from the residual melt less rapidly than expected based only on olivine fractionation. Removal of a Ni-rich immiscible melt would lead to an even more rapid removal of Ni, not the less rapid Ni removal observed. However, removal of a large amount of immiscible

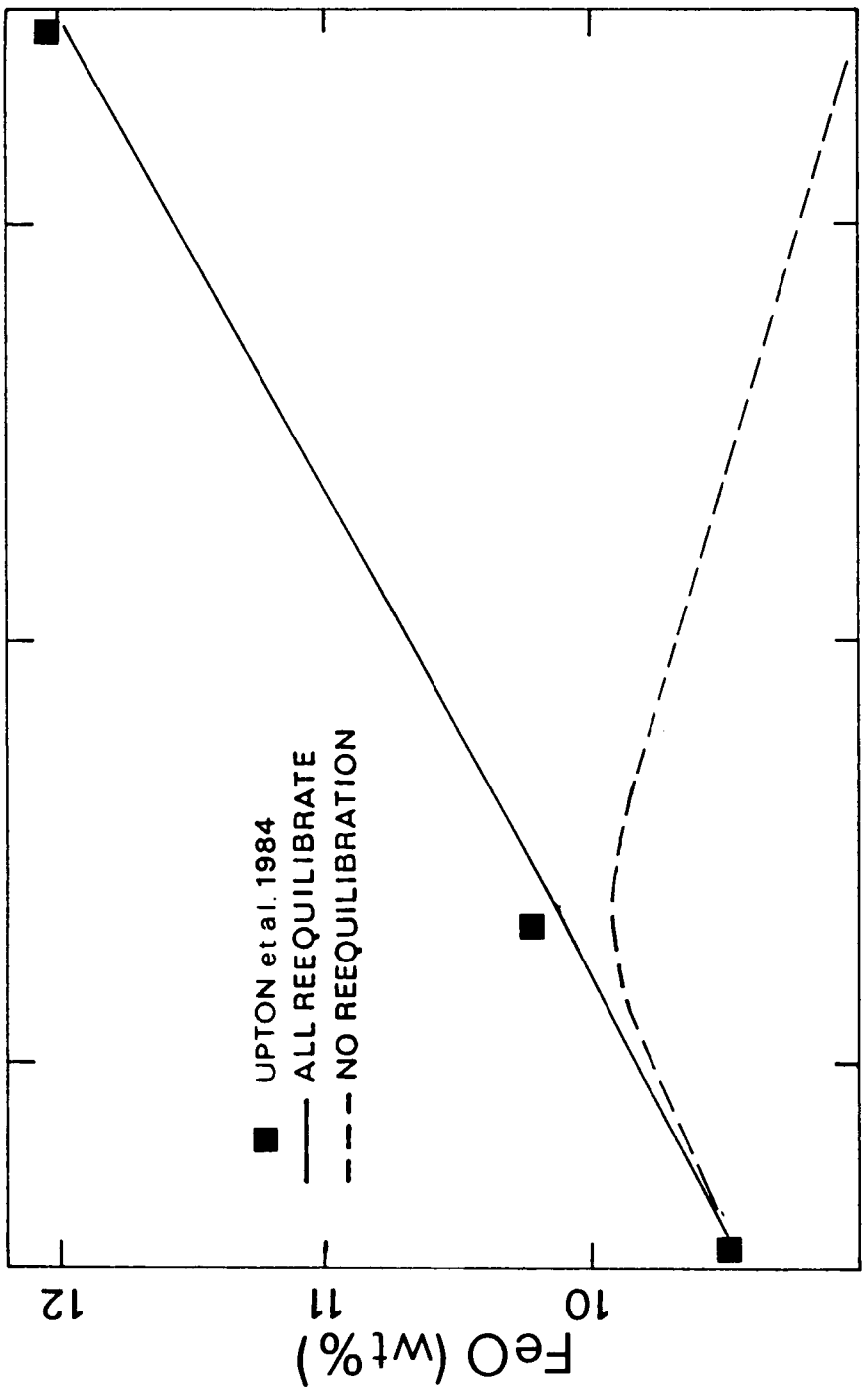

Figure 30. Comparison of projected FeO lines of descent when all elements reequilibrate to final conditions to the case when all elements continuously fractionally crystallize (data from Upton et al., 1984).

melt which is Ni-poor but of nearly the same composition as the parent melt in other elements would also explain the observed trends.

The conclusion reached in this study is that perfect fractional crystallization of olivine cannot explain chemical trends in the basalt suites studied. Some or all trace elements in olivine may reequilibrate with the melt even when major elements do not. Accumulation of equilibrated or partially equilibrated olivine may be more realistic than fractional crystallization. This might explain the success of the use of constant partitioning values in magma modeling studies. It is apparent from this study that rigorous thermodynamics can be useful in yielding additional insights into the nature of mechanisms of magma evolution.

CHAPTER 4

SUMMARY

Previously reported partitioning values between crystal and melt vary by 100% or more for single elements. This is the result of the combined effects of magma composition, temperature, and pressure. This study makes a systematic thermodynamic appraisal of the effects of temperature and composition on olivine/melt and orthopyroxene/melt partitioning. This alleviates the necessity of determining experimentally partitioning in each system of interest. Such modeling yields a better understanding of the nature of trace elements in silicate crystals and melt.

This study also models free energies of trace element exchange between crystal and melt as a function of trace element size. This makes it possible to estimate partitioning of elements which have not been experimentally investigated. In principle, the approach shows promise of being useful in modeling partitioning in other phases and in modeling kinetic processes, a wide applicability in experimental petrology.

Temperature and compositional dependence of partitioning is determined by evaluating the relation $\ln K = -\Delta G/RT$ for each element. This requires knowledge of the terms in the equilibrium constant, K. Therefore, the substitution mechanism must be known. For divalent trace cations in orthopyroxene and olivine, this entails a straightforward substitution of trace cation for divalent octahedral cations. However,

trivalent trace cation substitutions are complicated by charge balance restrictions. In orthopyroxene, an Al-Si coupled substitution on a tetrahedral site appears to charge balance trivalent trace cations. In olivine, at least two substitution mechanisms appear to be important: (1) a vacancy substitution ($n\square + 2nM^{+3} = 3nM^{+2}$) which is dominant for the larger cation substitutions, and (2) an Al-Si coupled substitution which is dominant for small trace cations.

In both olivine and orthopyroxene there is a tendency for Fe cations to congregate around large trace cations. The apparent nonidealities arising from this local ordering of Mg and Fe are modeled on the basis of differences in the Mg-Fe exchange energies between trace-cation-associated sites and normal octahedral sites. This interpretation offers both a conceptual explanation for the nonideality and a mathematical formulation for the dependence of the activity coefficient on temperature and composition.

Both ΔS and ΔH vary systematically with trace cation size. The variation of ΔH is modeled by formulating an expression for the change in lattice energy when the trace cation substitutes for Mg in olivine or orthopyroxene. This expression is of the form:

$$\Delta U = k(\Delta(Z^{+}Z^{-}/d^{2}))-L(\Delta(\exp(d/p)))$$

where Z = charge, d = internuclear distance, p = repulsion parameter, U = internal energy $\approx \Delta H$, and k and L are constants.

Application of these partition coefficients, which vary with temperature and pressure, to basaltic suites from Hawaii, Greenland, and

the Moon, reveal that in real petrologic systems the effective partition coefficients often do not vary with temperature and composition. It is inferred that elements in olivine often reequilibrate with the melt and that a fractional crystallization model may not be realistic. More realistic may be a model in which reequilibrated olivine is mechanically mixed or accumulated in a magma.

Visions of the Future

Results of this study can be applied to magma evolution studies. The main contribution to the realm of magma modeling is to allow confident constraints to be placed on equilibrium elemental distributions between phases. With equilibrium partitioning well constrained, the effects of other processes on magma composition can be investigated more readily.

However, the major contribution of this study is in the establishment of a model by which partitioning data can be synthesized. The ionic model used in this study simply and accurately models the energy relations of trace components in olivine, orthopyroxene, and melt. In future work, data for other phases might be synthesized by this model. A focus on determination of repulsion parameters for trace elements will make possible estimation of ΔH values for substitution of the trace element into any particular site in any phase of known structure. This will allow accurate modeling of trace element partitioning for all elements and phases based only on data from a few experiments.

Also, the approach is applicable to more than just partitioning studies. A similar approach has been adopted in recent work by Miyamoto

and Takeda (1980, 1983) and Miyamoto et al. (1982). Miyamoto and Takeda use the known crystal structure of olivine and derived repulsion parameters to compute ionic potentials for various cations on olivine sites. They are currently using these parameters to model intracrystalline partitioning and diffusion.

It is hoped that the approach demonstrated in this study will make possible a synthesis of the great amounts of data available in partitioning and related studies and provide a base for improving subsequent experiments.

BIBLIOGRAPHY

BIBLIOGRAPHY

Albarede, F. and Bottinga, Y., 1972, Kinetic disequilibrium in trace element partitioning between phenocrysts and host lava: Geochim. Cosmochim. Acta, v. 36, pp. 141-156.

Apted, M. F. and Boettcher, A. L., 1981, Partitioning of rare earth elements between garnet and andesite melt: an autoradiographic study of P-T-X effects: Geochim. Cosmochim. Acta, v. 45, pp. 827-837.

Atkins, P. W., 1978, Physical Chemistry: Oxford Univ. press, W. H. Freeman and Co., San Francisco.

Banno, S., and Matsui, Y., 1973, On the formulation of partition coefficients for trace elements distribution between minerals and magma: Chem.Geol., v. 11, pp. 1-15.

Benjamin, T., Heuser, W. R., Burnett, D. S., and Seitz, M. G., 1980, Actinide crystal-liquid partitioning for clinopyroxene and $Ca_3(PO_4)_2$: Geochim. Cosmochim. Acta, v. 42, pp. 1251-1264.

Bliznakov, G. and Dragonova, D., 1975, Distribution of cadmium and Ni vions in ammonium chloride at various temperatures and supersaturations and constant ratio of cocrystallization components: Sofii Univ. Khim. Fak. v. 66, pp. 415-431.

Bottinga, Y. and Weill, D. F., 1972, The viscosity of magmatic silicate liquids: a model for calculation: Am. Jrnl. Sci., v272, pp. 438-475.

Bowen, N. L., Schairer, J. F., and Posnjak, E., 1933, The system Ca_2SiO_4-Fe_2SiO_4: Am. Jrnl. Sci., v. 26, pp. 273-297.

Brown, G. E., 1970, The crystal chemistry of olivines: Ph.D. thesis, Virginia Polytechnic Institute and State University, Blacksburg, Virginia.

Buseck, P. R. and Veblen, D. R., 1978, Trace elements, crystal defects and high resolution electron microscopy: Geochim. Cosmochim. Acta, v. 42, pp. 669-678.

Colson, R. O., McKay, G. A., and Taylor, L. A., 1985, A model for trace element partitioning: orthopyroxene and melt: Lunar and Planetary Sci. XVI, Lunar and Planetary Inst., Houston, pp. 146-147.

Colson, R. O., Taylor, L. A., and McKay, G. A., 1984, REE between olivine and melt: a proposed substitution mechanism (abstr.): Lunar and Planetary Sci. XV, Lunar and Planetary Inst., Houston, pp. 178-179.

Cohen, M. L., 1981, Pseudopotentials and crystal structure: in O'Keefe, M. and Navrotsky, A. (eds.), Structure and Bonding in Crystals, pp. 25-48.

Compston, W., Berry, H., Vernon, M.J., Chappell, B. W., and Kaye, M. J., 1971,Rb-Sr chronology and chemistry of lunar material from the Ocean of Storms, Proc. Lunar Sci. Conf. 2nd, pp. 1471-1485.

Denbigh, K., 1963, The Principles of Chemical Equilibrium, Cambridge.

Donaldson, C. H., Williams, R. J., and Lofgren, G. E., 1975, A sample holdjB D^{J} trocedure: Geochim. Cosmochim. Acta, v. 42, pp. 679-683.

Drake, M. J. and Holloway, J. R., 1981, Partitioning of Ni between olivine and silicate melt: The "Henry's Law problem" reexamined: Geochim. Cosmochim. Acta, v. 45, pp. 431-437.

Drake, M. J. and Weill, D. F., 1972, New rare earth element standards for electron microprobe analysis: Chem. Geol., v. 10, pp. 179-181.

Drake, M. J., and Weill, D. F., 1975, Partition of Sr, Ba, Ca, Y, Eu^{+2}, Eu^{+3}, and other REE between plagioclase feldspar and magmatic liquid: an experimental study: Geochim. Cosmochim. Acta, v. 39, pp. 689-712.

Duke, J. M., 1976, Distribution of the period four transition elements among olivine, calcic clinopyroxene, and mafic silicate liquid: experimental results: Jrnl. of Pet., v. 17, pp. 499-521.

Ford, C. E., Russell, D. G., Craven, J. A., and Fisk, M. R., 1983, Olivine-liquid equilibria: temperature, pressure and composition dependence of the crystal/liquid cation partition coefficents for Mg, Fe^{2+}, Ca and Mn: Jrnl. of Pet., v. 24, pp. 256-265.

Freer, R., 1981, Diffusion in silicate minerals and glasses: a data digest andguide to the literature: Contr. Min. Pet., v. 76, pp. 440-454.

Fujimaki, H. and Tatsumoto, M., 1984a, Partition coefficients of Hf, Zr, and REE between ilmenite and liquid (abstr): Lunar and Planetary Science XV, Lunar and Planetary Inst, Houston, pp. 282-283.

Fujimaki, H. and Tatsumoto, M., 1984b, Partition coefficients of Hf, Zr, and REE between zircon, apatite, and liquid and their inferences to lunar granite petrogenesis (abstr): Lunar and Planetary Science XV, Lunar and Planetary Inst, Houston, pp. 280-281.

Gamble, R. P. and Taylor. L. A., 1980, Crystal/liquid partitioning in augite: effects of cooling rate: Earth Planet. Sci. Lett., v. 47, pp. 21-33.

Goldschmidt, V. M., 1937, The principle of distribution of chemical elements in minerals and rocks: Jrnl. Chem. Soc., pp. 655-672.

Green, D. H., Ringwood, A. E., Warc, N. G., Hibberson, W. D., Major, A., and Kiss, E., 1971, Experimental petrology and petrogenesis of Apollo 12 basalts: Proceedings Second Lunar Sci. Conf., pp. 601-615.

Green, T. H. and Pearson, N. J., 1983, Effect of pressure on rare earth elment partion coefficients in common magmas: Nature, v. 305, pp. 414-416.

Grove, T. L., 1981, Use of FePt alloys to eliminate iron loss problems in latm gas mixing experiments: theoretical and practical considerations: Contr. Min. Pet., v. 78, pp. 298-304.

Gunn, B. M., 1971, Trace element partition during olivine fractionation of Hawaiian basalts: Chem. Geol., v. 8, pp. 1-13.

Harrison, W. A., 1980, Electronic structure and the properties of solids, Freeman, San Francisco, California.

Harrison, W. J., 1978, Rare earth element partitioning between garnets, pyroxenes, and melts at low trace element concentrations: Carnegie Inst. Wash. Yearbook, v. 77, pp. 682-689.

Harrison, W. J., 1979a, An experimental investigation of the partitioning of aREE, Sm^{+3}, between garnets and melts at high pressures and temperatures: Progress in expermental petrology fourth progress report of research supported by NERC, pp. 59-67.

Harrison, W. J., 1979b, An experimental investigation of the partitioning of rare earth elements between garnets and liquids at high pressure and temperature with particular reference to nonHenry's Law behavior: Ph.D. thesis, Univ. of Manchester, England.

Harrison, W. J., 1981, Partitioning of REE between minerals and coexisting melts during partial melting of garnet lherzolite: Am. Min., v. 66, pp. 242-259.

Harrison, W. J. and Wood, B. J., 1982, An experimental investigation of the partitioning of REE between garnet and liquid with reference to the role of defect equilibrium: Contr. Min. Pet., v. 72, pp. 145-155.

Hart, S. R. and Davis, K. E., 1978, Nickel partitioning between olivine and silicate melt: Earth and Planet. Sci. Lett., v. 40, pp. 203-220.

Hazen, R. M., 1977, Effects of temperature and pressure on the crystal structure of ferromagnesian olivine: Am. Min., v. 62, pp. 286-295.

Hazen, R. M. and Finger, L. W., 1981, Module structure variation with temperature, pressure, and composition: a key to the stability of modular structures: in O'Keefe M. and Navrotsky A. (ed), Structure and Bonding in Crystals Vol. 2, pp. 109-116.

Henderson, P. and Williams, C. T., 1979, Variations in trace element partition (crystal/magma) as a function of crystal growth rate: Phys. Chem. Earth, v. 11, pp. 191-198.

Hervig, R. L. and Smith, J. V., 1984, Petrogenesis and crystallographic implications of minor and trace element content of lherzolite minerals (abstr.): Trans. Am. Geophys. Union, v. 65, p. 286.

Hodder, A. P. W., 1983, Cationic environments in hydrothermal silicate systems: determination from partition coefficients: Jrnl. Colloid and Interface Science, v. 91, pp. 294-297.

Hofmann, A. W. and Margaritz, M., 1977, Diffusion of Ca, Sr, Ba, and Co in a basalt melt: implications for the geochemistry of the mantle: Jrnl. Geophys. Res., v. 82, pp. 5432-5440

Holloway, J. R. and Drake, M. J., 1977, Quantitative microautoradiography by X-ray emission microanalysis: Geochim. Cosmochim. Acta, v. 41, pp. 1395-1397.

Huheey, J. E., 198?, Inorganic Chemistry: Principles of Structure and Reactivity, 3rd ed., Harper and Row, Cambridge.

Hume Rothery, W. and Raynor, G. V., 1954, The structure of metals and alloys, 3rd ed., The Institute of Metals, London.

Hurlbut, C. S. and Klein, C., 1977, Manual of Mineralogy after James D. Dana, 19th ed., John Wiley and Sons, New York.

Irving, A. J., 1978, A review of experimental studies of crystal/liquid trace element partitioning: Geochim. Cosmochim. Acta, v. 42, pp. 743-770.

Irving, A. J. and Frey, F. A., 1977, Experimental partitioning of trace elements between garnet and hydrous acidic melt, (abstr.): in papers presentedto the International Conference on Experimental Trace Element Geochemistry, pp. 59-61.

Irving A. J. and Frey, F. A., 1978, The distribution of trace elements between garnet megacrysts and volcanic liquids of kimberlitic to rhyolitic composition: Geochim. Cosmochim. Acta, v. 42, pp. 771-787.

Irving, A. J., Singleton, D. E., and Merrill, R. B., 1978, Partitioning of rare earth elements among armalcolite, ilmenite, and mare basalt liquid (abstr.): Lunar and Planetary Sci. IX, pp. 570-572.

Jones, J. H., 1984, Temperature- and pressure-independent correlations of olivine/liquid partition coefficients and their application to trace element partitioning: Contr. Min. Pet., v. 88, pp. 126-132.

Kerrick, D. M. and Darken, L. S., 1975, Statistical thermodynamic models for ideal oxide and silicate solid solutions, with application to plagioclase: Geochim. Cosmochim. Acta, v. 39, pp. 1431-1442.

Kern, R. and Weisbrod, A., 1967, Thermodynamics for Geologists, Freeman Cooper and Co., San Francisco.

Kittel, C., 1976, Introduction to Solid State Physics, 5th edition, John Wiley and Sons, New York.

Kring, D. A. and McKay, G. A., 1984, Chemical gradients in glass adjacent to olivine in experimental charges and Apollo 15 green glass vitrophyres (abstr.): Lunar and Planetary Science IV, Lunar and Planetary Inst., Houston, pp. 461-462.

Krivandina, E. A. and Kostyleva, E. E., 1973, Effect of the temperature gradient on the nature of impurity distribution during the growth of crystals from a melt: Kristallografiya, v. 18, pp. 885-887.

Lager, G. A., and Meagher, E. P., 1978, High temperature structural study of six olivines: Am. Min., v. 63, pp. 365-377.

Leeman, W. P., 1974, Experimental determination of partitioning of divalent cations between olivine and basaltic liquid: Ph.D. thesis, Univ. of Oregon.

Leeman, W. P., 1979, Partitioning of Pb between volcanic glass and coexisting sanidine and plagioclase feldspars: Geochim. Cosmochim. Acta, v. 43, pp. 171-175.

Levin, E. M., Robbins, C. R., and McMurdie, H. F., 1964, Phase diagrams for ceramists: The American Ceramic Society Inc.

Lindstrom, D. J., 1976, Experimental study of the partitioning of the transition metals between clinopyroxene and coexisting silicate liquids: Ph.D. thesis, Univ. of Oregon.

Lindstrom, D. J., 1983, Kinetic effects on trace element partitioning: Geochim. Cosmochim. Acta, v. 47, pp. 617-622.

Long, P. E., 1978, Experimental determination of partition coefficients for Rb, Sr, and Ba between alkali feldspar and silicate liquid: Geochim. Cosmochim. Acta, v. 42, pp. 833-846.

Lumpkin, G. R., Ribbe, P. H., and Lumpkin, N. E., 1983, Composition, order-disorder, and lattice parameters of olivines: determinative methods for Mg-Mn and Mg-Ca silicate olivines: Am. Min., v. 68, pp. 1174-1182.

McIntire, W. L., 1963, Trace element partition coefficients-a review of theory and application to geology: Geochim. Cosmochim. Acta, v. 39, pp. 621-634.

McKay, G. A., 1981, Experimental REE partitioning between olivine and Apollo 12 olivine basaltic liquids (abstr.): EOS, Trans. Am. Geophys. Union, v. 62,p. 1070.

McKay, G. A., 1982, Partitioning of REE between olivine, plagioclase, and synthetic baslatic melts: implications for the origin of lunar anorthosites (abstr.): Lunar and Planetary Sci. XII, Lunar and Planetary Inst., Houston, pp. 493-494.

McKay, G. A., 1986, Crystal/liquid partitioning of REE in basaltic systems: extreme fractionation of REE in olivine: Geochim. Cosmochim. Acta, January, inpress.

McKay, G. A. and Seymour, R. S., 1982, Electron microprobe analysis of trace elements in minerals at 10ppm concentrations: in Heinrich, K. (ed.), Microbeam Analysis 1982, Proc. 17th Annual Conference Microbeam Analytical Society, pp. 431-434.

McKay, G., Wagstaff, J., and Yang, F-R., 1986, Zirconium, hafnium, and rare earth element partition coefficients for ilmenite and other minerals in high-Ti lunar mare basalts: an experimental study: Proc. 16th Lunar Sci. Conf., in press.

McKay, G. A. and Weill, D. F., 1976, Petrogenesis of KREEP: Proc. Seventh Lunar Sci. Conf., pp. 2427-2447.

McKay, G. A. and Weill, D. F., 1977, KREEP petrogenesis revisited: Proc. Eighth Lunar Sci. Conf., pp. 2339-2355.

Melikhov, I. V., Nebylitsyn, B. D., and Rudin, V. N., 1975, Study of the surface structure of barium sulfate crystals in aqueous solution: Sov. Phys. Crystallogr., v. 19, pp. 521-524.

Miyamoto, M. and Takeda, H., 1980, An interpretation of the structures of mantle minerals at high pressure in terms of ionic forces: Geochem. Jrnl., v. 14, pp. 243-248.

Miyamoto, M. and Takeda, H., 1983, Atomic diffusion coefficients calculated for transition metals in olivine: Nature, v. 303, pp. 602-603.

Miyamoto, M., Takeda, H., Fujino, K., and Takéuchi, Y., 1982, The ionic compressibilities and radii estimated for some transition metals in olivine structures: Min. Jrnl., v. 11, pp. 172-179.

Morlotti, R. and Ottonello, G., 1984, The solution of trace amounts of Sm in forsterite olivine: an experimental study by EMF galvanic cell measurements: Geochim. Cosmochim. Acta, v. 48, pp. 1173-1181.

Morris, R. V., 1975, Electron paramagnetic resonance study of the site preference of Gd^{+3} and Eu^{+3} in polycrystalline silicate and aluminate minerals: Geochim. Cosmochim. Acta, v. 39, pp. 621-634.

Morse, S. A., 1984, Cation diffusion in plagioclase feldspars: Science, v. 225, pp. 504-505.

Mukhopadyay, D. K. and Lindsley, D. H., 1983, Phase relations in the join Kirschteinite ($CaFeSiO_4$)-Fayalite (Fe_2SiO_4): Am. Min., v. 68, pp. 1089-1094.

Mysen, B. D., 1975a, Rare earth partitioning between crystals and liquid in the upper mantle: Carnegie Inst. Wash. Yearbook, v. 74, pp. 656-659.

Mysen, B. D., 1975b, Nickel partitioning between upper mantle crystals and partial melts as a function of pressure, temperature, and nickel concentration: Carnegie Inst. Wash. Yearbook, v. 74, pp. 662-668.

Mysen, B. D., 1978a, Experimental determination of rare earth element partitioning between hydrous silicate melt, amphibole and garnet peridotitie menerals at upper mantle pressures and temperatures: Geochim. Cosmochim. Acta, v. 42, pp. 1253-1263.

Mysen, B. D., 1978b, Limits of solution of trace elements in minerals according to Henry's Law: A review of experimental data: Geochim. Cosmochim.Acta, v. 42, pp. 871-885.

Mysen, B. D. and Kushiro, I., 1979, The effect of pressure on the partitioning of nickel between olivine and aluminosilicate melt: Earth Planet. Sci. Lett., v. 42, pp. 383-389.

Mysen, B. D. and Seitz, M. G., 1975, Trace element partitioning determined by Beta track mapping: An experimental study using carbon and samarium as examples: Jrnl. Geophys. Res., v. 80, pp. 2627-2635.

Mysen, B. D. and Virgo, D., 1980, Trace element partitioning and melt structure: an experimental study at 1 atm pressure: Geochim. Cosmochim. Acta, v. 44, pp. 1917-1930.

Mysen, B. D., Virgo, D., and Kushiro, I., 1981a, Distribution of aluminum between structural units in silicate melts: Carnegie Inst. Wash. Yearbook, v. 80, pp. 304-305.

Mysen, B. D., Virgo, D., and Kushiro, I., 1981b, The structural role of aluminum in silicate melts-a Raman spectroscopic study at 1 atmosphere: Am. Min., v. 66, pp. 678-701.

Mysen, B. D., Virgo, D, and Seifert, F. D., 1982, The structure of silicate melts: implications for chemical and physical properties of natural magmas: Rev. Geophys. and Space Phys., v. 20, pp. 353-383.

Nabelek, P. I., 1980, Nickel partitioning between olivine and liquid in natural basalts: Henry's Law behavior: Earth and Plant. Sci. Lett., v. 48, pp. 293-302.

Nagasawa, H., 1966, Trace element partition coefficient in ionic crystals: Science, v. 165, pp. 767-769.

Nagasawa, H., Schreiber, H. D., and Morris, R. V., 1980, Experimental mineral/liquid partition coefficients of the Rare Earth Elements (REE), Sc, and Sr for perovskite, spinel, and melilite: Earth and Planet. Sci.Lett., v.46, pp. 431-437.

Naney, M. T., 1983, Iron redox kinetics in silicate liquids (abstr.): GSA abstracts, p. 650.

Nash, W. P. and Crecraft, H. R., 1985, Partition coefficients for trace elements in silicic magmas, Geochim. Cosmochim. Acta, v. 49, pp. 2309-2322.

Nathan, H. D. and VanKirk, C. K., 1978, A model of magmatic crystallization: Jrnl. of Pet., v. 19, pp. 66-94.

Navrotsky, A., 1978, Thermodynamics of element partitioning: (1) Systematics of transition metals in crystalline and molten sislicates and (2) Defect chemistry and "The Henry's Law problem": Geochim. Cosmochim. Acta, v. 42, pp. 887-902.

Navrotsky, A., Hon, R., Weill, D. F., and Henry, D. S., 1980, Thermochemistry of glasses and liquids in the system $CaMgSi_2O_6$-$CaAl_2Si_2O_8$- $NaAlSi_3O_8$, SiO_2-$CaAl_2Si_2O_8$-$NaAlSi_3O_8$, and SiO_2-Al_2O_3-CaO-Na_2O: Geochim. Cosmochim. Acta, v. 44, pp. 1409-1423.

Nicholls, I. A. and Harris, K. L., 1980, Experimental rare earth element partition coefficients for garnet, clinopyroxene, and amphibole coexisting with andesitic and basaltic liquids: Geochim. Cosmochim. Acta, v. 44, pp. 287-308.

Oestrike, R. and Kirkpatrick, R. J., 1984, Silicate glass structure in the system anorthite-diopside-forsterite: a high resolution solid state NMR study(abstr.): Trans. Am. Geophys. Union, v.65, p. 286.

O'Keefe, M., 1981, Some aspects of the ionic model of crystals: in O'Keefe, M.and Navrotsky, A. (eds.), Structure and Bonding in Crystals, Vol. 1, pp. 299-322.

O'Nions, R. K. and Powell, R., 1977, The thermodynamics of trace element distribution: in Fraser, D. G. (ed.), Thermodynamics in Geology, pp. 349-363.

Onken, H., 1965, Verfeinerung der kristall struktur von monticellite: Tschermak's Mineral. Petrogr. Mitt., v. 10, pp. 34-44.

Onuma, N., Higuchi, H., Wakita, H., and Nagasawa, H., 1968, Trace element partitioning between two pyroxenes and the host lava: Earth Planet. Sci. Lett., v. 5, pp47-57.

Papike, J. J. and Ross, M., 1970, Gedrites: crystal structures and intracrystalline cation distributions: Am. Min., v. 55, pp. 1945-1972.

Petersen, J., 1986, Jrnl. of Pet., in press.

Phillips, J. C., 1973, Bonds and Bands in Semiconductors: Academic Press, New York.

Phillips, J. C., 1981, Quantum theory and crystal chemistry: in O'Keefe, M. and Navrotsky, A. (eds.), Structure and Bonding in Crystals, pp. 25-48.

Pierozynski, W. J., 1977, The effects of varying bulk composition on the partitioning of Sr, Ba, and Rb between alkali-feldspar and coexisting silicate liquid (abstr.): Papers presented to the International Conference on Experimental Trace Element Geochemistry, pp. 98-99.

Philpotts, J. A., 1978, The law of constant rejection: Geochim. Cosmochim. Acta, v. 42, pp. 909-920.

Prewitt, C. T. (ed.), 1980, Reviews in Mineralogy vol. 7: Pyroxenes, Min. Soc. Am.

Räuber, A., 1976, Doping modulation by electric currents in lithium niobate during crystal growth: Mat. Res. Bull., v. 11, pp. 497-502.

Ray, G. L., Shimuzu, N., and Hart, S. R., 1983, An ion microprobe study of partitioning of trace elements between clinopyroxene and liquid in the system diopside-albite-anorthite: Geochim. Cosmochim. Acta, v. 47, pp. 2131-2140.

Rhodes, J. M., 1983, Homogeneity of lava flows: chemical data for historic Mauna Loan eruptions: Proc. 13th Lunar Sci. Conf., Jrnl. Geophys. Res. v. 88 supplement, pp. A869-A879.

Ribbe, P. H. (ed.), 1982, Reviews in Mineralogy, Vol. 5: Orthosilicates, Min. Soc. Am.

Ribbe, P. H. (ed.), 1983, Reviews in Mineralogy, Vol. 2: Feldspar Mineralogy, Min. Soc. Am.

Sack, R. O., Carmichael, I. S. E., Rivers, M., and Ghiorso, M. S., 1980, Ferric-ferrous equilibria in natural silicate liquids at 1 bar: Contr. Min. Pet., v. 75, pp. 369-376.

Sato, Motoaki, 1971, Electrochemical measurements and control of oxygen fugacity and other gaseous fugacities with solid electrolyte sensors: in Ulmer, G. C. (ed.), Research Techniques for High Pressure and High Temperature, pp. 43-49.

Schaefer, M. W., 1985, Site occupancy and two-phase character of "ferrifayalite": Am. Min., v. 70, pp. 729-736.

Schreiber, H. D. and Haskin, L. A., 1976, Chromium in basalts: Experimental determination of redox states and partitioning among synthetic silicate phases: Proc. seventh Lunar Sci. Conf., pp. 1221-1259.

Seifert, F., Mysen, B. O., and Virgo, D., 1981, Structures and properties of aluminum silicate melts with three-dimensional network structure: Carnegie Inst. Wash. Yearbook, v. 80, pp. 305-308.

Shannon, R. D. and Prewitt, C. T., 1969, Effective ionic radii in oxides and fluorides: Acta Crystallogr., Sect. B, 25, p. 925-946.

Shimuzu, N., 1974, An experimental study of the partitioning of K, Rb, Cs, Sr, and Ba between clinopyroxene and liquid at high P: Geochim. Cosmochim. Acta, v. 38, pp. 1789-1798

Shimuzu, N. and Kushiro, I., 1975, The partitioning of rare earth elements between garnet and liquid at high pressures: preliminary experiments: Geophys. Res. Lett., v. 2, pp. 413-416.

Shimuzu, N., Sangen, K, and Masuda, A., 1982, Experimental study on rare-earthelement partitioning in olivine and clinopyroxene formed at 10 and 20kb for basaltic systems: Geochim. Jrnl., v. 16, pp. 107-117.

Steele, I. M. and Lindstrom, D. J., 1981, Ni partitioning between diopside and silicate melt: a redetermination by ion microprobe and recognition of an experimental complication: Geochim. Cosmochim. Acta, v. 45, pp. 2177-2183.

Stosch, H. G.,1982, Rare earth element partitioning between minerals from anhydrous spinel peridotite xenoliths: Geochim. Cosmochim. Acta, v. 46, pp. 793-811.

Takahashi, E, 1978, Partitioning of Ni^{+2}, Co^{+2}, Fe^{+2}, Mn^{+2}, and Mg^{+2} between olivine and silicate melts: compositional dependence of partition coefficients: Geochim. Cosmochim. Acta, v. 42, pp. 1829-1845.

Terakado, Y. and Masuda, A., 1983, Kinetic effect of rare-earth element partitioning in the diopside-melt system: an experimental observation: Chem. Geol., v. 40, pp. 13-23.

Tosi, M., 1964, Cohesion of ionic solids in the Born model: Solid State Physics, v. 16.

Tsang, T., Philpotts, J. A., and Yin, L., 1978, Trace element partitioning between ionic crystal and liquid: Jrnl. Phys. Chem. Solids, v. 39, pp. 439-442.

Upton, B. G. J., Emeleus, C. H., and Beckinsale, R. D., 1984, Petrology of the northern east Greenland Tertiary flood basalts: Evidence from Hold with Hope and Wollaston Forland, Jrnl. of Pet., v. 25, pp. 151-184.

Veblen, D. R. (ed.), 1981, Reviews in Mineralogy vol. 9A: Amphiboles and other Hydrous Pyriboles--Mineralogy, Min. Soc. Am.

Volfinger, M., 1976, Effet dela température sur les distributions de Na, Rb, et Cs entre la sanidine, la muscovite, la phlogopite et une solution hydrothermale sous une pression de 1 kbar: Geochim. Cosmochim. Acta, v. 40, pp. 267-282.

Volfinger, M. and Robert, J. L., 1980, Structural controls of the distribution of trace elements between silicates and hydrothermal solutions: Geochim. Cosmochim. Acta, v. 44, pp. 1455-1461.

Walker, D., Longhi, J., Kirkpatrick, R. J., and Hays, J. F., 1976, Differentiation in an Apollo 12 picrite magma, Proc. Lunar Sci. Conf. 7th, pp. 1365-1389.

Walsh, D., Donnay, G., and Donnay, J. D. H., 1976, ordering of transition metal ions in olivine: Canadian Min., v. 14, pp. 149-150.

Watson, E. B., 1977, Partitioning of manganese between forsterite and silicateliquid: Geochim. Cosmochim. Acta, v. 41, pp. 1363-1374.

Watson, E. B. and Green, T. H., 1981, Apatite/liquid partition coefficients for the rare earth elements and strontium: Earth and Planet. Sci. Lett., v.56, pp. 405-421.

Weill, D. F. and McKay, G. A., 1975, The partitioning of Mg, Fe, Sr, Ce, Sm, Eu, and Yb in lunar igneous systems and a possible origin of KREEP by equilibrium partial melting: Proc. 6th Lunar Sci. Conf., pp. 1143-1158.

Williams, R. J. and Mullins, O., 1981, JSC systems using solid ceramic oxygen electrolyte cells to measure oxygen fugacities in gas-mixing systems: NASA technical memorandum 58234.

Whittaker, E. J. W. and Muntus, R., 1970, Ionic radii for use in geochemistry: Geochim. Cosmochim. Acta, v. 34, pp. 945-956.

Wood, B. J., 1976, Samarium distribution between garnet and liquid at high pressure: Carnegie Inst. Wash. Year Book, v. 75, pp. 659-668.

Zhizhong, P., 1980, A discussion on order-disorder of deficiency in the seriesof fayalite-ferrifayalite crystal structure and its genesis: Acta Geol. Sinica, v. 2, pp. 1-10.

APPENDICES

APPENDIX A

PROCEDURES FOR PREPARATION OF BASALTIC GLASS

A synthetic glass of basaltic composition can be generated by the proper proportional mixing of five basic components: Mg, Fe, Al, Ca, and Si. Compounds typically used in mixing are either the oxides or carbonates of these metals, and are listed MgO, Fe_2O_3, Al_2O_3, $CaCO_3$, SiO_2.* Although it is possible to use different compounds or compound combinations, these are chosen to minimize problems with weight percent calculation, hydration, oxidation, and the general production or acquisition of the compound. In addition, it is useful to consider the crystal state of the compound to be used, since a very stable configuration would not dissolve in the melt as readily as a higher energy crystal. Therefore, it would be ideal to have Al_2O_3 in the γ-Al_2O_3 state rather than as corundum and SiO_2 as α-crystobalite, as these are less stable forms which dissolve more readily. The techniques for production and dehydration of these basic compounds are outlined below, along with procedures for the homogeneous mixing of the predetermined composition and the preparation of the synthetic basaltic glass. Many of these procedures are summarized in figure A1.

---

*If K_2O and Na_2O are required, they are added as carbonates and prepared in a manner similar to $CaCO_3$. TiO_2 is added as TiO_2; it is prepared like Fe_2O_3 since it will develop a defect solution if heated to too high a temperature. Ni, Cr, Mn, etc., are added as oxides: again, they are prepared like Fe_2O_3. Finally if P is to be added, the Na or K should (at least in part) be added as their phosphates. They are prepared like $CaCO_3$.

	MgO	Fe_2O_3	Al_2O_3	$CaCO_3$	SiO_2
	500°C-- 6 hrs	350°C-- 6-12 hrs	500°C-- 6 hrs	300°C to 500°C	500°C-- 6 hrs
	750°C-- 6 hrs		700°C-- 6-12 hrs	6-12 hrs	heat in small amounts until reaches total
	1000°C-- 6 hrs				750°C-- 6 hrs
	1300°C-- 12 hrs				1000°C-- 12 hrs

Day 1:					
8:00 a.m.	Lindberg at 500°C	Thermolyne at 350°C	Lindberg at 500°C	Thermolyne at 350°C	Lindberg at 500°C (add in increments)
4:00 p.m.	Lindberg to 700°C				
Day 2:					
8:00 a.m.	Lindberg to 1000°C	Remove to desiccator; turn off Thermolyne	Remove to desiccator		Lindberg to 1000°C
8:00 p.m.	Lindberg to 1300°C				Remove to desiccator

Day 3:
8:00 a.m. Remove to desiccator--cool Lindberg to 500°C.
Weigh and mix desired composition.
4:00 p.m. Heat mixture in Pt-Au crucible in Lindberg at 500°C.

Day 4:
8:00 a.m. Turn Lindberg to 750°C.
2:00 p.m. Turn Lindberg to 1000°C.

Day 5:
8:00 a.m. Turn to melting temperature desired.
12:00 p.m. Remove and quench--regrind-remix-repeat melting twice more.

Figure A1. An efficient schedule for preparing a basaltic glass using a high-temperature Lindberg furnace (500-1500°C) and a lower-T Thermolyne furnace (200-700°C).

The appropriate compounds should be gathered--typically MgO, Fe_2O_3, $CaCO_3$, $AlCl_3 \cdot (H_2O)_6$, and silicic acid (although Al_2O_3 (corundum)and quartz could be used if correspondingly greater difficulty in getting a good mixture is acceptable)--as well as appropriate mixing, grinding, and drying vessels and utensils. Such equipment should be reserved exclusively for that single compound with which it is used.

Approximate amounts to be weighed out initially for each of the compounds should be calculated based on the final bulk composition desired. This is done in order to minimize wasted effort and chemicals. To minimize the inevitable weighing errors, these amounts should also be concordant with a final mixture of 10-20 g. Since there will be an inevitable loss of material in the succeeding process and dehydration will result in significant weight changes, exact measurements are rather futile at this stage.

Once these compounds have been weighed in the approximate proportions ultimately desired, it is necessary that $AlCl_3 \cdot (H_2O)_6$ and silicic acid be converted to the desired forms (γ-Al_2O_3 and α-crystobalite). All the compounds must be dehydrated so water content will not confuse the weighing process. This requires the use of furnaces with available temperature ranges from 300°C to 1300°C. (Depending on the targeted composition, it may be necessary to go somewhat higher than this when melting the mixture later.) Here, the process will be described with the use of a Lindberg furnace with temperature ranges of 500°C to 1500°C and a smaller Thermolyne furnace with a lower temperature range. Since the preparation process for each of the compounds differs slightly, each will be described separately.

The first consideration is the relative tendency to hydrate. MgO has a very strong tendency and so it should be dried last. The general order of tendency to hydrate from greatest to least is MgO, Fe_2O_3, Al_2O_3, $CaCO_3$, SiO_2. This is the reverse order of drying. (It is also the ideal order in which to do the final weighing.) Also, it is advisable to heat the powders slowly, in stages from lower temperatures. This is done for two reasons: to prevent "explosion" of the compounds from rapid release of volatiles and to minimize the number of times the furnace must be opened when at the higher temperatures. Safety precautions must be taken with the furnaces, especially at the higher temperatures when considerable radiation is generated in the furnace. Use of asbestos gloves and a face mask with a radiation shield for the eyes is essential as is the use of tongs to move the compound-containing vessel in and out of the furnace.

The silicic acid must be dehydrated and converted to α-crystobalite before it is weighed. This is done with a silica crucible and the Lindberg furnace. Initially, only small charges (1 gm) are heated so that gases can escape. Start heating the crucible of silicic acid at a lower temperature (about 500°C) and heat for about 30 minutes. Remove the crucible and add more silicic acid; repeat the process until the desired amount of silicic acid has been dehydrated. Then move the temperature to about 1000°C and heat for another 12 hours. This completes the conversion to dehydrated crystobalite. As with all the following compounds, it is necessary to get the chemical into a dessicator before there is a significant uptake of H_2O from the air.

Carefully take the crucible from the furnace and allow to cool to a few hundred degrees before placing in an aluminum desicator. If the dessicator is glass, the crucible must be allowed to cool further. Alternatively, you may wish to turn the furnace to a lower temperature before removing the crucible and allow it to cool in the furnace to avoid taking the compound containing the crucible from the furnace at the higher temperatures.

The $CaCO_3$ should be heated to between 300°C and 500°C. This is just high enough to effect dehydration but not so high as to decomposed the compound. The CO_2 must be retained until the final weighing is complete so that the final weight percent will not be thrown off. A corundum crucible and the Thermolyne furnace can be used at these lower temperatures.

In order to decompose the $AlCl_3 \cdot (H_2O)_6$ compound to γ-Al_2O_3 and to dehydrate it, the compound must be heated to approximately 700°C. It should be heated in several stages in a corundum crucible, and again precautions should be taken in using the Lindberg furnace. The decomposition releases HCl gas; the room must be well ventilated and exposure to the fumes should be kept to a minimum.

Due to the tendency of Fe_2O_3 to contaminate everything with which it is used, vessels and utensils should be expressly reserved only for this compound. A corundum crucible of Fe_2O_3 is heated to approximately 350°C to drive off water. Additional heating (to much beyond 500°C) results in the production of maghemite, which would cause problems in weighing because the stoichiometry of the compound is variable.

MgO must be heated to 1300°C to effect dehydration, so it is necessary to use a Pt crucible. As is the case with the other compounds, it should be placed in an aluminum desicator as soon as it is cool enough. Because of MgO's strong tendency to hydrate, this is especially important.

Before beginning to weigh out compounds, the amounts needed should be calculated and expressed as a fraction of MgO. This will allow the absolute amount of MgO to vary without changing the precalculated amounts wanted of the other compounds. This eliminates tedious, time-consuming weighing of MgO while it soaks up water from the air. Since, in weighing the compounds, some of the material may stick to the paper used in weighing, it is more accurate to determine the weight of the paper after weighing the total. Also, during the final fusion of the material to be done later, Fe_2O_3 tends to be absorbed into the precious metal crucible used in the final fusions. Adding approximately 5% (of the total Fe_2O_3 in the final mix) more Fe_2O_3 than is actually wanted offsets this effect. However, in general, it is not necessary to get an exact composition glass, and extremely precise weighing may be more work and take more time than it is worth.

The compounds are weighed out in the desired proportions, beginning with MgO, and then ground under acetone with an agate grinder. It is convenient to dump the compounds directly into the agate mortar once they are weighed. Before use, the grinder should be cleaned by grinding quartz sand and acetone in it for a few minutes.) To minimize losses, the agate should not be cleaned again until after all grinding steps

with this composition are completed. This mixture is then ground with acetone until mixed thoroughly (about 20 minutes),dried in air, and placed in an Au-Pt alloy crucible for melting in the Lindberg furnace. Melting temperatures typically are between 1300°C-1400°C, but the mixture should be heated gradually in order to allow gases from the breakdown of $CaCO_3$ to escape and to allow any residual acetone to burn off. Starting at 500°C, the crucible could be placed on the furnace lip to allow acetone to ignite and burn. The crucible is left at 500°C for 6-12 hours. The temperature should be increased in 200-250°C increments and the mixture left at each temperature for 6-12 hours. Molten mixtures rich in Fe will have a tendency to "crawl out" of the crucible due to surface tension effects. This can be offset somewhat by a higher gold content in the crucible. However, for high-Fe mixtures, it should be recognized that a significant portion of the mixture may be lost, and that a tight lid may be welded onto the crucible by the crawling silicate melt.

The mixture is left at the final melting temperature (1200-1400°C) for 12 hours, whereupon it is taken from the furnace and quenched by plunging the crucible into a basin about half full of water. A lid on the crucible will prevent the freeqing melt from popping out of the crucible. (The lid also prevents contamination of the material from furnace insulation that might fall in while the crucible is still in the furnace.) The glass inside will crack and shatter to the point where over 90% can be removed by a simple tap on the base. Attempting to scrape out the glass not only consumes time but scratches and dents the

surface, resulting in greater problems the next time the crucible is used. This glass is then crushed, reground, remixed, and remelted.

The process outlined above is repeated two more times to insure a homogeneous mixture. A small portion of the glass powder should be examined optically in immersion oil to insure complete melting is occurring. After all crushing and grinding operations for the composition are completed, the agate grinder should be cleaned with sand; all other tools should be cleaned appropriately. A piece of the resulting glass can then be analyzed to determine the "true" composition, and the rest of the glass powdered for use in the experiments to be run. If adjustments to the composition or additions of minor and trace components are required, these can be added to the glass powder and the material re-fused either as small batches or a large batch as required by the experiment.

The mixtures used in this study are reported in tables A1 and A2.

Table A1. Bulk compositions of starting materials. These compositions were mixed in various proportions and trace elements were added for each experiment. All are fused to insure an homogeneous mixture except 75% MgO end, 50% MgO end, and Olivine field mix.

Mixture	(grams)	Analysis	(wt%)	Mixture	(grams)	Analysis	(wt%)
	MgO end				FeO-MgO end		
SiO_2	6.085g	SiO_2	49.44	SiO_2	5.599g	SiO_2	46.23
MgO	1.800g	MgO	13.86	MgO	1.113g	MgO	9.13
$CaCO_3$	2.913g	CaO	13.16	$CaCO_3$	2.148g	CaO	9.81
Al_2O_3	2.955g	Al_2O_3	23.31	Al_2O_3	2.197g	Al_2O_3	17.90
				Fe_2O_3	2.237g	FeO	16.63
	75% MgO end				50% MgO end		
SiO_2	0.874g	SiO_2	46.23	SiO_2	0.864g	SiO_2	47.01
MgO	0.238g	MgO	9.13	MgO	0.215g	MgO	11.30
$CaCO_3$	0.399g	CaO	9.81	$CaCO_3$	0.373g	CaO	11.24
Al_2O_3	0.405g	Al_2O_3	17.90	Al_2O_3	0.3809	Al_2O_3	20.61
Fe_2O_3	0.084g	FeO	16.63	Fe_2O_3	0.168g	FeO	8.70
	A				B		
SiO_2	4.101g			SiO_2	4.654g		
MgO	0.984g			MgO	1.757g		
$CaCO_3$	1.138g			$CaCO_3$	1.218g		
Al_2O_3	1.157g			Al_2O_3	1.242g		
Fe_2O_3	1.681g			Fe_2O_3	0.736g		
	C				D		
SiO_2	3.121g			SiO_2	3.290g		
MgO	0.982g			MgO	1.599g		
$CaCO_3$	0.330g			$CaCO_3$	0.323g		
Al_2O_3	0.345g			Al_2O_3	0.331g		
Fe_2O_3	1.674g			Fe_2O_3	0.670g		
	Olivine field mix						
SiO_2	0.465g						
MgO	0.273g						
Fe_2O_3	0.546g						
FeO-MgO end	1.000g						

Table A2. Bulk compositions of individual experiments. Weighing uncertainties for trace elements are as large as 100% of the weighed value.

Mixture	Grams	Mixture	Grams
68Yb		78Yb	
FeO-MgO end	0.07939	50% MgO end	0.07894
Yb_2O_3	0.0017	Yb_2O_3	0.00183
79aYb		79bYb	
FeO-MgO end	0.25425	FeO-MgO end	0.07922
Yb_2O_3	0.00519	Yb_2O_3	0.0008
79Sm		79Gd	
FeO-MgO end	0.23047	FeO-MgO end	0.22838
Sm_2O_3	0.01086	Gd_2O_3	0.00466
80Gd		81Yb	
FeO-MgO end	0.22835	FeO-MgO end	0.25425
Gd_2O_3	0.00466	Yb_2O_3	0.00519
82Gd		85Yb	
50% MgO end	0.07193	50% MgO end	0.08095
Gd_2O_3	0.00147	Yb_2O_3	0.00165
85Gd		85Sm	
50% MgO end	0.07838	50% MgO end	0.07212
Gd_2O_3	0.0016	Sm_2O_3	0.00339
89Yb		90Yb	
50% MgO end	?	MgO end	0.07507
Yb_2O_3	?	SiO_2	0.002
		MgO^2	0.00133
		Yb_2O_3	0.0016
92Yb		94Yb	
75% MgO end	0.05984	Ol field mix	0.0782
Yb_2O_3	0.00122	Yb_2O_3	0.00176
94Gd		99Sm	
Ol field mix	0.07187	50% MgO end	0.07761
Gd_2O_3	0.00147	Sm_2O_3	0.00345
101aYb		101bYb	
Ol field mix	0.07204	Ol field mix	0.07506
Yb_2O_3	0.00117	Yb_2O_3	0.00053
		TiO_2	0.00229

Table A2. (continued)

Mixture	Grams	Mixture	Grams
103		104	
A	0.0748	B	0.0822
Yb_2O_3	0.00057	Yb_2O_3	0.0006
Gd_2O_3	0.00067	Gd_2O_3	0.0008
Sm_2O_3	0.00062	Sm_2O_3	0.0007
105		106a	
C	0.0805	B	0.082
Yb_2O_3	0.0006	C	0.0826
Gd_2O_3	0.0006	Gd_2O_3	0.0012
Sm_2O_3	0.0005	Sm_2O_3	0.0014
106b		107b	
106a mix	0.0774	A	0.03968
Yb_2O_3	0.0008	B	0.04365
		Yb_2O_3	0.0009
		Gd_2O_3	0.0005
		Sm_2O_3	0.0006
108a		108b	
A	0.0779	108a mix	0.0809
C	0.0901	Yb_2O_3	0.0005
Gd_2O_3	0.0017		
Sm_2O_3	0.0016		
109		110a	
A	0.085	B	0.0804
Yb_2O_3	0.0004	Yb_2O_3	.000
Gd_2O_3	0.0005	Gd_2O_3	.000
Sm_2O_3	0.0006	Sm_2O_3	0.0007
111a		111b	
MgO end	0.0507	MgO end	0.0513
FeO-MgO end	0.0498	FeO-MgO end	0.0505
NiO	0.0007	ZnO	0.0003
$AgNO_3$	0.0022	ZrO	0.0023
Y_2O_3	0.0009	$Sr(NO_3)_2$	0.0126
Eu_2O_3	0.0013		
Co_3O_4	0.001		
112a		112b	
FeO-MgO end	0.0838	FeO-MgO end	0.0769
$Sr(NO_3)_2$	0.0076	Sc_2O_3	0.0005
NiO	0.0002		
CoO	0.0004		
Sc_2O_3	0.0006		

Table A2. (continued)

Mixture	Grams	Mixture	Grams
113a		113b	
B	0.0398	B	0.039
D	0.0393	D	0.0394
Yb_2O_3	0.0004	Gd_2O_3	0.0005
Sm_2O_3	0.0006	NiO	0.0004
114a,b		115a,b	
MgO end	0.08059	C	0.0799
FeO-MgO end	0.0801	D	0.0815
Yb_2O_3	0.0012	Gd_2O_3	0.0001
Sc_2O_3	0.0008	Sm_2O_3	0.0009
		Sc_2O_3	0.0003
117a,b		118a,b	
A	0.0804	D	0.1612
D	0.0819	Yb_2O_3	0.0006
Yb_2O_3	0.0006	Gd_2O_3	0.0013
Gd_2O_3	0.0013	Sm_2O_3	0.0016
Sm_2O_3	0.001	Sc_2O_3	0.0005
Sc_2O_3	0.0013		
119a,b		120a	
B	0.1625	A	0.0402
Yb_2O_3	0.0009	B	0.041
Gd_2O_3	0.0038	Gd_2O_3	0.0025
Sm_2O_3	0.002	NiO	0.0013
Sc_2O_3	0.0012	Sc_2O_3	0.0007

APPENDIX B

PROCEDURES FOR Fe-PLATING Pt LOOPS

Solution of thermodynamic equations and determination of energy parameters in experimental systems is most readily accomplished when the system can be considered closed to mass transfer. However, experimental "basaltic" systems can potentially lose material to the Pt loop or capsule which suspends the sample in the furnace. Since the mass transfer reaction is of the form $M^{+2}_{melt} + 2e^{-} = M_{Pt}$ the amount of material lost to the Pt loop is a function of the elemental oxidation potential as well as the solubility of the element in Pt. Due to the difficulty in reducing Al^{+3}, Ca^{+2}, Si^{+4}, and Mg^{+2} under basaltic conditions these ions are not lost from the charge to any significant extent. However, the more readily reduced Fe and Ni may be lost to the Pt. Iron loss is especially critical since it is a major component of basaltic systems. This loss of mass from the experimental charge can be minimized by presaturating the Pt loop with respect to the components involved. This can be done in two ways.

1. A sample chemically identical to the planned experimental charge is placed in the furnace at the same T, P, and fO_2 as is planned for the actual experiment and allowed to equilibrate. The sample is quenched and dissolved from the loop with HF, leaving a "saturated" loop which can be used in the experiment.
2. Iron, the major element lost to the Pt, can be electroplated onto the loop in the appropriate amount and allowed to homogenize in the Pt by diffusion during annealing.

The latter technique was used in this study and is described here.

Given the T, fO_2, and composition of the experimental charge, the "appropriate" amount of Fe to electroplate onto the loops can be determined from the data reported by Grove (1981). However, a typographical error in Grove (1981) results in an incorrect reported equation. The correct equation used in this study was

$$a^{alloy}_{Fe} = a^{liq}_{FeO} / K_2 \cdot (a^{gas}_{O2})^{0.5} \quad .$$

K_2 is then determined from the graphs of Grove (1981) at a given T. The relation of a^{alloy}_{Fe} to X^{alloy}_{Fe} can also be determined from Grove.

Loops were suspended by alligator clips in a 0.8 molal solution of ferrous sulfate at 35-38°C. To insure a uniform plating on all the loops, the clips were thoroughly cleaned before each use and areas of the loop where Fe was not desired were isolated from the solution by adhesive plastic strips (scotch tape). The loops were moved slowly through the solution by an electric motor.

Since the rate of Fe-plating is linearly dependent on current flow, a voltage regulator was used to control current through the solution. To maximize speed and efficiency of the plating, the current was held in the vicinity of 30 mA (appr. 0.45v). Due to fluctuations in resistivity of the system, values varied from the average by ±20%. The amount of Fe plated onto the Pt was determined by carefully weighing the loops before and after the electroplating. Weight percent Fe = wtFe/(wtFe + wt of portion of loop plated). Plating rates vs current flow are shown in figure B1. The large fluctuations in the graph reflect the poor current control.

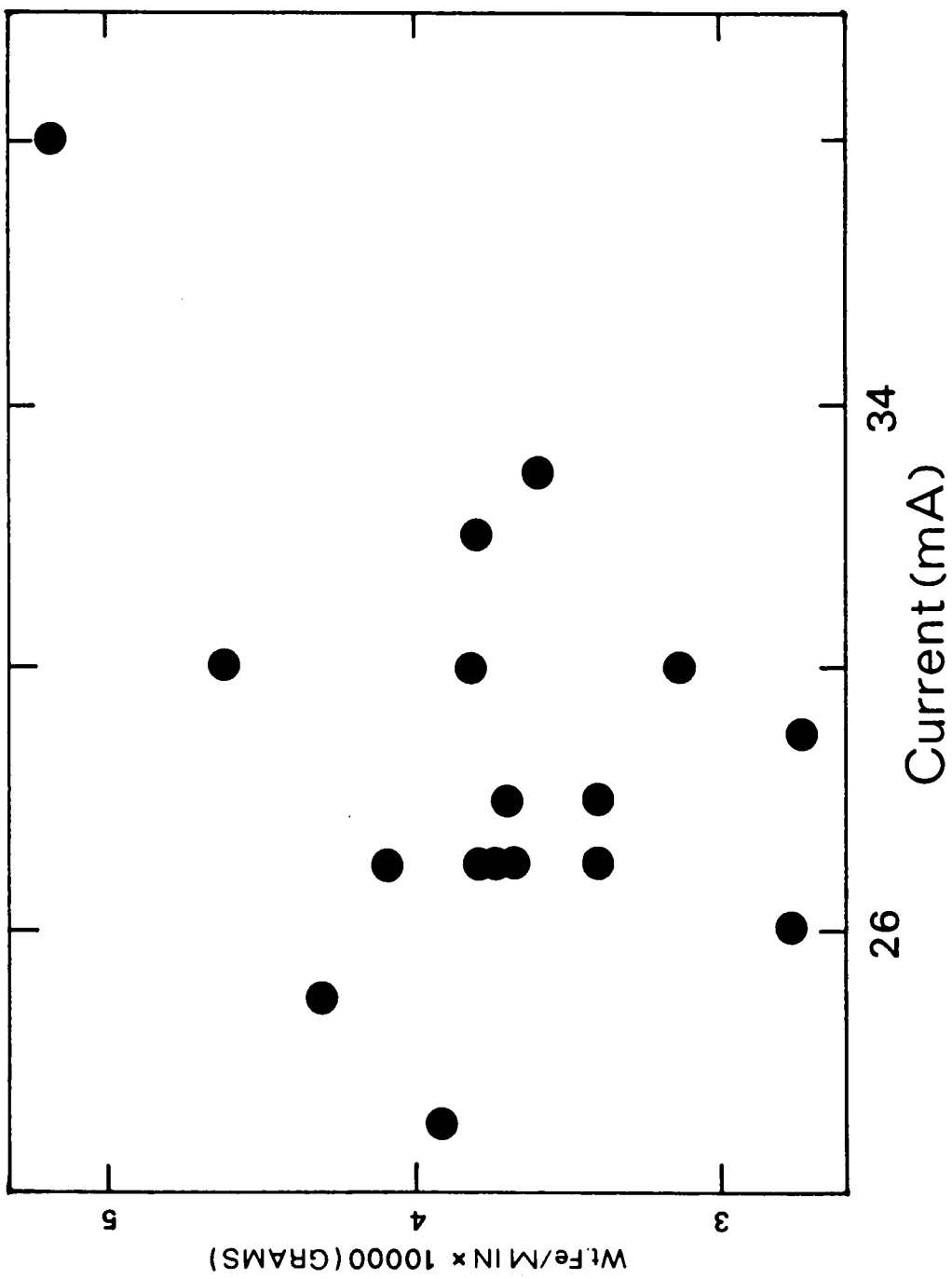

Figure B1. Plot of rate of Fe-plating versus applied current. Scatter illustrates the poor current control.

Once plated with the desired weight of Fe, the loops can be annealed (appr. 24 hrs.) to homogenize the iron. Storage of the loops in acetone prevents rusting.

APPENDIX C

ANALYTICAL PROCEDURES

Major Elements

Values reported for major element analyses were performed on an automated Cameca Microbeam Electron Microprobe at 15kv accelerating potential and 20-30na beam current. Corrections were made for an electronically imposed dead time. Matrix corrections for analyses of experiments numbered 101 or less invoke Bence-Albee procedures, all others used the Cameca ZAF routine. Standards with compositions are listed below in table C1. Spot checks of analyses of major elements using different standards and correction procedures on an ARL-EMX microprobe and a MAC 400s automated microprobe yield good multi-instrument reproducibility (The ARL-Cameca analyses are generally within standard deviation, while the MAC-Cameca analyses are within 0.5% to 2% relative for all elements).

Trace Elements

Values reported were determined either on an ARL-EMX electron microprobe using techniques described by McKay and Seymour (1982) or on an automated Cameca Microbeam Electron Microprobe using techniques described by McKay (1986). In both cases a 30kv accelerating potential was used. A beam current of 600-800na was used for the ARL analyses and a current of 200-250na was used with the Cameca. For all elements for each instrument the profile across the peak was carefully examined for

Table C1. Table of standards used in major element analyses. PR3 is inhomogeneous on the 5μm scale.

Spring Mountain Kaersutite: Std for Si, Al, Ca, Fe, Mg, Ti
(JSC/NASA microprobe lab, Houston, TX)
Si: 39.70 Ti: 5.73 Al: 14.69 Fe: 11.87 Mn: 0.12 Mg: 11.6
Ca: 9.71 Na: 2.75 K: 1.6

REE1: Std for Gd, Eu (Drake and Weill, 1972)
Si: 26.96 Al: 30.52 Ca: 25.16 Eu: 4.20 Gd: 4.46
Tb: 4.35 Tm: 4.35

REE2: Std for Yb, Sm (Drake and Weill, 1972)
Si: 27.07 Al: 30.63 Ca: 25.26 Nd: 4.26 Sm: 4.26
Yb: 4.26 Lu: 4.26

PR3: Std for Sc (not a good std)
(mixed from oxides for this study)
Si: 47.66 Al: 13.95 Ca: 7.53 Fe: 17.82 Mg: 11.64
Na: 0.06 Sc: 0.32

---

minor peaks and nonlinearities in the background. Such nonlinearities are potentially significant for elements at very low concentrations.

ARL

The Yb peak profile (on glass containing appr. 2% Yb, using LIF crystal with 10 second counts per spectrometer setting) for the ARL analyses is shown in figure C1. Since spectrometer #1 appears to have lower resolution it was chosen as the "background" spectrometer. A background offset of +0.04 was made from the peak position (LIF geared spectrometer settings). No Gd was present in the Yb samples analyzed so there was no problems with interference from the Gd $L_{\beta 5}$ and Gd $L_{\beta 7}$ peaks. Spectrometer #2 was set on the Yb peak. The detector HV was optimized in the vicinity of 1900v for each spectrometer for each analysis. The PHA window was set to eliminate low energy noise and higher energy pulses but to admit the entire Yb peak.

Beam size was approximately 5 micrometers on the olivine and 20 micrometers on the glass (the larger area of the beam on the glass avoids sample damage). Counting times were 200 seconds for olivine and 20 seconds on the glass (difference was determined by estimating the counting times which result in equal statistical error for both glass and crystal).

A more detailed analysis of the Yb peak in both olivine and glass is shown in figure C2. Two observations are noted:

1. There appears to be a "double Yb peak" in both glass and olivine.

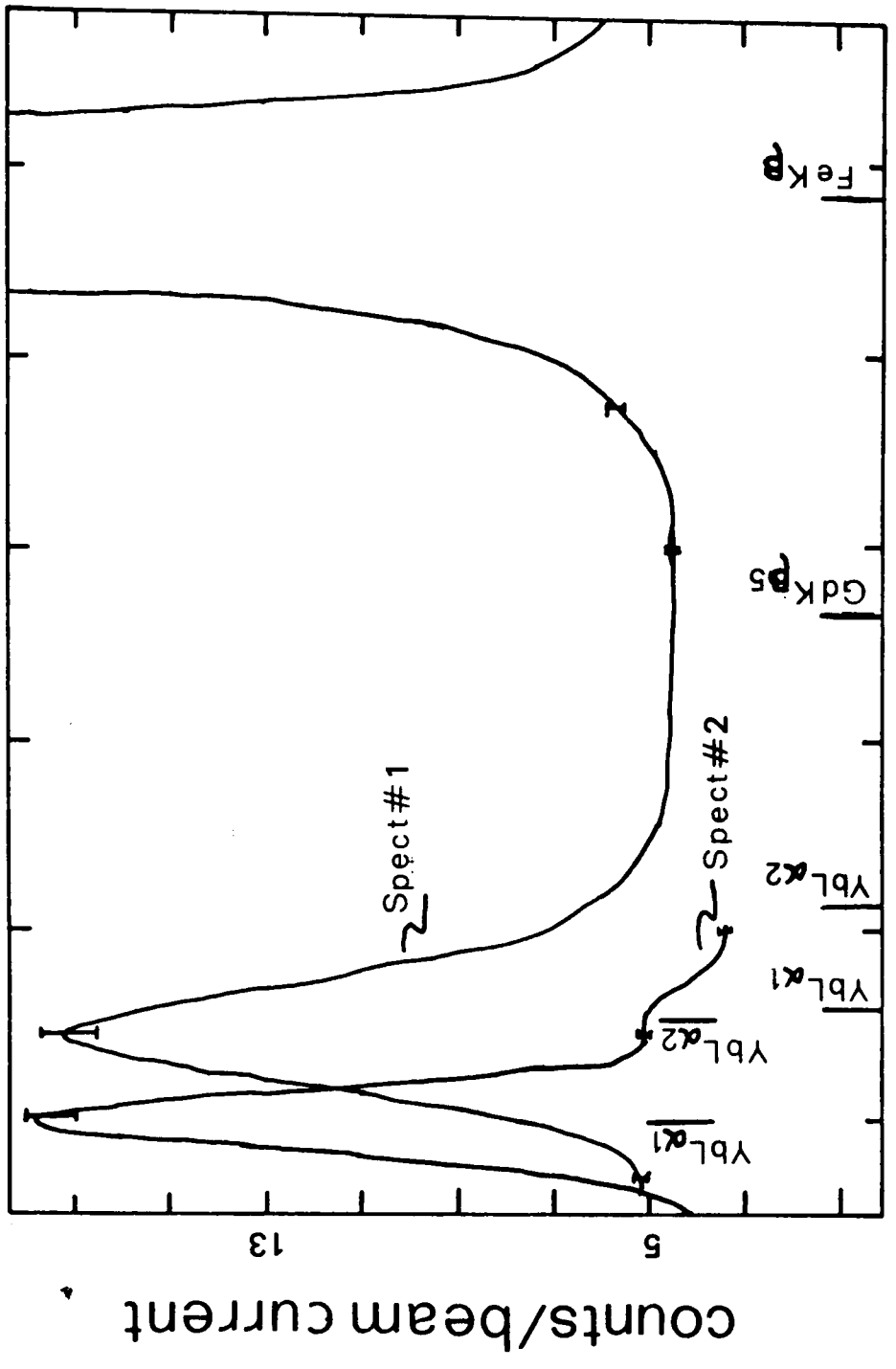

Figure C1. Yb peak profile performed on ARL microprobe on silicate glass. Ten second analyses are approximately 0.004 apart (LIF geared spectrometer settings). Bars represent 4 sigma standard deviations.

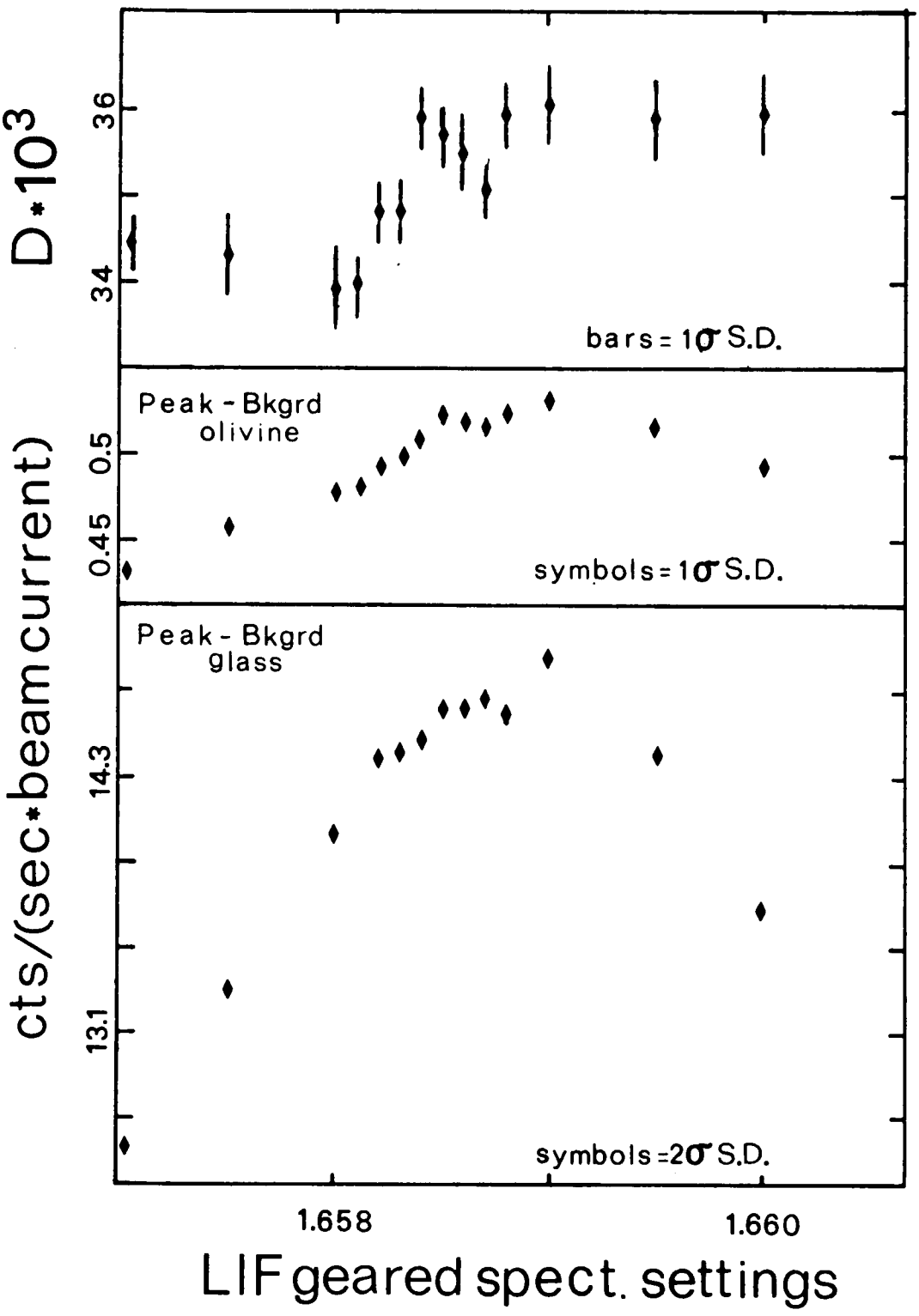

Figure C2. Detailed Yb peak profile on glass and olivine performed on ARL microprobe; partitioning values at each spectrometer setting are included.

2. The apparent measured partitioning coefficient changes as the Yb peak is crossed.

Two such profiles were done across the Yb, and both of these effects were consistent in each, though significant only at the 75-85% confidence level. Whether the first effect is "real" representing a splitting of the energy of the Yb $L_{\alpha 1}$ transition in these silicates is not resolved. It is possible that the variation across the Yb peak represents interference from the Ni K_{α} peak, at least in part, but this too is uncertain. Therefore care was taken to find the center of the Yb peak for each analysis. Similar approaches were used for the Gd and Sm analyses.

Cameca

Since the Cameca microprobe was automated, it was desirable to analyze several elements with a single set-up to avoid losing time in resetting the instrument during overnight runs. Because of this the HV detectors were not always optimized for each element. However, because of the much greater sensitivity of the Cameca instrument, this was not critical. Another difference (between the ARL and Cameca analyses) was that no upper window PHA setting was made for the Cameca. In addition, the technique used for analysis was considerably different (and more reliable) as described by McKay et al. (1986).

Examples of the peak profiles for Sc, Mn, and Gd are shown in figure C3. For Sc in olivine the background appears fairly linear. The background in olivine was readily interpolated on the basis of the innermost four background points. However, for the glass there is

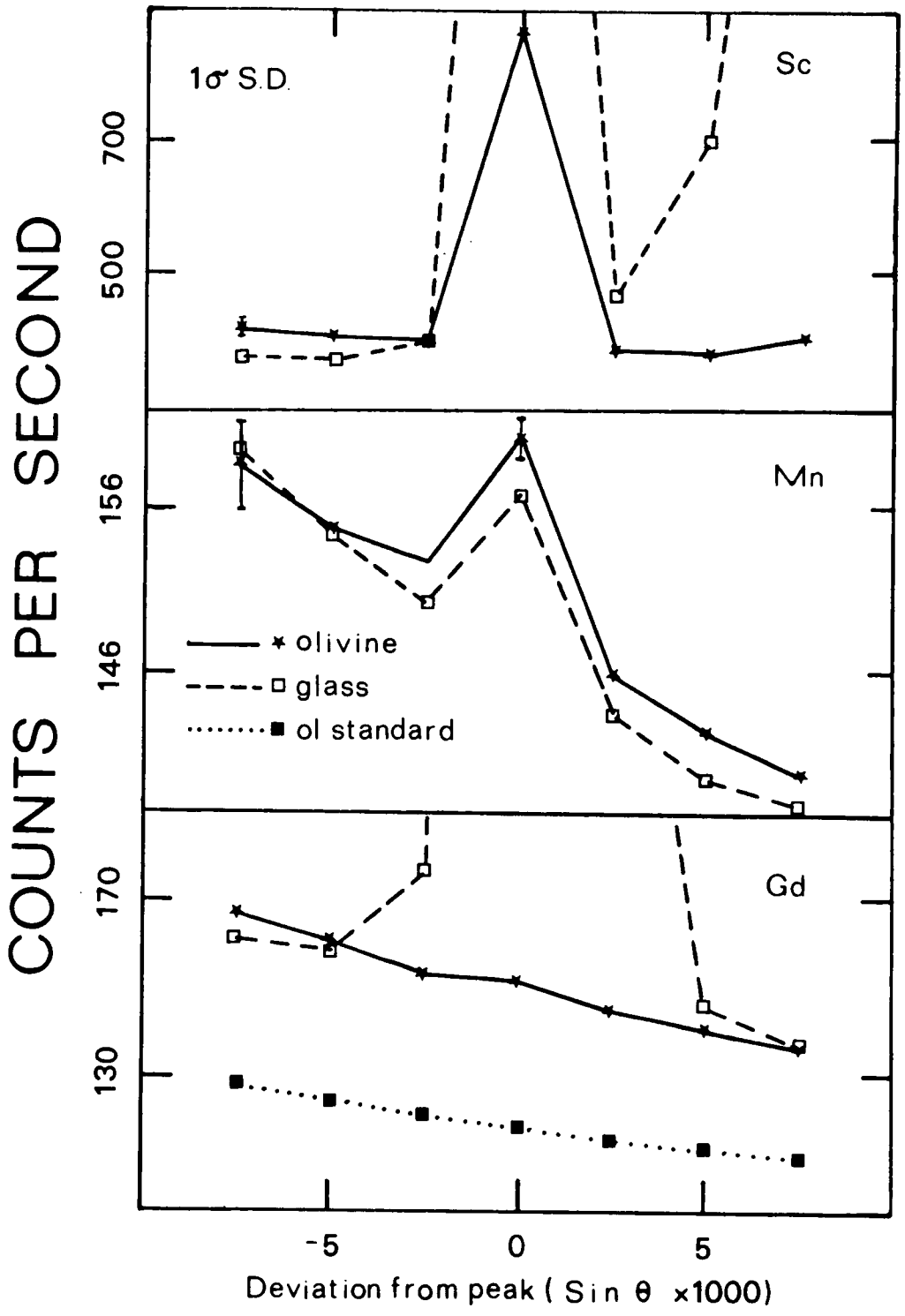

Figure C3. Glass and olivine peak profiles performed on the Cameca microprobe for the purpose of determining partitioning values. Sc, Mn, and Gd peaks are shown. Mn concentrations are only ≈ 400ppm.

interference apparent to the right of the Sc peak. Because of this, the background was extrapolated from only the left most three points on the basis of the apparent slope.

Concentrations of Sc are fairly high (near the percent level) and easy to analyze. The Mn peak illustrates the significance of the analyses at lower concentrations (appr. 40 ppm). Total counting times were two hours for each glass or olivine point. Again the background is linear and readily interpolated.

However, the Gd peak has a significant shoulder. From the glass profile this shoulder was computed as a fraction of peak-minus-background and subtracted out of the background for both olivine and glass. For glass, the outer four points were used to interpolate background; for olivine the innermost four points were used after the "shoulder" effect was removed.

Ti, Zr, Y, Eu, Sm, and Yb partitioning values were computed similar to Gd. Considerable interference around the K_α peak was encountered for the elements Sr, Ni, Al, and Ca. For the latter two, the high concentrations in both olivine and glass reduced the significance of the uncertainty in the background. No successful analysis of Sr was made and the Ni D values of run #120a which are reported were made using the Ni L_α peak which had less interference than the Ni K_α peak. Most of the Ni interference was from minor REE peaks.

The reproducibility between instruments/techniques is good for the Yb data. This is illustrated in figure C4. However, the analyses of Gd D values were systematically different between the ARL and Cameca.

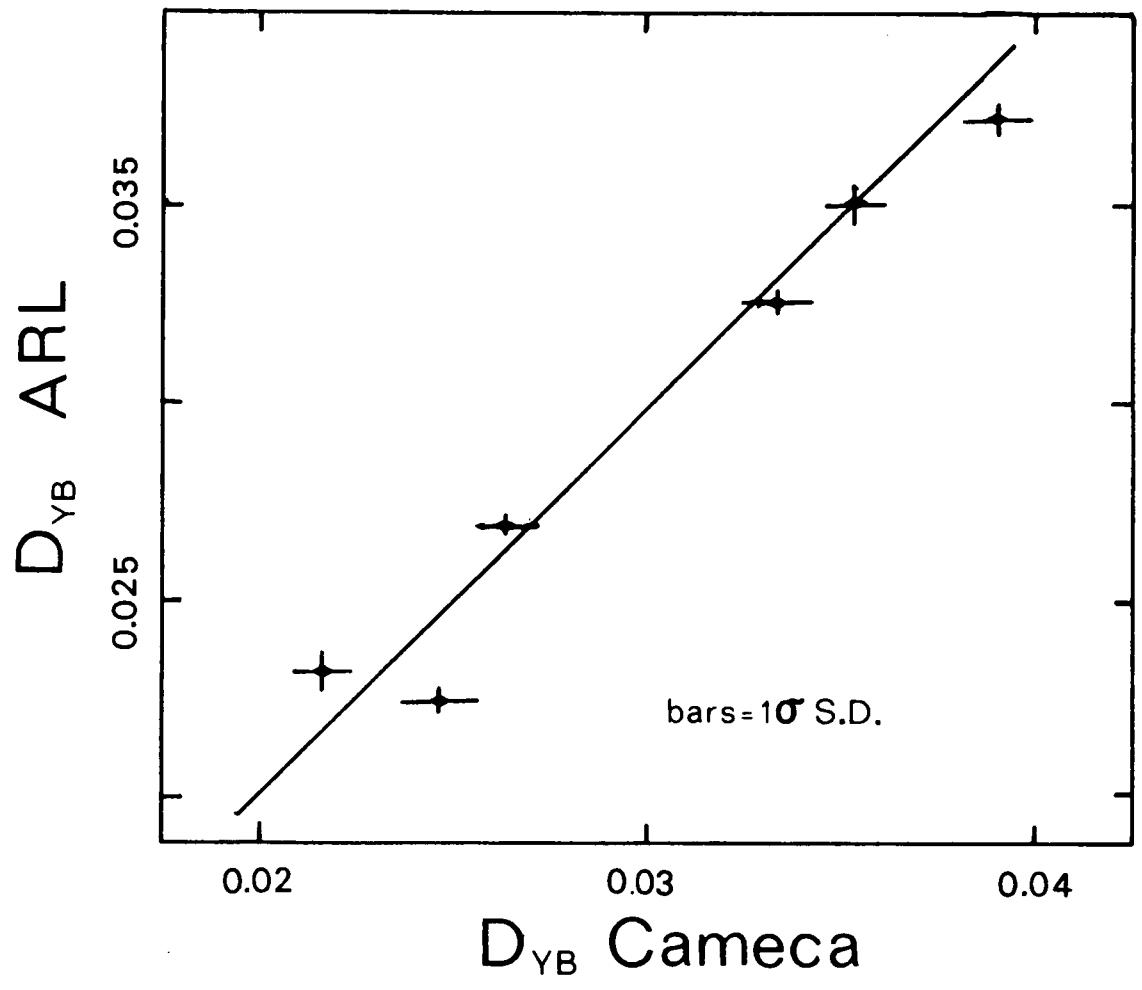

Figure C4. Comparison of Yb partitioning values determined on the ARL microprobe to those determined on the Cameca microprobe.

This remains unexplained, but the Cameca analyses are considered more reliable and it is the Cameca values for Gd which are reported.

β-Track Mapping

A series of experiments containing 10 to 40 ppm Sm^{151} were conducted. Sm^{151}, being a β emitting radioactive isotope, is readily analyzed by the β-track mapping techniques described by Mysen and Seitz (1975). These experiments were conducted with the hope of testing the "Henry's Law" assumption. Samples were cut and mounted in epoxy before being carefully polished to 1μm. Since "topography" increases the β particle half-distance (air being less dense than the glass or crystalline medium) it was especially important to get a flat surface. To insure this, acetate polishing paper was used.

Exposures were made on K-5 Ilford 25μm emulsions. These emulsions were kept refrigerated until a few hours before they were used. If they are not allowed to warm up and dry out, the emulsion will stick to the sample and either pull the sample out of the epoxy or expose the emulsion with an electrostatic discharge resulting when they are pulled apart.

At 40ppm Sm in the bulk composition, the Sm concentrations in glass and olivine are expected to be approximately 49ppm and 49ppb respectively. Specifications for the Sm^{151} solution used are given in table C2. For a target of 10^7 tracks per square centimeter, projected exposure times are 10 minutes for glass and 7 days for olivine.

Because of the large difference in Sm concentrations in glass and olivine, stray β particles or X-rays wandering into the olivine region

Table C2. Specifications for the Sm^{151} solution used in β-track experiments.

Isotope	Sm151
Concentration	7.36mCi/ml
Specific Activity	18.3mCi/ml
Solids	0.403mgSm/ml

of the emulsion from the glass may become significant after 7 days. Mysen and Seitz (1975) calculate β particle ranges in geologic materials of 1 to 3 μm (reported in their paper as density times range). These ranges are small enough to not be significant in these experiments in which olivine crystals are 50 to 500 μm across.

Figure C5 illustrates β-tracks for an exposure time of two weeks. Glass,olivine, and plagioclase are illustrated. However, there is an apparent zoning in the crystals which gives them "fuzzy edges." A fuzzy edge is also seen between the glass and the epoxy. This is magnified in figure C6.

It is seen that the band of fuzzines is more than 50μm wide and cannot be explained by compositional zoning. This is much greater than the 3μm track range predicted by Mysen and Seitz (1975). It is believed Mysen and Seitz (1975) calculations are in error (D. Lindstrom, pers. comm.). Time was not available to search outways to make the β-track mapping technique useful in this study.

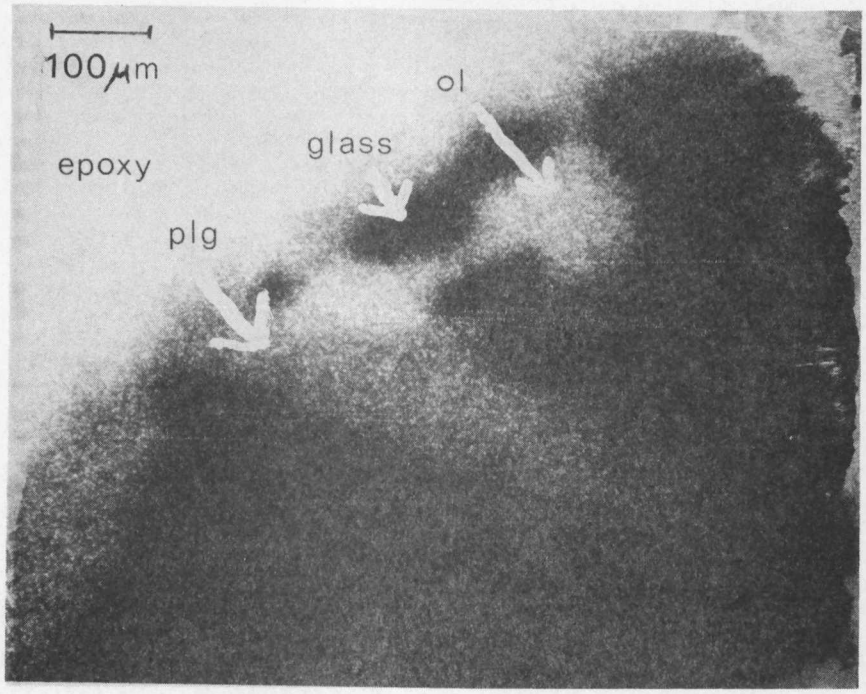

Figure C5. β-tracks for a two week exposure of glass, epoxy, plagioclase, and olivine containing Sm^{151}. Note the "fuzzy edges" around the crystals and glass.

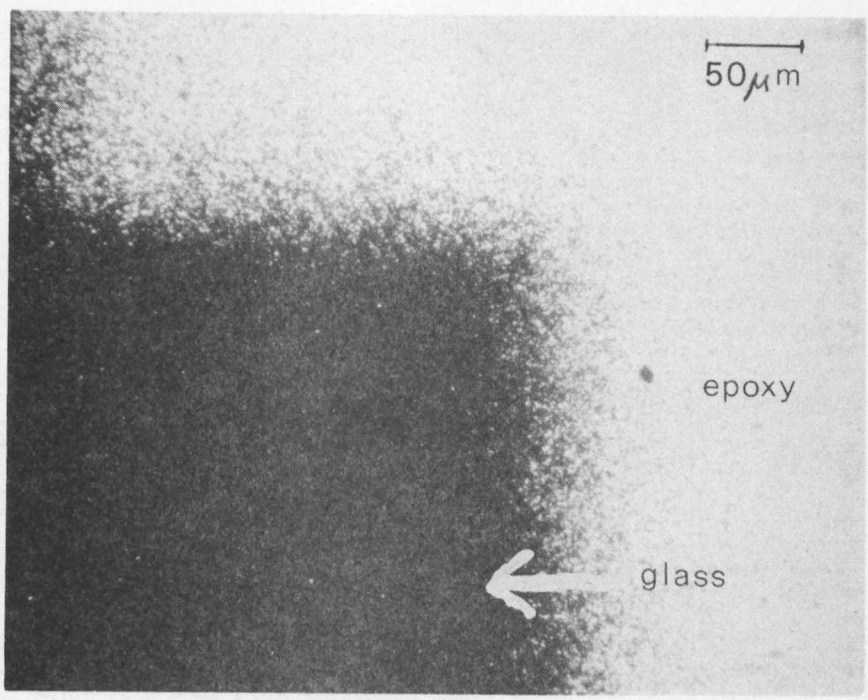

Figure C6. β-tracks for a two week exposure of glass, containing Sm^{151}, and epoxy.

APPENDIX D

THERMODYNAMICALLY VALID CRYSTAL FRACTIONATION

(A PROGRAM IN PASCAL)

APPENDIX D

THERMODYNAMICALLY VALID CRYSTAL FRACTIONATION
(A PROGRAM IN PASCAL)

```
PROGRAM CLFRACTIONATION (INPUT,OUTPUT,TRENDS);


CONST
  TCEILING=1477;

TYPE
  ONEELEM=RECORD
                ELEMENT:PACKED ARRAY[1..2] OF CHAR;
                VALENCE:INTEGER;
                DISTANCE:REAL;
                WT:REAL;
                MOLAR:REAL;
                CLWT:REAL
               END;
  ELEMDATA=ARRAY[1..92] OF ONEELEM;

VAR
ELEMDAT:ELEMDATA;
  FE2,FE3,FO,FA,T,WTFRACOL,WTSUM,MGHOLD,NIHOLD:REAL;
  NEXTELEMENT,ELEMENTNO,ATNO:INTEGER;
  ENDCASE,HOLDNI,QUIT,FINISHEDWCOMP:BOOLEAN;
  WTSAVE:ARRAY[1..92] OF REAL;
  TRENDS:FILE OF CHAR;
  PROCTYPE,ANSWER:CHAR;
  FEA,FEB:INTEGER;
  WTFE:REAL;  (*JUGGLES FE2O3,FEO*)

PROCEDURE CONVTOMOLAR (VAR ELEMDAT : ELEMDATA);
VAR
  SUMOFMOLES:REAL;
BEGIN
  SUMOFMOLES:=(3*ELEMDAT[1].WT/18)+(3*ELEMDAT[6].WT/44)+
     (ELEMDAT[15].WT*7/142)+(ELEMDAT[11].WT*3/62)+
     (ELEMDAT[12].WT*2/40.3)+(ELEMDAT[13].WT*5/102)+
     (ELEMDAT[19].WT*3/94.2)+(ELEMDAT[20].WT*2/56)+
     (ELEMDAT[22].WT*3/79.9)+(ELEMDAT[26].WT*FEA/WTFE)+
     (ELEMDAT[14].WT*3/72);

     ELEMDAT[1].MOLAR:=(2*ELEMDAT[1].WT/18)/SUMOFMOLES;
     ELEMDAT[6].MOLAR:=(2*ELEMDAT[6].WT/44)/SUMOFMOLES;
     ELEMDAT[11].MOLAR:=(2*ELEMDAT[11].WT/62)/SUMOFMOLES;
     ELEMDAT[12].MOLAR:=(1*ELEMDAT[12].WT/40.3)/SUMOFMOLES;
     ELEMDAT[13].MOLAR:=(2*ELEMDAT[13].WT/102)/SUMOFMOLES;
     ELEMDAT[14].MOLAR:=(1*ELEMDAT[14].WT/72)/SUMOFMOLES;
     ELEMDAT[15].MOLAR:=(2*ELEMDAT[15].WT/142)/SUMOFMOLES;
     ELEMDAT[19].MOLAR:=(2*ELEMDAT[19].WT/94.2)/SUMOFMOLES;
     ELEMDAT[20].MOLAR:=(1*ELEMDAT[20].WT/56)/SUMOFMOLES;
     ELEMDAT[21].MOLAR:=(1*ELEMDAT[21].WT/45)/SUMOFMOLES;
     ELEMDAT[22].MOLAR:=(1*ELEMDAT[22].WT/79.9)/SUMOFMOLES;
     ELEMDAT[23].MOLAR:=(1*ELEMDAT[23].WT/51)/SUMOFMOLES;
     ELEMDAT[24].MOLAR:=(1*ELEMDAT[24].WT/52)/SUMOFMOLES;
     ELEMDAT[25].MOLAR:=(1*ELEMDAT[25].WT/55)/SUMOFMOLES;
     ELEMDAT[26].MOLAR:=(FEB*ELEMDAT[26].WT/WTFE)/SUMOFMOLES;
```

```
    ELEMDAT[27].MOLAR:=(1*ELEMDAT[27].WT/59)/SUMOFMOLES;
    ELEMDAT[28].MOLAR:=(1*ELEMDAT[28].WT/58.7)/SUMOFMOLES;
    ELEMDAT[29].MOLAR:=(1*ELEMDAT[29].WT/63.5)/SUMOFMOLES;
    ELEMDAT[30].MOLAR:=(1*ELEMDAT[30].WT/65.4)/SUMOFMOLES;
    ELEMDAT[31].MOLAR:=(1*ELEMDAT[31].WT/69.7)/SUMOFMOLES;
    ELEMDAT[37].MOLAR:=(1*ELEMDAT[37].WT/85.5)/SUMOFMOLES;
    ELEMDAT[38].MOLAR:=(1*ELEMDAT[38].WT/87.6)/SUMOFMOLES;
    ELEMDAT[39].MOLAR:=(1*ELEMDAT[39].WT/88.9)/SUMOFMOLES;
    ELEMDAT[40].MOLAR:=(1*ELEMDAT[40].WT/91.2)/SUMOFMOLES;
    ELEMDAT[41].MOLAR:=(1*ELEMDAT[41].WT/92.9)/SUMOFMOLES;
    ELEMDAT[56].MOLAR:=(1*ELEMDAT[56].WT/137.3)/SUMOFMOLES;
    ELEMDAT[57].MOLAR:=(1*ELEMDAT[57].WT/139)/SUMOFMOLES;
    ELEMDAT[58].MOLAR:=(1*ELEMDAT[58].WT/140)/SUMOFMOLES;
    ELEMDAT[62].MOLAR:=(1*ELEMDAT[62].WT/150.4)/SUMOFMOLES;
    ELEMDAT[63].MOLAR:=(1*ELEMDAT[63].WT/152)/SUMOFMOLES;
    ELEMDAT[64].MOLAR:=(1*ELEMDAT[64].WT/157.3)/SUMOFMOLES;
    ELEMDAT[65].MOLAR:=(1*ELEMDAT[65].WT/159)/SUMOFMOLES;
    ELEMDAT[66].MOLAR:=(1*ELEMDAT[66].WT/162.5)/SUMOFMOLES;
    ELEMDAT[70].MOLAR:=(1*ELEMDAT[70].WT/173)/SUMOFMOLES;
    ELEMDAT[71].MOLAR:=(1*ELEMDAT[71].WT/175)/SUMOFMOLES;
    ELEMDAT[72].MOLAR:=(1*ELEMDAT[72].WT/178.5)/SUMOFMOLES;
    ELEMDAT[73].MOLAR:=(1*ELEMDAT[73].WT/181)/SUMOFMOLES;
    ELEMDAT[90].MOLAR:=(1*ELEMDAT[90].WT/232)/SUMOFMOLES
  END;

PROCEDURE LIQUIDUST (ELEMDAT : ELEMDATA; FE2 : REAL; VAR  FO,FA,T : REAL);

    (*AFTER NIELSEN AND DUNGAN, 1983 *)
    (*ASSUMES CLIVINE IS ON THE LIQUIDUS *)


  VAR
    MG,FE,NI,SI:REAL;
    EQN1,EQN2,EQN3:REAL;
    TEST1,TEST2,TEST3:REAL;
    FO1,FO2,FO3:REAL;
    NETMOD,NETFORM:REAL;
    ITERATIONS:INTEGER;

  BEGIN
    NETMOD:=ELEMDAT[12].MOLAR+ELEMDAT[26].MOLAR+
              (ELEMDAT[13].MOLAR-ELEMDAT[11].MOLAR-
              ELEMDAT[19].MOLAR)+ELEMDAT[20].MOLAR+
              ELEMDAT[22].MOLAR+ELEMDAT[28].MOLAR+
              ELEMDAT[1].MOLAR;

    NETFORM:=ELEMDAT[14].MOLAR+ELEMDAT[11].MOLAR+
               ELEMDAT[19].MOLAR;

    MG:=ELEMDAT[12].MOLAR/NETMOD;
    FE:=FE2/NETMOD;
    NI:=ELEMDAT[28].MOLAR/NETMOD;
    SI:=ELEMDAT[14].MOLAR/NETFORM;

    EQN1:=(3.73-LN(MG)-0.5*LN(SI))/6700;
    EQN2:=(-1.143+LN(FE)-1.02597*LN(MG)-0.01299*LN(SI));
    EQN3:=(0.512+LN(NI)-1.6761*LN(MG)-0.3381*LN(SI));

    FO1:=0.01;
    FO2:=0.98;
```

```
      FO3:=0.5;

      FOR ITERATIONS:=1 TO 15 DO
       BEGIN
        TEST1:=EXP(-1.02597*LN(FO1))-EXP(-0.02597*LN(FO1))-EXP(EQN2)-
                EXP(EQN3)*EXP(0.6501*LN(FO1));
        TEST2:=EXP(-1.02597*LN(FO2))-EXP(-0.02597*LN(FO2))-EXP(EQN2)-
                EXP(EQN3)*EXP(0.6501*LN(FO2));
        TEST3:=EXP(-1.02597*LN(FO3))-EXP(-0.02597*LN(FO3))-EXP(EQN2)-
                EXP(EQN3)*EXP(0.6501*LN(FO3));

        IF TEST3 < 0 THEN
         IF TEST2 > 0 THEN
          FO1:=FO3
         ELSE IF TEST1 > 0 THEN
          FO2:=FO3
               ELSE
                BEGIN
                 FO1:=(FO3+FO1)/2;
                 FO2:=(FO3+FO2)/2
                END
        ELSE
         IF TEST2 < 0 THEN
          FO1:=FO3
         ELSE IF TEST1 < 0 THEN
          FO2:=FO3
               ELSE
                BEGIN
                 FO1:=(FO3+FO1)/2;
                 FO2:=(FO3+FO2)/2
                END;
        FO3:=(FO1+FO2)/2;
       END;(*OF FOR LOOP*)
        WRITELN(FO3);

      FA:=1-FO3-EXP(EQN3)/EXP(-1.6761*LN(FO3));
      FO:=FO3;
      T:=1/(EQN1+LN(FO)/6700)
    END;(*OF PROCEDURE LIQUIDUST*)

PROCEDURE FEVALENCE (ELEMDAT : ELEMDATA; VAR FE2,FE3,FO,FA,T : REAL);

      (* AFTER SACK ET AL, 1980 *)
      (* ASSUMES MELT IS BUFFERED ON QFM *)

    VAR
     OXIDESUM,RATIO,INTERACTION,T1,LNFO2 : REAL;
    BEGIN
     OXIDESUM:=ELEMDAT[14].MOLAR + ELEMDAT[13].MOLAR/2 + ELEMDAT[26].MOLAR
       +ELEMDAT[12].MOLAR + ELEMDAT[20].MOLAR + ELEMDAT[11].MOLAR/2 +
       ELEMDAT[19].MOLAR/2;

     INTERACTION:= -2.15036*(ELEMDAT[14].MOLAR/OXIDESUM) - 8.35163*
       (ELEMDAT[13].MOLAR/(2*OXIDESUM)) - 4.49508*(ELEMDAT[26].MOLAR/
       OXIDESUM) - 5.43639*(ELEMDAT[12].MOLAR/OXIDESUM) + 0.073113*(
       ELEMDAT[20].MOLAR/OXIDESUM) + 3.54148*(ELEMDAT[11].MOLAR/(2*
       OXIDESUM)) + 4.1868d*(ELEMDAT[19].MOLAR/(2*OXIDESUM));

     FE2:=ELEMDAT[26].MOLAR;
     LIQUIDUST (ELEMDAT,FE2,FO,FA,T);
```

```
    REPEAT (*UNTIL TEMPERATURE CHANGES LESS THAN 1 DEGREES*)
      LNFO2:= -61663.6/T + 15.646; (*QFM ASSUMED*)

      RATIO:= EXP(0.21813*LNFO2 + 13184.7/T - 4.49933 + INTERACTION);

      FE3:= ELEMDAT[26].MOLAR*RATIO/(RATIO + 0.5);

      FE2:= ELEMDAT[26].MOLAR - FE3;

      T1:=T;

      LIQUIDUST (ELEMDAT,FE2,FO,FA,T);
      UNTIL ABS(T-T1) < 1;
  END; (*OF PROCEDURE FEVALENCE*)

PROCEDURE OLCOMP (VAR ELEMDAT : ELEMDATA; FE2, FE3, FO, FA, T : REAL);
  VAR
   AL,MG,D,NETFORM,NETMOD,EXCESS,H4:REAL;
   MOLEFRACT,WTFRACT,SUMWTFRACT:REAL;
   NEXTELEMENT:INTEGER;

  BEGIN
   NETMOD:=ELEMDAT[12].MOLAR+ELEMDAT[26].MOLAR+
       ELEMDAT[11].MOLAR+ELEMDAT[19].MOLAR+ELEMDAT[20].MOLAR+
       ELEMDAT[22].MOLAR+ELEMDAT[28].MOLAR+ELEMDAT[1].MOLAR;

   NETFORM:=ELEMDAT[14].MOLAR+ELEMDAT[13].MOLAR;

   MG:=ELEMDAT[12].MOLAR/NETMOD;
    IF NOT HOLDM THEN
     BEGIN
      MGHOLD:=MG;
      NIHOLD:=ELEMDAT[28].MOLAR/NETMOD
     END;
   AL:=ELEMDAT[13].MOLAR/NETFORM;
   SUMWTFRACT:=0;

   FOR NEXTELEMENT:=1 TO 92 DO
    IF ELEMCAT[NEXTELEMENT].WT > 0.000001 THEN
     BEGIN
     H4:=-0.075+0.465*(1/ELEMDAT[NEXTELEMENT].DISTANCE - 1.205);
     EXCESS:=LN((EXP(H4*10000/T)/FA)/(1+FO*EXP(H4*10000/T)/FA));
     CASE NEXTELEMENT OF
       28,27,25,70,21,20,13:
         CASE NEXTELEMENT OF
          28:D:=EXP(-LN(MGHOLD/FO)-2.65+5410/T-EXCESS);
          27:D:=EXP(-LN(MG/FO)-0.196-230/T-EXCESS);
          25:D:=EXP(-LN(MG/FO)+0.445-3050/T-EXCESS);
          20:D:=EXP(-LN(MG/FO)+0.272-9450/T-EXCESS);
          13:D:=EXP(-1.5*LN(MG/FO)-6.67+80/T-EXCESS);
          21:D:=EXP(-1.5*LN(MG/FO)-0.78-3940/T-EXCESS);
          70:D:=EXP(-1.5*LN(MG/FO)-0.001-8580/T-EXCESS)
         END;
      90,72,23,22,40:D:=EXP(2*LN(MG/FO)-1.58*(1/
              (ELEMDAT[NEXTELEMENT].DISTANCE*       (*TETRAVALENT*)
              ELEMDAT[NEXTELEMENT].DISTANCE*
              ELEMDAT[NEXTELEMENT].DISTANCE)-1.75)+12.15*
              (ELEMDAT[NEXTELEMENT].VALENCE/
              (ELEMDAT[NEXTELEMENT].DISTANCE+1.32)-0.9434)*10000/T-
              52*(EXP((3.578-(1.32+ELEMDAT[NEXTELEMENT].DISTANCE)/
```

```
          0.707)/0.208)*ELEMDAT[NEXTELEMENT].VALENCE-16.21)/T-
          125900/T-EXCESS);
 2,65,66,71,73,63,58,57,31,39,62,64,41:D:=EXP(-1.5*LN(MG/FO)-1.58*(1/
          (ELEMDAT[NEXTELEMENT].DISTANCE*  (*TRIVALENT*)
          ELEMDAT[NEXTELEMENT].DISTANCE*
          ELEMDAT[NEXTELEMENT].DISTANCE)-1.75)+12.15*
          (ELEMDAT[NEXTELEMENT].VALENCE/
          (ELEMDAT[NEXTELEMENT].DISTANCE+1.32)-0.9434)*10000/T-
          136*(EXP((3.578-(1.32+ELEMDAT[NEXTELEMENT].DISTANCE)/
          0.707)/0.208)*ELEMDAT[NEXTELEMENT].VALENCE-16.21)/T-
          57300/T-EXCESS-0.693);
  30,29,56,38:D:=EXP(-LN(MG/FO)-1.58*(1/
          (ELEMDAT[NEXTELEMENT].DISTANCE*   (*DIVALENT*)
          ELEMDAT[NEXTELEMENT].DISTANCE*
          ELEMDAT[NEXTELEMENT].DISTANCE)-1.75)+12.15*
          (ELEMDAT[NEXTELEMENT].VALENCE/
          (ELEMDAT[NEXTELEMENT].DISTANCE+1.32)-0.9434)*10000/T-
          52*(EXP((3.578-(1.32+ELEMDAT[NEXTELEMENT].DISTANCE)/
          0.707)/0.208)*ELEMDAT[NEXTELEMENT].VALENCE-16.21)/T+
          1100/T-EXCESS);
  11,19,37:D:=EXP(-2*LN(MG/FO)+LN(AL)-1.58*(1/
          (ELEMDAT[NEXTELEMENT].DISTANCE*    (*UNIVALENT*)
          ELEMDAT[NEXTELEMENT].DISTANCE*
          ELEMDAT[NEXTELEMENT].DISTANCE)-1.75)+12.15*
          (ELEMDAT[NEXTELEMENT].VALENCE/
          (ELEMDAT[NEXTELEMENT].DISTANCE+1.32)-0.9434)*10000/T-
          52*(EXP((3.578-(1.32+ELEMDAT[NEXTELEMENT].DISTANCE)/
          0.707)/0.208)*ELEMDAT[NEXTELEMENT].VALENCE-16.21)/T+
          52370/T-4.2);
  15:D:=0;
  12,26,14:
END;
IF (NEXTELEMENT <> 13) OR (NEXTELEMENT <> 2) THEN
  IF (NEXTELEMENT=28) THEN
     MOLEFRACT:=(D*0.2857)*NIHOLD
  ELSE
  MOLEFRACT:=(D*0.2857)*(ELEMDAT[NEXTELEMENT].MOLAR/NETMOD)
ELSE IF NEXTELEMENT = 2 THEN
  MOLEFRACT:= (D*0.2857)*(FE3/NETMOD)
ELSE
  MOLEFRACT:=(D*0.2857)*(ELEMDAT[NEXTELEMENT].MOLAR/NETFORM);

CASE NEXTELEMENT OF
  15:WTFRACT:=MOLEFRACT*(71);
  28:WTFRACT:=MOLEFRACT*(58.7);
  27:WTFRACT:=MOLEFRACT*(58.93);
  25:WTFRACT:=MOLEFRACT*(70.9);
  20:WTFRACT:=MOLEFRACT*(56.1);
  30:WTFRACT:=MOLEFRACT*(65.4);
  29:WTFRACT:=MOLEFRACT*(63.5);
  56:WTFRACT:=MOLEFRACT*(137.3);
  38:WTFRACT:=MOLEFRACT*(87.6);
  62:WTFRACT:=MOLEFRACT*(150.4);
  64:WTFRACT:=MOLEFRACT*(157.3);
  21:WTFRACT:=MOLEFRACT*(45.0);
  70:WTFRACT:=MOLEFRACT*(173);
  13:WTFRACT:=MOLEFRACT*(51.0);
  39:WTFRACT:=MOLEFRACT*(88.9);
  31:WTFRACT:=MOLEFRACT*(69.7);
  41:WTFRACT:=MOLEFRACT*(92.9);
```

```
        23:WTFRACT:=MOLEFRACT*(50.9);
        22:WTFRACT:=MOLEFRACT*(79.9);
        40:WTFRACT:=MOLEFRACT*(91.2);
        11:WTFRACT:=MOLEFRACT*(31.0);
        19:WTFRACT:=MOLEFRACT*(47.1);
        37:WTFRACT:=MOLEFRACT*(85.5);
        57:WTFRACT:=MOLEFRACT*(139);
        58:WTFRACT:=MOLEFRACT*(140);
        63:WTFRACT:=MOLEFRACT*(152);
        65:WTFRACT:=MOLEFRACT*(159);
        66:WTFRACT:=MOLEFRACT*(163.5);
        71:WTFRACT:=MOLEFRACT*(175);
        72:WTFRACT:=MOLEFRACT*(178.5);
        73:WTFRACT:=MOLEFRACT*(181);
        90:WTFRACT:=MOLEFRACT*(232);
        12:WTFRACT:=FO*0.2857*40.3;
        26:WTFRACT:=FA*0.2857*WTFE/FEB;
         2:WTFRACT:=MOLEFRACT*(WTFE/FE8); (*TRIVALENT FE*)
        14:WTFRACT:=8.59
      END;
    ELEMDAT[NEXTELEMENT].OLWT:=WTFRACT;
    SUMWTFRACT:=SUMWTFRACT+WTFRACT
  END;(*OF IF STATEMENT*)
   ELEMDAT[26].OLWT:=ELEMDAT[26].OLWT + ELEMDAT[2].OLWT;
   FOR NEXTELEMENT:=1 TO 92 DO
    ELEMDAT[NEXTELEMENT].OLWT:=(ELEMDAT[NEXTELEMENT].OLWT/
                                        SUMWTFRACT)*100;
    IF NOT HOLDNI THEN
      WRITELN (ELEMDAT[30].OLWT);
   ELEMDAT[2].OLWT:=0
END;

BEGIN (*MAIN PROGRAM*)
  REWRITE(TRENDS);
  ELEMDAT[1].ELEMENT:=' H';
  ELEMDAT[6].ELEMENT:=' C';
  ELEMDAT[11].ELEMENT:='NA';
  ELEMDAT[12].ELEMENT:='MG';
  ELEMDAT[13].ELEMENT:='AL';
  ELEMDAT[14].ELEMENT:='SI';
  ELEMDAT[15].ELEMENT:=' P';
  ELEMDAT[19].ELEMENT:=' K';
  ELEMDAT[20].ELEMENT:='CA';
  ELEMDAT[21].ELEMENT:='SC';
  ELEMDAT[22].ELEMENT:='TI';
  ELEMDAT[23].ELEMENT:=' V';
  ELEMDAT[24].ELEMENT:='CR';
  ELEMDAT[25].ELEMENT:='MN';
  ELEMDAT[26].ELEMENT:='FE';
  ELEMDAT[27].ELEMENT:='CO';
  ELEMDAT[28].ELEMENT:='NI';
  ELEMDAT[29].ELEMENT:='CU';
  ELEMDAT[30].ELEMENT:='ZN';
  ELEMDAT[31].ELEMENT:='GA';
  ELEMDAT[37].ELEMENT:='RB';
  ELEMDAT[38].ELEMENT:='SR';
  ELEMDAT[39].ELEMENT:=' Y';
  ELEMDAT[40].ELEMENT:='ZR';
  ELEMDAT[41].ELEMENT:='NB';
  ELEMDAT[56].ELEMENT:='BA';
```

```
ELEMDAT[57].ELEMENT:='LA';
ELEMDAT[58].ELEMENT:='CE';
ELEMDAT[62].ELEMENT:='SM';
ELEMDAT[63].ELEMENT:='EU';
ELEMDAT[64].ELEMENT:='GD';
ELEMDAT[65].ELEMENT:='TB';
ELEMDAT[66].ELEMENT:='DY';
ELEMDAT[70].ELEMENT:='YB';
ELEMDAT[71].ELEMENT:='LU';
ELEMDAT[72].ELEMENT:='HF';
ELEMDAT[73].ELEMENT:='TA';
ELEMDAT[90].ELEMENT:='TH';
ELEMDAT[1].VALENCE:=1;
ELEMDAT[2].VALENCE:=3; (*TRIVALENT FE*)
ELEMDAT[6].VALENCE:=4;
ELEMDAT[11].VALENCE:=1;
ELEMDAT[12].VALENCE:=2;
ELEMDAT[13].VALENCE:=3;
ELEMDAT[14].VALENCE:=4;
ELEMDAT[15].VALENCE:=5;
ELEMDAT[19].VALENCE:=1;
ELEMDAT[20].VALENCE:=2;
ELEMDAT[21].VALENCE:=3;
ELEMDAT[22].VALENCE:=4;
ELEMDAT[23].VALENCE:=4;
ELEMDAT[24].VALENCE:=3;
ELEMDAT[25].VALENCE:=2;
ELEMDAT[26].VALENCE:=2;
ELEMDAT[27].VALENCE:=2;
ELEMDAT[28].VALENCE:=2;
ELEMDAT[29].VALENCE:=2;
ELEMDAT[30].VALENCE:=2;
ELEMDAT[31].VALENCE:=3;
ELEMDAT[37].VALENCE:=1;
ELEMDAT[38].VALENCE:=2;
ELEMDAT[39].VALENCE:=3;
ELEMDAT[40].VALENCE:=4;
ELEMDAT[41].VALENCE:=3;
ELEMDAT[56].VALENCE:=2;
ELEMDAT[57].VALENCE:=3;
ELEMDAT[58].VALENCE:=3;
ELEMDAT[62].VALENCE:=3;
ELEMDAT[63].VALENCE:=3;
ELEMDAT[64].VALENCE:=3;
ELEMDAT[65].VALENCE:=3;
ELEMDAT[66].VALENCE:=3;
ELEMDAT[70].VALENCE:=3;
ELEMDAT[71].VALENCE:=3;
ELEMDAT[72].VALENCE:=4;
ELEMDAT[73].VALENCE:=3;
ELEMDAT[90].VALENCE:=4;
ELEMDAT[2].DISTANCE:=0.73; (*TRIVALENT FE*)
ELEMDAT[11].DISTANCE:=1.10;
ELEMDAT[12].DISTANCE:=0.80;
ELEMDAT[13].DISTANCE:=0.61;
ELEMDAT[14].DISTANCE:=0.46;
ELEMDAT[15].DISTANCE:=0.25;
ELEMDAT[19].DISTANCE:=1.46;
ELEMDAT[20].DISTANCE:=1.08;
ELEMDAT[21].DISTANCE:=0.83;
```

```
ELEMDAT[22].DISTANCE:=0.69;
ELEMDAT[23].DISTANCE:=0.67;
ELEMDAT[24].DISTANCE:=0.70;
ELEMDAT[25].DISTANCE:=0.91;
ELEMDAT[26].DISTANCE:=0.86;
ELEMDAT[27].DISTANCE:=0.83;
ELEMDAT[28].DISTANCE:=0.77;
ELEMDAT[29].DISTANCE:=0.81;
ELEMDAT[30].DISTANCE:=0.83;
ELEMDAT[31].DISTANCE:=0.70;
ELEMDAT[37].DISTANCE:=1.57;
ELEMDAT[38].DISTANCE:=1.21;
ELEMDAT[39].DISTANCE:=0.98;
ELEMDAT[40].DISTANCE:=0.80;
ELEMDAT[41].DISTANCE:=0.78;
ELEMDAT[56].DISTANCE:=1.44;
ELEMDAT[57].DISTANCE:=1.13;
ELEMDAT[58].DISTANCE:=1.09;
ELEMDAT[62].DISTANCE:=1.04;
ELEMDAT[63].DISTANCE:=1.03;
ELEMDAT[64].DISTANCE:=1.02;
ELEMDAT[65].DISTANCE:=1.00;
ELEMDAT[66].DISTANCE:=0.99;
ELEMDAT[70].DISTANCE:=0.95;
ELEMDAT[71].DISTANCE:=0.94;
ELEMDAT[72].DISTANCE:=0.79;
ELEMDAT[73].DISTANCE:=0.75;
ELEMDAT[90].DISTANCE:=1.08;

REPEAT (*UNTIL QUIT*)
 FOR NEXTELEMENT:=1 TO 92 DO
  BEGIN
   ELEMDAT[NEXTELEMENT].WT:=0;
   ELEMDAT[NEXTELEMENT].MOLAR:=0;
   ELEMDAT[NEXTELEMENT].CLWT:=0
  END;
 WRITELN(TTYOUTPUT,'HOW MANY ELEMENTS?');
 IF EOLN(TTY) THEN GET(TTY);
 READ(TTY,ELEMENTNO);
 WRITELN(TTYOUTPUT,'FOR EACH ELEMENT GIVE THE ATOMIC NUMBER AND WT% OXIDE');
  FOR NEXTELEMENT:=1 TO ELEMENTNO DO
   BEGIN
    WRITELN (TTYOUTPUT,'ATOMIC NUMBER?');
    READ (TTY,ATNO);
    WRITELN (TTYOUTPUT,'WT%?');
    READ (TTY,WTSAVE[ATNO]);
     IF ATNO= 26 THEN
      BEGIN
       WRITELN ('IS INPUT IN FORM OF FE2O3? (Y,N)');
       READ (TTY,ANSWER,ANSWER);
        IF ANSWER= 'Y' THEN
         BEGIN
          FEA:=5;
          FEB:=2;
          WTFE:=159.2
         END
        ELSE
         BEGIN
          FEA:=2;
          FEB:=1;
```

```
          WTFE:=71.85
        END
      END
  END;

ENDCASE:=FALSE;
WHILE NOT ENDCASE DO
  BEGIN
   WRITELN('DO YOU WANT TO USE PROCEDURE "A" OR "B"?');
   WRITELN('FOR DESCRIPTIONS OF A AND B TYPE "Z"');
   READ (TTY,PROCTYPE,PROCTYPE);
   CASE PROCTYPE OF
     'Z':BEGIN
         WRITELN('PROCEDURE "A" INCREMENTALLY ADDS OLIVINE TO THE INPUT COMPOSITION');
         WRITELN('ASSUMING THAT THE COMPOSITION HAS DESCENDED FROM A HIGHER-TEMPERATURE');
         WRITELN('MAGMA BY FRACTIONAL CRYSTALLIZATION OF OLIVINE.  OLIVINE');
         WRITELN('COMPOSITION (MAJORS AND TRACE) AND TEMPERATURE ARE RECOMPUTED');
         WRITELN('FOR EACH INCREMENT AND PLACED IN THE TRENDS FILE.');
         WRITELN;
         WRITELN('PROCEDURE "B" SUBTRACTS OLIVINE FROM THE INPUT COMPOSITION');
         WRITELN('ASSUMING COMPOSITIONS IN A SUITE ARE RELATED BY MECHANICAL');
         WRITELN('REMOVAL OF OLIVINE.  OLIVINE COMPOSITION IS ASSUMED CONSTANT');
         WRITELN('AT A VALUE DETERMINED BY THE COMPOSITION AND LIQUIDUS');
         WRITELN('TEMPERATURE OF THE INPUT COMPOSITION.');
       END;

     'A':BEGIN
REPEAT (*UNTIL FINISHED WITH COMPOSITION*)
 T:=0;
 FOR NEXTELEMENT := 1 TO 92 DO
  ELEMDAT[NEXTELEMENT].WT:=WTSAVE[NEXTELEMENT];
WRITE (TRENDS,'TEMP(K)  ');
 FOR NEXTELEMENT:=1 TO 92 DO
  IF ELEMDAT[NEXTELEMENT].WT > 0 THEN
   WRITE (TRENDS,'    ',ELEMDAT[NEXTELEMENT].ELEMENT,'   ');
WRITELN (TRENDS);
WRITELN (TTYOUTPUT,'WITH WHAT WT FRACTION OLIVINE DO YOU WANT TO INCREMENT?');
READ (TTY,WTFRACOL);
WRITELN ('DO YOU WANT NI TO REEQUILIBRATE TO FINAL CONDITIONS?');
READ (ANSWER,ANSWER);
HOLDNI:=FALSE;
WHILE T < TCEILING DO
 BEGIN
  CONVTOMOLAR(ELEMDAT);
  FEVALENCE(ELEMDAT,FE2,FE3,FO,FA,T);
  WRITE (TRENDS,T:4:0,'   ');
  FOR NEXTELEMENT:=1 TO 92 DO
   IF ELEMDAT[NEXTELEMENT].WT > 0 THEN
     WRITE (TRENDS,ELEMDAT[NEXTELEMENT].WT:9);
  WRITELN (TRENDS);
    OLCOMP(ELEMDAT,FE2,FE3,FO,FA,T);
  IF ANSWER = 'N' THEN
    HOLDNI:=FALSE
  ELSE HOLDNI:=TRUE;
  WTSUM:=0;
  FOR NEXTELEMENT:=1 TO 92 DO
    BEGIN
     ELEMDAT[NEXTELEMENT].WT:=ELEMDAT[NEXTELEMENT].WT+
                       ELEMDAT[NEXTELEMENT].OLWT*WTFRACOL;
     WTSUM:=WTSUM+ELEMDAT[NEXTELEMENT].WT
```

```
      END;
    FOR NEXTELEMENT:=1 TO 92 DO
       ELEMDAT[NEXTELEMENT].WT:=ELEMCAT[NEXTELEMENT].WT*
                                          100/WTSUM;
  END;(*OF WHILE LOOP*)
  WRITELN (TTYOUTPUT,'DO YOU WANT TO REPEAT WITH A DIFFERENT OL INCREMENT? (Y,N)');
  READ (TTY,ANSWER,ANSWER);
  IF ANSWER <> 'N' THEN
    FINISHEDWCOMP:=FALSE
  ELSE
    FINISHEDWCOMP:=TRUE
UNTIL FINISHEDWCOMP;
WRITELN('DO YOU WANT TO TRY A DIFFERENT PROCEDURE?(Y,N)');
READ(TTY,ANSWER,ANSWER);
IF ANSWER = 'N' THEN
  ENDCASE:=TRUE
END;
       'B':BEGIN
  REPEAT (*UNTIL FINISHED WITH COMPOSITION*)
   T:=0;
   FOR NEXTELEMENT := 1 TO 92 DO
    ELEMDAT[NEXTELEMENT].WT:=WTSAVE[NEXTELEMENT];
  WRITE (TRENDS,'TEMP(K)  ');
   FOR NEXTELEMENT:=1 TO 92 DO
    IF ELEMDAT[NEXTELEMENT].WT > 0 THEN
     WRITE (TRENDS,'    ',ELEMDAT[NEXTELEMENT].ELEMENT,'   ');
  WRITELN (TRENDS);
  WRITELN (TTYOUTPUT,'WITH WHAT WT FRACTION OLIVINE DO YOU WANT TO INCREMENT?');
  READ (TTY,WTFRACOL);
    CONVTOMOLAR(ELEMCAT);
    FEVALENCE(ELEMCAT,FE2,FE3,FO,FA,T);
    CLCOMP(ELEMCAT,FE2,FE3,FC,FA,T);
    T:=0;
    WHILE T < TCEILING DO
    BEGIN
    WRITE (TRENDS,T:4:0,'   ');
    FOR NEXTELEMENT:=1 TO 92 DO
     IF ELEMDAT[NEXTELEMENT].WT > 0 THEN
       WRITE (TRENDS,ELEMDAT[NEXTELEMENT].WT:9);
    WRITELN (TRENDS);
    WTSUM:=0;
    FOR NEXTELEMENT:=1 TO 92 DO
      BEGIN
       ELEMCAT[NEXTELEMENT].WT:=ELEMCAT[NEXTELEMENT].WT+
                          ELEMDAT[NEXTELEMENT].OLWT*WTFRACOL;
       WTSUM:=WTSUM+ELEMDAT[NEXTELEMENT].WT
      END;
    FOR NEXTELEMENT:=1 TO 92 DO
       ELEMDAT[NEXTELEMENT].WT:=ELEMCAT[NEXTELEMENT].WT*
                                          100/WTSUM;
    CONVTOMOLAR(ELEMCAT);
    FEVALENCE(ELEMCAT,FE2,FE3,FC,FA,T)
  END;(*OF WHILE LOOP*)
  WRITELN (TTYOUTPUT,'DO YOU WANT TO REPEAT WITH A DIFFERENT OL INCREMENT? (Y,N)');
  READ (TTY,ANSWER,ANSWER);
  IF ANSWER <> 'N' THEN
    FINISHEDWCOMP:=FALSE
  ELSE
    FINISHEDWCOMP:=TRUE
UNTIL FINISHEDWCOMP;
```

```
WRITELN('DO YOU WANT TO TRY A DIFFERENT PROCEDURE?(Y,N)');
READ(TTY,ANSWER,ANSWER);
IF ANSWER = 'N' THEN
  ENDCASE:=TRUE
END
END (*OF CASE*)
END;(*OF PROCEDURE-TYPE WHILE LOOP*)

WRITELN (TTYOUTPUT,'DO YOU WANT TO INPUT ANOTHER COMPOSITION? (Y,N)');
READ (TTY,ANSWER,ANSWER);
IF ANSWER <> 'N' THEN
  QUIT:=FALSE
ELSE
  QUIT:=TRUE
UNTIL QUIT
END.
```

VITA

Russell Owen Colson was born in Red Cloud, Nebraska, on March 5, 1959, and grew up on a farm near Esbon, Kansas. He graduated from Esbon High School in 1977. In May 1981 he received a B.S. in geology at the University of Kansas, Lawrence, and the following fall was accepted into the graduate program at the University of Tennessee, Knoxville. There he met and married Mary Rita Cudzil.

Russell Colson worked the first year at the University of Tennessee as a teaching assistant and later as a graduate teaching assistant within the geology department. In the ensuing three years he was a NASA graduate fellow, working alternately at U.T. and the Johnson Space Center, Houston. He plans to assume the position NRC postdoctoral fellow at the Johnson Space Center following completion of his degree.

Following is a list of published abstracts and reports given at professional meetings:

Colson, R. O., McKay, G. A., and Taylor, L. A., 1983, REE crystal liquid distribution coefficients in basalt systems: Reevaluation of experimental determinations (abstract). Trans. Am. Geophys. Union 64, 343.

Colson, R. O., McKay, G. A., and Taylor, L. A., 1983, Compositionally dependent complexities in experimentally determined REE partitioning coefficients (abstract). Geol. Soc. Amer. Ann. Mtg., 349.

Colson, R. O., Taylor, L. A., and McKay, G. A., 1984, REE between olivine and melt: A proposed substitution mechanism. In The Lunar and Planetary Sci. XV, 178-179, Lunar and Planetary Institute.

Colson, R. O., McKay, G. A., and Taylor, L. A., 1985, A model for trace element partitioning: orthopyroxene and melt. In The Lunar and Planetary Sci. XVI, 146-147, Lunar and Planetary Institute.